NASA Technical Memorandum 104566, Vol. 35

SeaWiFS Technical Report Series

Stanford B. Hooker and Elaine R. Firestone, Editors

Volume 35, AMT-1 Cruise Report and Preliminary Results

David B. Robins, Anthony J. Bale, Gerald F. Moore, Nigel W. Rees, Stanford B. Hooker, Christopher P. Gallienne, Anthony G. Westbrook, Emilio Marañón, William H. Spooner, and Samuel R. Laney

April 1996

NASA Technical Memorandum 104566, Vol. 35

SeaWiFS Technical Report Series

Stanford B. Hooker, Editor
NASA Goddard Space Flight Center, Greenbelt, Maryland

Elaine R. Firestone, Technical Editor
General Sciences Corporation, Laurel, Maryland

Volume 35, AMT-1 Cruise Report and Preliminary Results

David B. Robins, Anthony J. Bale, Gerald F. Moore, and Nigel W. Rees
Plymouth Marine Laboratory, Plymouth, United Kingdom

Stanford B. Hooker
NASA Goddard Space Flight Center, Greenbelt, Maryland

Christopher P. Gallienne and Anthony G. Westbrook
University of Plymouth, Plymouth, United Kingdom

Emilio Marañón and William H. Spooner
IMS/University of Southampton, Southampton, United Kingdom

Samuel R. Laney
Brookhaven National Laboratory, Upton, New York

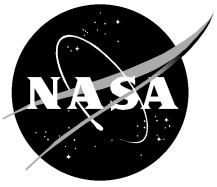

National Aeronautics and
Space Administration

Goddard Space Flight Center
Greenbelt, Maryland 20771

1996

Abstract

This report documents the scientific activities on board the Royal Research Ship (RRS) *James Clark Ross* during the first Atlantic Meridional Transect (AMT-1), 21 September to 24 October 1995. The ship sailed from Grimsby (England) for Montevideo (Uruguay) and then continued on to Stanley (Falkland Islands). The primary objective of the AMT program is to investigate basic biological processes in the open Atlantic Ocean over very broad spatial scales. For AMT-1, the meridional range covered was approximately 50°N to 50°S or nearly 8,000 nmi. The measurements to be taken during the AMT cruises are fundamental for the calibration, validation, and continuing understanding of remotely sensed observations of biological oceanography. They are also important for understanding plankton community structure over latitudinal scales and the role of the world ocean in global carbon cycles. During AMT-1 a variety of instruments were used to map the physical, chemical, and biological structure of the upper 200 m of the water column. Ocean color measurements were made using state-of-the-art sensors, whose calibration was traceable to the highest international standards. New advances in fluorometry were used to measure photosynthetic activity, which was then used to further interpret primary productivity. A unique set of samples and data were collected for the planktonic assemblages that vary throughout the range of the transect. These data will yield new interpretations on community composition and their role in carbon cycling. While the various provinces of the Atlantic Ocean were being crossed, the partial pressure of CO_2 was related to biological productivity. This comparison revealed the areas of drawdown of atmospheric CO_2 and how these areas relate to the surrounding biological productivity. These data, plus the measurements of light attenuation and phytoplankton optical properties, will be used as a primary input for basin-scale biological productivity models to help develop ecosystem dynamics models which will be important for improving the forecasting abilities of modelers. The AMT program is also attempting to meet the needs of international agencies in their implementation of Sensor Intercomparison and Merger for Biological and Interdisciplinary Ocean Studies (SIMBIOS), a program to develop a methodology and operational capability to combine data products from the various ocean color satellite missions.

1. INTRODUCTION

Twice a year, the Royal Research Ship (RRS) *James Clark Ross* (JCR) steams a meridional transect of the Atlantic Ocean to resupply the British Antarctic Survey (BAS). In September, the ship sails from Grimsby (England) to Montevideo (Uruguay) and then on to Stanley (Falkland Islands) before setting sail for the Antarctic; the April transect is simply the reverse of the southbound transect. The ship is operated for the Natural Environmental Research Council (NERC) by the BAS. A technical summary of the ship's capabilities is presented in Appendix A.

Plymouth Marine Laboratory† (PML), in collaboration with BAS and in association with the Southampton Oceanography Center (SOC) and the University of Plymouth (UoP) have started a series of Atlantic Meridional Transects (AMTs). This program was initiated utilizing funding from NERC for additional ship time. The scientific objectives of the first AMT cruise (AMT-1) were supported with funds from NERC, as well as the National Aeronautics and Space Administration (NASA) Goddard Space Flight Center (GSFC). Funding for the former was provided by the NERC Special Topic Plankton Reactivity in the Marine Environment (PRIME) program, while the latter was through the Sea-viewing Wide Field-of-view Sensor (SeaWiFS) Project (Hooker and Esaias 1993).

The primary objective of the AMT program is to investigate basic biological processes in the open Atlantic Ocean over very broad spatial scales. For AMT-1, the meridional range covered was approximately 50°N to 50°S. The measurements to be taken during the AMT cruises are fundamental for the calibration, validation, and continuing understanding of remotely sensed observations of biological oceanography. They are also important for understanding plankton community structure over latitudinal scales and the role of the world ocean in global carbon cycles. The AMT program forms a significant component of two NERC Special Topic PRIME projects:

P19 The optical characterization of zooplankton in relation to ocean physics; discrimination of seasonal, regional, and latitudinal variations (D. Robins, R. Harris, and D. Pilgrim); and

P20 Holistic biological oceanography: meso- to basin-scale and seasonal studies of phytoplankton processes linked to the functional interpretation of bio-optical signatures and biogeochemistry (J. Aiken and P. Holligan).

† This publication constitutes an official PML cruise report and its content have been approved by the Director, R.F.C. Mantoura.

The AMT program is also attempting to meet the needs of international agencies in their implementation of Sensor Intercomparison and Merger for Biological and Interdisciplinary Ocean Studies (SIMBIOS), a program to develop a methodology and operational capability to combine data products from the various ocean color satellite missions. In the longer term, the AMT project aims to enhance the modeling of global primary production (at basin scales) and to help develop ecosystem dynamics models for improving the forecasting abilities of modelers.

AMT-1 is the first in a series of Atlantic transects over the next three years whose objectives are as follows:

- Acquire data for the calibration of remotely sensed observations (primary validation);
- Secondary validation of remotely sensed products (e.g., chlorophyll concentration);
- Develop models that enable the interpretation of satellite imagery in terms of total water column properties;
- Interpret basin-scale remote sensing observations;
- Understand further the interaction between physical processes and biological production;
- Identify and quantify latitudinal changes in biogeochemical provinces;
- Determine phytoplankton characteristics and photosynthetic parameters;
- Relate the partial pressure of CO_2 (pCO_2) in surface waters with the biological production;
- Identify nutrient regimes; and
- Characterize plankton community structure, including the accurate determination of carbon values in accordance with Joint Global Ocean Flux Study (JGOFS) protocols (JGOFS 1991).

1.1 Methodology

The research strategy for the AMT-1 cruise brought together state-of-the-art marine technology with well established methodologies for investigating basin-scale oceanographic processes. A combination of this approach, together with the spatial scales resulting from the transect, provided a unique opportunity to improve the application of physical and biogeochemical oceanography to the interpretation of remote sensing imagery.

Two different sampling strategies were used during the AMT-1 cruise:

i) Underway sampling of surface water while the ship steamed at approximately 11.5 kts, and

ii) A daily (local) noon station which lasted approximately 1–2 hours.

On station, a range of parameters were measured by vertical profiles to a maximum of 200 m and discrete samples were taken from bottle samples as well as the ship's uncontaminated seawater supply for further analyses.

1.2 Physical Measurements

The undulating oceanographic recorder (UOR) was deployed three times a day (exceptions were primarily due to sampling restrictions in territorial waters):

1. From 0600 until 30 minutes before the noon station, the UOR was towed approximately 400 m behind the ship.
2. At the start of the noon station, the UOR was lowered vertically to a depth of 200 m to obtain a fluorescence profile.
3. After the completion of the noon station, the UOR was towed until 2200.

The undulating tows, between 10–80 m, provided vertical sections of the physical structure in the waters adjacent to each station.

Continuous underway surface logging of temperature and salinity related the daily station measurements to the wider physical structure of the Atlantic Ocean. In addition, hydrographic data was collected from the On-line Real-time Knowledge-based Analysis (ORKA) system, expendable bathythermographs (XBTs) from the UK Hydrographic Office, and conductivity, temperature, and depth (CTD) profiles taken during the noon station. An Acoustic Doppler Current Profiler (ADCP) was run continuously for logging ocean current velocities in the upper 250 m of the water column.

1.3 Bio-optical Measurements

As with many of the other types of measurements, bio-optical data was collected underway and on station. The UOR and a Wetlabs nine-channel absorption and attenuation meter (AC-9) provided the former, whereas, the latter were provided by two different multispectral profilers that were mounted on the same deployment rig: the SeaWiFS Optical Profiling System (SeaOPS), based on Satlantic† radiance and irradiance sensors, and the Profiling Reflectance Radiometer-600 (PRR-600) made by Biospherical Instruments, Inc. (BSI). Underway surface irradiance was provided by SeaOPS and a photosynthetically available radiation (PAR) sensor; the latter was JCR equipment.

A summary of the bio-optical sampling used to interpret the biogeochemical fields was as follows:

a) Discrete vertical profiles of the *in situ* light field using the PRR-600 and SeaOPS multispectral instruments;

b) Synoptic measurements of surface optical properties using the UOR light sensors and beam transmissometer; and

† Identification of commercial equipment does not imply recommendation or endorsement, nor does it imply the equipment identified is necessarily the best available.

c) Underway measurements of the underlying inherent optical properties of absorption and attenuation using the AC-9 instrument.

The UOR, PRR-600, and SeaOPS light sensors all measured optical properties at SeaWiFS wavelengths. The AC-9 was coupled to the uncontaminated seawater supply and its data may be used to interpret and model the optical measurements made by the light sensors. Additionally, the AC-9 provided the interpretation of the other underway measures when *in situ* optical observations were unavailable. For the light measurements, the diffuse attenuation coefficient (K_d) of the water was used as a quicklook product to determine the efficacy of the sensors.

1.4 Biogeochemical Measurements

Water samples were taken to support the following biological and chemical analyses:

- Nutrients (nitrate, nitrite, phosphate, and silicate);
- Autonomous pCO_2;
- Particulate organic carbon (POC);
- Particulate organic nitrogen (PON);
- Chlorophyll;
- Pigments;
- Size-fractionated production;
- Phytoplankton;
- Microzooplankton and zooplankton (net samples) carbon; and
- Community size structure and taxonomy.

The samples were taken from the underway pumping system between stations or from vertical profiles at each station, or both.

Nutrients were analyzed using a four-channel Technicon segmented-flow auto-analyzer. The pCO_2 system measured both atmospheric CO_2 (at bridge level) and CO_2 in seawater from the uncontaminated supply, thus providing estimates of the air-sea concentration difference. Simultaneous measurements of atmospheric pressure and seawater temperature were made to support the analysis of data.

Chlorophyll samples were extracted using acetone and analyzed using fluorometric techniques on board the ship. Individual samples for pigment analysis using high performance liquid chromatography (HPLC) were taken and frozen in liquid nitrogen for subsequent analysis in the laboratory. Size-fractionated primary production experiments were conducted at each station, and ^{14}C analyses were performed on board the ship. A fast repetition rate fluorometer (FRRF) was run underway and at all stations to investigate photosynthetic parameters and ocean productivity.

Samples for various fractions and total carbon to nitrogen ratio (C/N) were taken for the size range less than 1 μm to zooplankton over 2,000 μm in accordance with JGOFS protocols (JGOFS 1991). These samples were processed on board in preparation for analysis back in the laboratory. Samples for phytoplankton, microzooplankton, and zooplankton distribution and composition were taken and preserved on the cruise for analysis by microscope back in the laboratory. The ADCP was used for logging zooplankton distribution and abundance from acoustic backscatter. Automated analyses were carried out for zooplankton community size structure, using the Optical Plankton Counter (OPC) and a high-speed video camera.

1.5 Document Organization

The rest of this document begins with detailed summaries of the sampling strategies, instrumentation, and analysis techniques (Section 2) used during the AMT-1 cruise track (Section 3). This material is followed by a presentation of preliminary results from a low productivity station (Section 4), a day of underway sampling through high productivity water (Section 5), and a synopsis of the entire transect (Section 6). The results are strictly preliminary, and in many cases, the instrumentation has not been completely calibrated. The idea is to expose the reader to the types of products that will be produced from the AMT-1 data set. The report concludes with a discussion of the overall cruise experience and future plans (Section 7).

2. INSTRUMENTATION

Most of the sampling during AMT-1, in terms of time spent collecting data, was while the ship was underway. Close to noon, however, the ship stopped for 1–2 hours of vertical sampling. The daily stations were numbered the same as the sequential day of the year (SDY). Departures from this schedule were usually the result of avoiding sampling restrictions in territorial waters, that is, exclusive economic zones (EEZs). In keeping with the SeaWiFS optical protocols (Mueller and Austin 1995), however, every effort was made to ensure station sampling during suitable sun angles, that is, zenith angles less than 60°(e.g., Table 1). In many cases, this required the ship to steam at an above normal cruising speed during evening transects (when the UOR was not in the water) or an early termination of the UOR tow to allow enough high speed transit time to the next station.

The basic sampling strategy at each station was to slow the ship to 6 kts and bring the UOR on board, which was then immediately used to obtain a fluorescence profile (there was no fluorometer on the CTD rosette) and establish the basic water structure of the station. Once the UOR profile had begun, the optical instruments and the zooplankton net were deployed. The depth of the optical cast (a cast is a down and then up deployment of the sensors involved) was determined in real time based on the ambient light field; the net casts were always to a nominal depth of 200 m (the actual depth reached was recorded

Table 1. Solar zenith angles (in degrees) for SDY 280 (accuracy ±0.5°).

Degrees	*Greenwich Mean Time (GMT)*									
Latitude	0800	0900	1000	1100	1200	1300	1400	1500	1600	1700
35	85.1	73.3	62.2	52.4	44.8	41.0	41.8	47.0	55.4	65.8
30	84.3	71.7	59.7	49.0	40.5	36.0	37.0	43.0	52.4	63.6
25	83.4	70.2	57.5	45.8	36.3	31.1	32.2	39.2	49.5	61.6
20	82.6	68.8	55.5	42.9	32.4	26.2	27.5	35.6	47.0	59.8
15	81.9	67.6	53.7	40.4	28.7	21.3	22.9	32.3	44.7	58.3
10	81.2	66.6	52.2	38.2	25.4	16.5	18.6	29.4	42.8	57.0
5	80.6	65.8	51.1	36.5	22.7	11.8	14.6	27.2	41.3	56.0
0	80.0	65.1	50.2	35.4	20.8	7.6	11.5	25.6	40.3	55.2
−5	79.6	64.7	49.8	34.8	19.9	5.0	10.0	24.9	39.8	54.7
−10	79.2	64.4	49.7	34.9	20.3	6.6	10.8	25.1	39.8	54.6
−15	78.9	64.4	49.9	35.6	21.7	10.5	13.5	26.3	40.4	54.8
−20	78.7	64.6	50.6	36.9	24.1	15.1	17.3	28.2	41.4	55.2
−25	78.5	65.0	51.6	38.7	27.2	19.9	21.6	30.8	42.9	56.0
−30	78.5	65.6	52.9	40.9	30.7	24.8	26.1	33.8	44.8	57.0
−35	78.6	66.3	54.5	43.6	34.6	29.7	30.7	37.3	47.0	58.4

by a self-logging temperature and depth probe attached to the net strops). The CTD was then deployed to a depth of 200 m, during which, the UOR cast was terminated and the fluorescence data analyzed.

The optical and net casts were finished while the bottle depths were agreed upon using the CTD down cast data and the UOR fluorescence data. While the CTD was being brought back to the surface, the optical cast was finished and an XBT was dropped. In some cases, the optical casts were repeated to a shallower depth and a shorter boom length from the ship to quantify the effects of ship shadow. The final operation on station was bringing the CTD on board, after which, the UOR was redeployed at 6 kts. Because the ship's crew were willing to have several wires over the side at the same time, elapsed time on station was frequently on the order of one hour.

A complete summary of the scientific data collected during AMT-1 is presented in Appendices B–L. These appendices are the logs for the various instruments or sampling programs undertaken during the cruise. The scientists involved and their affiliations are given in Appendix M.

2.1 Hydrography

A variety of hydrographic instruments were deployed during AMT-1 and several of them provided duplicate data, e.g., temperature or pressure. This duplication allowed a vicarious calibration of data whose calibration was either unknown or obviously incorrect.

2.1.1 XBT

The deployment of an XBT yields a trace of temperature as a function of depth from the sea surface into the deep ocean. Interpretation of the temperature profile leads to a greater understanding of the underlying physical structure and hydrography of the oceanographic provinces being sampled. During AMT-1, XBTs were launched in conjunction with the deployment and recovery of the UOR and at the noon station. Sippican Mark 7 XBTs were used. These probes have an operational depth of approximately 760 m and give deeper readings than the UOR and CTD, which were deployed to depths of approximately 80 and 200 m, respectively. The XBT data was recorded by the Sippican MK9/MS-DOS data acquisition system (version 5.1); post-trace analysis was performed using the accompanying display software (version 3.1). A summary of the XBT deployments during AMT-1 is presented in Appendix B.

2.1.2 UOR

The UOR (Fig. 1) is a towed vehicle that incorporates a programmable servo which controls the attitude of a diving plane and causes the vehicle to undulate through a preset pattern, typically 5–75 m every 9 minutes. The UOR can operate at speeds between 10–12 kts. In the configuration used for AMT-1, it was towed at 11.5 kts. At speeds in excess of 6 kts, the servo unit is powered by an alternator, which is driven by a propeller on the rear of the body. Comprehensive details of the UOR vehicle are given by Aiken (1985).

2.1.2.1 UOR Hydrographic Instruments

The UOR used for AMT-1 was instrumented with a Chelsea Instruments CTD and fluorometer package, a Sea-Tech 25 cm path length transmissometer, tilt and roll sensors, and an array of upwelling and downwelling radiance and irradiance sensors (Table 2). The sensor packages are autonomous, powered by dry cell batteries and logged to

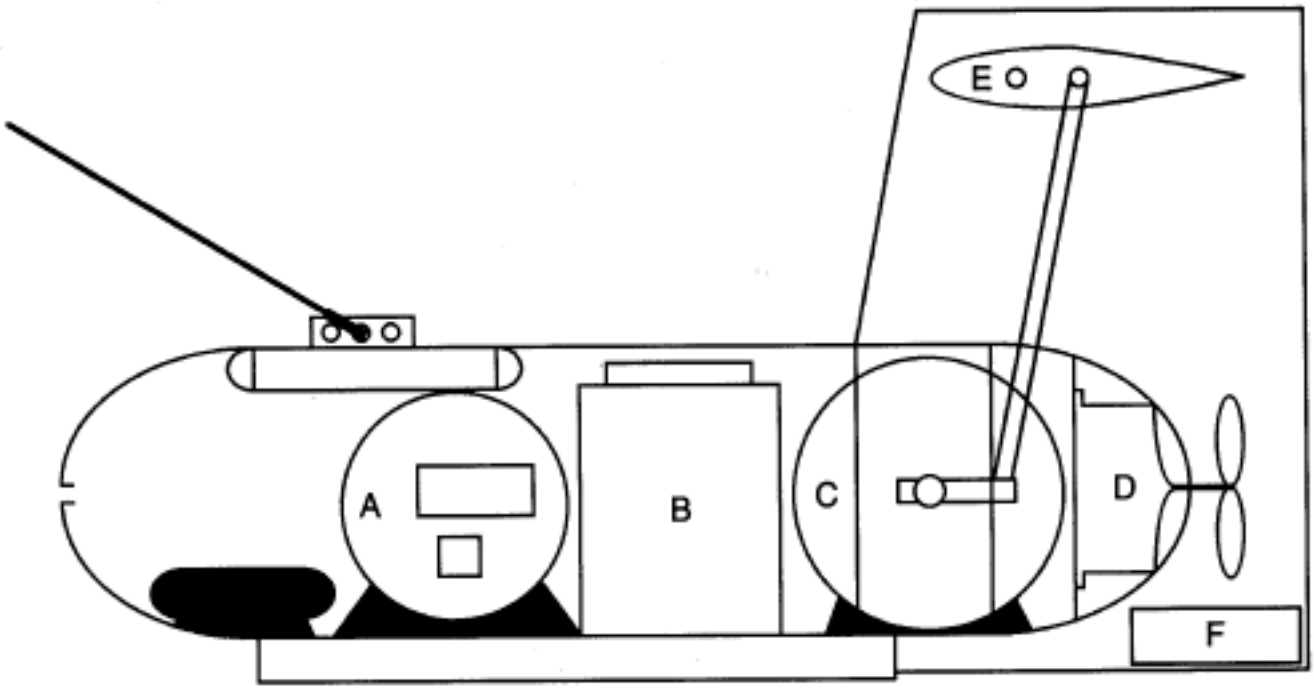

Fig. 1. A schematic of the UOR: A is the sensor package, B is the data logging package, C is the servo unit, D is the alternator, E is the dive control plane, and F is one of four light sensor modules.

an onboard, solid-state, data logger. With a sampling interval of 4 s, the logger has a capacity of approximately 16 hours of measurements over 22 data channels, which is compatible with battery duration. The last 6 channels use multiplexing technology; channel 11 is a hi-lo switch which controls channels 12–17 to allow an additional six channels to share the same data streams. Data frequency on the multiplexed channels is, therefore, every 8 s. On processing, the multiplexed data streams are separated to provide channels 18–23.

Table 2. A list of channels recorded by the UOR data logger in the setup employed for AMT-1.

Channel	*Parameter*	*Channel*	*Parameter*
1	Time	12	$E_d(412)$
2	Depth	13	$E_u(443)$
3	Temperature	14	$E_d(514)$
4	Conductivity	15	$E_u(490)$
5	Chlorophyll	16	$E_d(665)$
	Fluorescence	17	$E_u(554)$
6	Pitch	18	$E_d(443)$
7	Roll	19	$L_u(443)$
8	Transmittance	20	$E_d(490)$
9	$L_u(412)$	21	$L_u(490)$
10	$L_u(514)$	22	$E_d(554)$
11	Hi-Lo	23	$L_u(554)$

The temperature and conductivity sensors were calibrated in the laboratory before the cruise. During the cruise, they were cross-referenced against the precision reversing thermometers and salinity bottle measurements taken at each CTD station.

2.1.2.2 Routine Operations

Towing was carried out each day from 0600–2200 (ship time), except during passage in certain territorial waters. The UOR was recovered prior to the noon station and used for vertical profiling on station. Insufficient resources were available to support overnight towing, but the strategy employed provided data for approximately 7 hours before and after each station, which represents approximately 160 nmi of track or about 60% of the total track. The overnight period was used to increase speed over that adopted for towing and make good the slight deficiency in progress incurred by UOR launch and recovery operations as well as station work.

Using 500 m of 8 mm galvanized steel wire rope, the UOR routinely achieved a depth profile of 10–77 m which, for the most part, allowed the position of the thermocline and deep chlorophyll maximum (DCM) to be defined. In parallel with each tow, a navigation file was logged every 10 minutes and archived on a SUN work station for subsequent merging, using time (GMT), with the UOR data files.

Following each tow or profile, the logger memory card was removed from the UOR, exchanged for a blanked memory card, and the logger reset for the next towing operation. Data was downloaded from the memory card to a

personal computer (PC) where the values were calibrated and converted to engineering units from sensor voltage output using a C program containing calibration coefficients for each channel. For quick reference and evaluation of the vehicle performance and sensor output, the calibrated data was imported into a commercial software package. Plots of parameter versus time, and contour plots in a depth versus time frame were produced to help build up a picture of the mixed layer structure. For future presentation purposes and for subsequent publication, the final data set will be referenced to position using the merged navigational file mentioned previously.

On each daily station, with the vessel stopped, the UOR was reconfigured by mounting the sensors externally. The UOR was then profiled vertically to a depth of 200 m in order to measure the chlorophyll fluorescence distribution. This information was used to determine the optimum depths for GoFlo™ CTD bottles to be tripped on the subsequent CTD rosette cast.

2.1.3 CTD

Measurements of temperature and salinity were obtained from vertical profiles of a CTD and from a thermosalinometer which provided underway data from the uncontaminated seawater supply.

2.1.3.1 CTD Profiles

A Neil Brown Mark IIIB (Instrument Systems, Inc.) CTD instrument with a rosette sampling system, fitted with 12 (10 l) General Oceanics water bottles, was deployed to 200 m at each station (where water depth allowed). Data on the temperature and salinity profiles at each station were logged on the ship's computing system for further data processing. Temperature was also recorded using two reversing thermometers (RTM 4002) manufactured by Sensoren-Instrumente Systeme (SIS) on each deployment. These thermometers gave accurate readings to three decimal places from the standard *surface* depth of 7 m (used at all stations) and the deepest bottle depth at each station, which varied from station to station. All of these instruments were JCR equipment.

The temperature profile, together with the fluorescence profile from the UOR and light profiles from SeaOPS, were used to select the depths from which water was collected for the biological measurements of primary production, photosynthetic activity, pigments, dissolved organic carbon (DOC), POC, and plankton taxonomy. A standard comprehensive suite of samples were taken for five depths at all stations and a more limited set of analyses were carried out on two additional depths (see Appendix C).

2.1.3.2 Underway Hydrography

At every station, salinity bottles were taken from the *surface* (7 m) CTD water bottle and, synchronous with the CTD surface bottle collection, from the uncontaminated seawater supply. Normal precautions for rinsing and storing salinity bottle samples were observed and the samples were analyzed in batches of 12–20 using a Guildline Autosal™ (model 8400) precision salinometer standardized with the International Association for the Physical Sciences of the Ocean (IAPSO) standard seawater according to the manufacturer's instructions.

Salinity was also calculated from conductivity and temperature logged by the underway Ocean Logger as measured by a Sea-Bird Electronics (SBE) thermosalinograph, which was fed from the uncontaminated seawater supply. The output from the thermosalinometer was recorded by the level-B computer at a 1 Hz frequency. Bottle samples were taken from the salinometer effluent at a time coincident with the CTD cast. These were analyzed for salinity using the aforementioned Guildline Autosal.

2.1.4 ORKA

ORKA analyzes a variety of oceanographic data captured from hull-mounted or underway sensors in real time, and displays the results to the user in the form of a probability indicting the strength of frontal activity. The detection of potential forewarning signals of frontal activity is achieved by analyzing the ingested data in the context of the known and expected hydrology of the region. Once started, the system runs autonomously; the reading, analyzing, and updating of the data and graphic displays occurs once every 5 s.

The ORKA analysis algorithms are written in the Interactive Data Language (IDL), as is the graphical user interface (GUI), which is menu based and capable of displaying up to nine oceanographic parameters on screen simultaneously. The system resides on a Sun Microsystems (Sun) Sparc +20 workstation running the Solaris operating system (version 2.3).

2.2 Optics

The custom-built profiling rig to carry the PRR-600 and SeaOPS sensor systems was developed with a geometry that ensured both radiance sensors did not view any part of the support. The narrow geometry of the rig was designed to provide the minimum optical cross section. The field of view of the irradiance sensors was only influenced by the 7 mm wire, the first meter of which was covered with black tape. Careful attention was paid to the balance of the rig, since at present, neither SeaOPS or the PRR-600 have tilt or roll sensors. The rig was trimmed with lead weights in air, accounting for the in-water weights of the sensors; after final assembly of the rig, visual checks for correct trim were carried out in calm water.

The SeaOPS rig was deployed from a stern crane with a reach of about 8–9 m over the side of the ship. The typical lowering and raising speed of the winch used was

approximately 1 m in 5 s or 20cm s^{-1}. Since the crane was on the starboard side of the ship, the sun was kept on the starboard side during all stations except during adverse weather conditions. In addition, sea- and sky-state photographs were taken during the up cast whenever the optical instruments were deployed.

The commissioning and integration of the optical equipment presented several problems that were all completely resolved. The communications and power connections for the system, for example, presented two problems. The SeaOPS sensor went into RS-232 setup mode, due to an electrical leakage between the RS-232 input and RS-232 output of the connector; retermination with adequate insulation solved this problem. Commissioning the PRR-600 proved more difficult, because the connectors provided by the manufacturer were supplied with an incorrect wiring diagram. When the correct wiring was established, the PRR-600 failed to work with the length of cable used (approximately 260 m). The fault was eventually traced to inadequate power being supplied by the PRR-600 deck box. Using an alternative power supply to provide a higher voltage to overcome the cable resistance solved this problem. This remains a problem for discussion with BSI, since the cable resistance (14.8 Ω) was well within the manufacturer's specification.

Data was logged on two separate PC compatibles using the software supplied by the manufacturers for both SeaOPS and the PRR-600. There were initial problems with the Satlantic Proview program, because it failed to work on the laptop system intended for the work. This problem was caused by a below specification communications port on the laptop (the Proview manual warns about this potential problem). The PRR-PROF program operated without problems. The Satlantic Proview program, however, lost several files during initial deployments, apparently due to disk fragmentation and memory management problems on the PC. Removing disk caches and a number of drivers on the PC cured this problem. The program did overwrite data without warning, unfortunately, which caused the loss of half of one cast; this problem needs to be fixed.

The major task in terms of software was the integration of both the PRR-600 and SeaOPS data streams, since they were deployed on the same winch system. The deck irradiance and in-water data from SeaOPS proved relatively easy to integrate, since Proview provided an integrated data stream. Initial plans were to use time synchronization of the data to integrate the data from the PRR-600 and SeaOPS. Although adequate attention was paid to the setting of both PC clocks to the Radiocode master clock on the ship, this approach proved impossible to implement, since there was no clock information in either of the data streams, and any noise spikes resulting in lost information immediately destroyed the synchronization of the data streams.

The final approach was to merge the data based on depth, after binning the data to 0.2 m resolution. There was a difference in readings from the pressure sensors of approximately 5% after correction for surface offsets; at present, a final depth calibration is not available and all results have to be taken as provisional.

2.2.1 SeaOPS

SeaOPS is composed of an above-water and in-water set of sensors comprising five subsystems (Fig. 2). The in-water sensors are a downward-looking radiance sensor which measures upwelling radiance, L_u, and an upward-looking irradiance sensor which measures downwelling irradiance, E_d. The former is a Satlantic ocean color radiance (OCR-200) sensor (S/N 021), and the latter a Satlantic ocean color irradiance (OCI-200) sensor (S/N 029). The two units send their analog signals to an underwater data unit, a Satlantic DATA-100 (S/N 016), that converts the analog signals to RS-485 serial communications. The above water unit, a Satlantic Multichannel Visible Detector System (MVDS), measures the incident solar irradiance, E_s. The MVDS unit (S/N 009), is composed of an OCI-200 irradiance sensor (S/N 030) packaged with an analog-to-digital (A/D) module that converts the analog output of the OCI-200 unit to RS-485 serial communications.

All of the SeaOPS radiometers take measurements in the same spectral bands (Table 3) which have been selected to support SeaWiFS calibration and validation activities (McClain et al. 1992). During AMT-1, the underwater SeaOPS sensors were deployed on a T-shaped frame with the OCI-200 and OCR-200 sensors on one side of the frame and a PRR-600 on the other side (Fig. 2). A discussion of the PRR-600 is given in Section 2.2.2.

Table 3. Center wavelengths (CWLs) for the Satlantic sensors deployed on AMT-1 in association with SeaWiFS bands. All of the sensors have 10 nm bandwidths.

SeaWiFS Band	OCR-200 (L_u)	OCI-200 (E_d)	MVDS (E_s)
1	412.8	412.8	412.8
2	443.6	443.2	442.3
3	489.5	490.5	490.5
4	509.2	509.2	509.2
5	555.4	555.5	555.0
6	665.7	665.6	664.8
6	683.2	683.8	682.6

The RS-485 signals from the MVDS and the DATA-100 are combined in a Satlantic deck box, the DECK-100 (S/N 008), and converted to RS-232 communications for computer logging. The DECK-100 also provides the (computer controlled) direct current (DC) power for all the sensors and is designed to avoid instrument damage

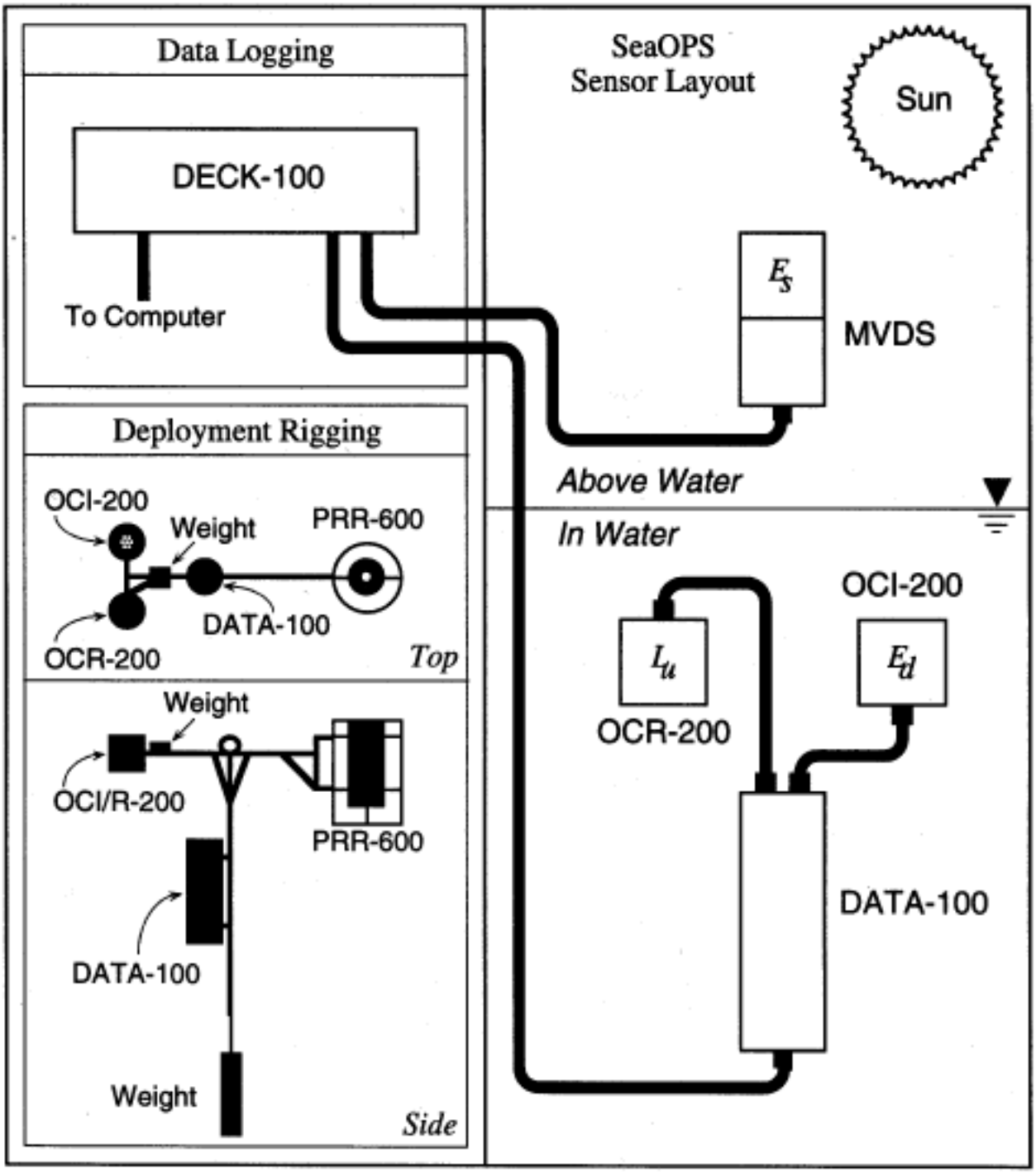

Fig. 2. A schematic of the sensor layout, cabling pathways, and deployment rigging for SeaOPS during AMT-1.

due to improper power-up sequences over varying cable lengths. For AMT-1, the MVDS cable length was approximately 200 m whereas the DATA-100 cable length was about 260 m (250 m on the winch and 10 m from the winch to the DECK-100). The unit also acts as a useful diagnostic should telemetry problems be encountered.

2.2.2 PRR-600

The PRR-600 measures downwelling irradiance and upwelling radiance over SeaWiFS bands 1, 3, 4, 5, and 6 (Table 4), as well as temperature and depth. The method of deployment was developed in an effort to conform to the SeaWiFS optics protocols (Mueller and Austin 1995) with regards to instrument tilt and roll. Meeting these challenging requirements is greatly aided by the stability of, and facilities offered by, the JCR.

Table 4. Basic operational specifications of the PRR-600 channels. The band entry refers to the SeaWiFS band number, and the last column gives the channel bandwidth in nanometers.

Band	*Channel*	*Sensor(s)*	*Width*
1	412	E_d L_u	10
2	443	E_d L_u	10
3	490	E_d L_u	10
4	510	E_d L_u	10
5	555	E_d L_u	10
6	665	E_d L_u	10
	PAR	E_d	10
6	683	L_u	10

The PRR-600 was deployed to measure ocean color using the SeaWiFS band set. The data obtained will be used to simulate and calibrate the information obtained from the SeaWiFS and the Ocean Color Temperature Sensor (OCTS) satellite systems. The data obtained will be compared with mathematical models of the underwater light field and with the other biogeochemical measurements taken on AMT-1. The Coastal Zone Color Scanner (CZCS) subset of bands will be compared with the discrete fluorometric chlorophyll *a* concentrations to determine the utility of the historical CZCS algorithms. The PRR-600 and the SeaOPS instruments were deployed on the same platform (Fig. 2). Comparison of the data will serve to validate calibration procedures and instrument design.

2.2.3 UOR Light Sensors

The UOR was fitted with four banks of three light sensors which were multiplexed on six logger channels and one bank of two sensors which had dedicated channels. These sensors were designed and fabricated at PML (Aiken and Bellan 1990) and were mounted externally on the upper and lower edges of the vertical tail planes of the UOR such that the sensors were not shaded by the vehicle. Each sensor collected light within a narrow wavelength band. Two sensor blocks were mounted on each side of the UOR and oriented so that, of each pair, one collected downwelling light and the other upwelling.

The spectral response of the UOR light sensors were determined to an accuracy of ±0.2 nm. The bandwidths were all in the range 8–12 nm around their nominal centers. Irradiance sensors were calibrated with a 1,000 W FEL lamp (number 81523). The radiance sensors were calibrated with an integration sphere, the output of which had been calibrated by transferring the FEL lamp irradiance scale. The linearity of the sensors was determined using a dysprosium discharge lamp and neutral density filters. With the exception of cosine response, radiance field of view, and immersion effect, the procedures conformed to the SeaWiFS ocean optics protocols (Mueller and Austin 1995). It is anticipated that these measurements will be carried out during the postcruise calibration.

The UOR was fitted with a Sea Tech, 25 cm path length, transmissometer with a 660 nm source. Transmission is the residual signal measured after light from a standard source has been subject to scattering and absorption. A transmission value of 100% implies total transmission, whereas 0% transmission equates to total light obscuration. In open ocean waters, low transmission values reflects areas of high productivity, since phytoplankton both scatter and absorb light. In coastal waters, inorganic suspended particles are major sources of light attenuation.

Operationally, the UOR transmissometer signal was sampled every four seconds and logged with the physical data. For calibration purposes during the AMT-1 survey, the transmissometer *air* and *dark* values were measured at intervals when the UOR was on deck. The transmissometer data was logged at the same frequency as the physical parameters.

2.2.4 AC-9

The AC-9 is a nine-channel (412, 440, 488, 510, 555, 630, 650, 676, and 715 nm) 25 cm pathlength transmissometer and reflective tube absorbance meter. The instrument consists of a dual path unit: the first path is a conventional transmissometer enclosed in a non-reflective tube; the second path consists of a collimated light source with a diffuse detector, enclosed in a reflective tube. These two beams give measurements that approximate the inherent optical properties c (the beam attenuation coefficient) and a (the absorption coefficient), where c is the sum of the scattering coefficient b and a.

With suitable knowledge of the scattering properties of seawater, it is possible to use the instrument to predict the other apparent optical properties of seawater, particularly reflectance (R) and K_d. In any practical instrument, these measurements are approximations of the true inherent optical properties. When measuring c, it is always necessary to use a finite collector angle, hence, a practical measurment of c will always measure some photons that

have been forward scattered in the direction of the collector. Consequently, the measured c will be reduced by a factor dependent on the geometry of the instrument:

$$\tilde{c} \;=\; a \;+\; \int_0^{90-\Delta} \beta(\theta) d\theta \qquad (1)$$

where $\tilde{c}$ is the measured value of c.

The measurement of a presents similar problems, since the reflective tube system does not collect photons that are backscattered towards the light source, and the measured a ($\tilde{a}$) will be increased, by a factor dependent on the backscatter of the water and the geometry of the instrument:

$$\tilde{a} \;=\; a \;+\; \int_0^{40} \beta(\theta) d\theta \qquad (2)$$

where $\beta(\theta)$ is the scattering phase function. These theoretical considerations are fundamental for the interpretion of the data from the AC-9 instrument, especially when considering a transect that covers waters ranging from particle dominated to clear oligitrophic waters.

2.2.4.1 Deployment Considerations

The AC-9 presents particular problems in mounting for underway deployment. The transmissometer path can be deployed at almost any angle, and is no more difficult to deploy than a conventional single wavelength transmissometer. The absorption tube, however, is more sensitive to orientation. Any bubbles or trapped air in the system will reduce the efficiency of either the diffuse collector or the reflective tube. The arrangements for mounting the system are shown in Fig. 3. The instrument was mounted at 45° and flow was under positive pressure from below. The instrument was orientated so that the outlet from the tube was upward. A bubble trap was fitted in the water supply before the instrument. The efficiency of this trap could be verified by visual observation. On initial startup or cleaning of the instrument, the c readings settled down within about 30 seconds, and the a readings after about 3–5 minutes. No problems were observed with spikes or short-term drift throughout the cruise.

2.2.4.2 Calibration and Processing

The instrument was supplied with the original Wetlabs air and pure water calibration. The air calibration values for the instrument were verified before deployment of the instrument and were found to agree within better than 0.1%. During the cruise, the instrument was thoroughly cleaned and new air calibration values were obtained. These values showed shifts with respect to the original precruise Wetlabs values. Postprocessing will determine whether to use the cruise air values or the nominal manufacturer's values. As a calibration test, seawater and *clean water* filtered with a Gelman high volume 0.2 μm filter was passed though the system after air calibration. The filtered seawater provided reliable results; however, it proved impossible to obtain reliable results from clean water values.

The data were logged using the Wetlabs `Wetview` program. This program performed the initial calibration of the instrument. The program does not correct for the temperature dependent absorption of water at 715 nm; however, the transect was within 1° of the calibration value, and in this case, the error is less than 0.2%. Normalized absorption values were calculated using the assumption that $a_p(715)$ can be assumed to be zero, and that the particle backscatter dominates. This is a standard method for processing AC-9 data, but has potential problems when used in oligotrophic waters where the backscatter from water dominate the particle backscatter at longer wavelengths.

2.2.5 PAR

The JCR PAR sensor is fitted as part of the Ocean Logger system. It is manufactured by Delta-T Instruments and was mounted on a mast just forward of the bridge. The digitized output of this sensor was recorded by the level-B logging system.

2.3 Fluorometry

Fluorescence measurements connect ocean biology to ocean optics, as fluorescence itself is a measurable effect of phytoplankton responding to irradiance, which is the initial transformation of solar energy into biological energy. Traditionally, fluorescence has been used as a general indicator of phytoplankton biomass, and good correlations of fluorescence signal to chlorophyll concentration have been well established. However, various sources of signal degradation and convolution, such as fluorescent detritus, physiological fluorescence quenching mechanisms, zooplankton, and solar blinding effects in surface water, have prevented field researchers from understanding the basic dynamics of phytoplankton-irradiance interactions. Although recent introductions in field instrumentation have addressed some of these issues individually, no one instrument can deliver a comprehensive picture of the interactions in question. Consequently, when designing an oceanographic bio-optical experiment, it becomes extremely important to consider the various fluorescence instrumentation available and to design a complementary suite of instruments and sampling methodology which can best reconstruct the underlying dynamics governing the observed fluorescence signal.

Such issues in field fluorescence measurements were well understood during the planning stages of AMT-1, and steps were taken to secure instrumentation which could be used to observe fluorescence signals through various methodologies. Consequently, AMT-1 is the first cruise to integrate many of the newer fluorometric instruments and, thus, the first to give a detailed look into many of the characteristics of basin-scale fluorescence measurements which

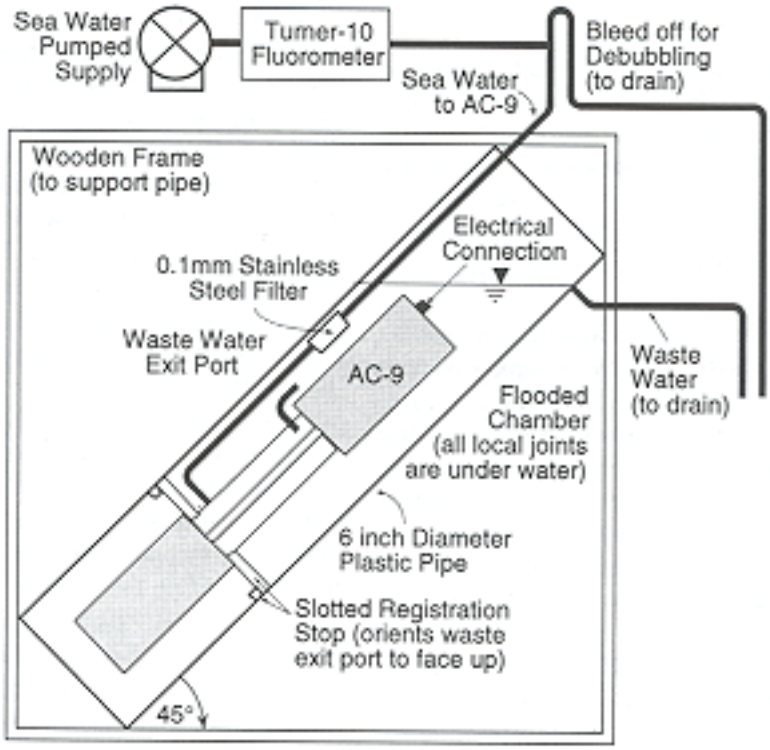

Fig. 3. A schematic of the deployment geometry for the AC-9 instrument during AMT-1.

one (or even two) instruments independently would quite likely fail to explain. In some cases, AMT-1 was the first instance where two fluorescence techniques were used concurrently, offering the first chance to compare data generated by different methodologies. Four different active and two different passive systems were employed during AMT-1; these systems were towed, profiled, used in flow-through mode and with individual samples, or in various combinations. Three of the active systems are explained here in detail; the passive (optical) systems (as passive fluorescence is a component of the signal in SeaWIFS band 6) are covered in Section 2.2.

2.3.1 Underway Fluorometer

Chlorophyll fluorescence for the JCR Ocean Logger system was measured using a Turner Model 10 fluorometer in flow-through mode. The Turner fluorometer was placed in line with the SBE thermosalinograph and a flow meter. The fluorometer used the standard Turner Designs chlorophyll fluorescence filter set. The data from the fluorometer was logged into the JCR Ocean Logger system using the internal A/D converter and range output. On acquisition, the data was adjusted to account for the current range of the fluorometer; no information was logged as to this range setting.

At the start of the cruise, the fluorometer flow-though cell was cleaned and the dessicant changed. Subsequently, the cell was checked regularly for fouling. The fluorometer zero was set with a *clean water* blank at the beginning of the cruise, and all ranges were checked for a zero reading on the analog output.

The data logged by the underway system, and the fluorometer showed initial problems with auto ranging: the fluorometer was switching ranges every 5–10 minutes. Although no offset between ranges was aparent on the analog reading, considerable offset shifts were observed in the logged data. At this point, it was decided to fix the range at a level consistent with the anticipated levels in the Mauritian upwelling (see Section 5.3.1 for results).

2.3.2 UOR Fluorometer

The UOR fluorometer was employed to map the location and variation of the subsurface chlorophyll maximum at high resolution while underway, and also to determine the vertical distribution of chlorophyll by vertically profiling the UOR and its sensor packages while stopped on station. The chlorophyll sensor carried on the UOR is a PML development (Aiken 1981) with characteristics designed specifically for autonomous deployment. Excitation is by means of a xenon discharge flash every 4 s providing saturation illumination with peak energy at 490 nm. The detector employs narrow band interference filters that receive fluorescence at 685 nm: the sample volume is 2 ml. The UOR fluorescence detector was factored to a nominal chlorophyll response which could be subsequently recalibrated against chlorophyll values derived from discrete samples extracted and measured on board.

2.3.3 FRRF

A benchtop FRRF, on loan from the Department of Energy (DOE) Brookhaven National Laboratory (BNL), was used for transect and profile measurements during the AMT-1 cruise. The FRRF is an active fluorometric system, utilizing a xenon flashtube excitation source to stimulate phytoplankton fluorescence similar to commercial active fluorometers. Unlike standard active fluorometers, however, the FRRF excitation and emission systems operate on a time scale several orders of magnitude smaller, providing the ability to resolve fluorescence signals to 60 ns and to produce controlled stimulation flashlets of approximately 2 μs width at a repetition rate of 200 KHz. Time resolution at this scale allows examination of biophysical processes and structure related to phytoplankton capture and utilization of incoming photon energy. Inspection of these characteristics provide qualification of the relative phytoplankton photosynthetic activity in a given environment.

Detailed explanations of the FRRF methodology and technology are well documented (Kolber and Falkowski 1993; Falkowski et al. 1992; Kolber and Falkowski 1992; and Kolber et al. 1990) and will not be reiterated here. During AMT-1, the benchtop instrument was operated using a flow cell, continually analyzing water samples tapped from the ship's (uncontaminated) seawater supply. Simultaneously, ambient measurements of seawater temperature, conductivity, fluorescence, PAR, and ship's position were logged into the FRRF from the shipboard computer platform. Since changes in environmental conditions affect biophysical characteristics in phytoplankton, some on the order of minutes, proper analysis of FRRF data records require a detailed matching record of the environmental state.

FRRF data were also obtained from bottle samples collected from daily CTD casts. Biophysical parameters were measured and examined over depth. Sampling was grouped around the subsurface fluorescence maximum as indicated by the active fluorometer system mounted in the UOR.

2.4 Photosynthesis and Calcification

Sampling for photosynthesis and calcification experiments was conducted at five depths on each daily station. Samples for determining photosynthetic parameters were taken at two selected depths: surface (7 m) and the depth of the chlorophyll maximum. In both cases, seawater samples were taken from the Niskin bottles and filtered through a 200 μm sieve in order to remove mesozooplankton. In addition to the vertical profiles, underway measurements of photosynthesis and calcification rates were conducted at selected areas by taking water samples from the uncontaminated water supply (approximately) every 4 hours.

Photosynthetic and calcification rates were measured by the ^{14}C method (Balch et al. 1992). Duplicate 70 ml polycarbonate bottles were filled with the seawater sample, spiked with 370 KBq (10 μCi) of $NaH^{14}CO_3$ (Amersham Life Science; specific activity, 2.0 GBq mmol^{-1}) and incubated in an on-deck incubator refrigerated with surface water. Incubations were carried out between 1400 and 2000 (ship time) and lasted for approximately 5 hours. At the end of the incubation, each sample was divided into two aliquots and each filtered through 0.2 μm pore size Poretics polycarbonate filters under low pressure (less than 100 mm Hg).

One of the filters (filter *a*) was carefully rinsed with filtered seawater and placed in a dessicator for 24 hours. This treatment has been shown to remove any soluble labelled carbonate still adsorbed to the filter (Joint and Pomroy 1983). The second filter (filter *b*) was rinsed and decontaminated by adding 1 ml of 1.0 N HCl as described in Lean and Burnison (1979). Radioactivity on each filter was determined by using a Beckman LS6000SC scintillation counter on board the ship. Radioactivity in filter *b* measures the photosynthetic carbon incorporation, whereas calcification was calculated as the difference between the radiactivity measured on filters *a* and *b*.

Individual samples to measure size-fractionated photosynthetic rates were incubated as described earlier, and filtered sequentially through 20, 2, and 0.2 μm Poretics polycarbonate filters. Decontamination and counting of the samples were conducted as previously indicated.

Production-irradiance (P-I) experiments were carried out in a laboratory incubator equipped with a 100 W halogen lamp, which provided a range of light intensities from approximately 6–900 μE m^{-2} s^{-1}. The samples were cooled with circulating uncontaminated seawater and the incubation lasted for three hours. Filtering, decontamination, and counting of the samples were conducted as described above.

The original AMT-1 research plan involved having two types of FRRF instruments on board: a benchtop laboratory unit and a submersible profiler. Used in tandem, these instruments can produce a detailed assessment of the biophysical parameters influencing primary productivity for *in situ* measurements of phytoplankton fluorescence. Each unit has a slightly different focus in observing photosynthetic properties that contribute to primary production. The benchtop unit is better suited for very sensitive measurements in low chlorophyll areas, whereas the submersible unit, designed for profiling, gives better *in situ* estimates of steady state photosynthetic rates in the water column.

Due to the timing of the experiment and because of prior commitments, the submersible FRRF unit was unavailable for use during AMT-1; consequently, the benchtop unit's role was expanded to include not only the transect work in low chlorophyll regions, where its sensitivity is

of particular benefit, but also to include measuring photosynthetic properties in parallel with the discrete incubation samples described above. Used together, incubation studies and FRRF data can provide a more complete picture of photosynthetic activity than either can alone. The facilities and equipment on board the JCR were especially well suited for doing tandem studies of photosynthesis and production.

In order to best assess the trends in FRRF data with regards to productivity, FRRF measurements were conducted on the same samples used for the incubation studies. In addition to the fluorescence properties measured by the FRRF, the natural variability of maximum quantum yield of photosynthesis ($\Delta\Phi_{\max}$) was of special interest in comparing the FRRF data to productivity estimates. Laboratory and certain field measurements using the FRRF, support the theory that maximum quantum yields for a population vary in the ocean by as much as a factor of five, and thus would be a significant physiological factor controlling primary production. One of the most important field study areas used to obtain these data was the upwelling region off Mauritania, West Africa, which the JCR passed through during AMT-1, and would again traverse during future AMT cruises. Such transects through the upwelling area are critical in assessing the parameters, photochemical and otherwise, controlling primary production in ocean water masses.

2.5 Pigment Extractions

The objective of the pigment extraction effort was to characterize the water column to enable detailed comparison with the profiled light data. Consequently, the sampling strategy concentrated on determining the optical significance of the biophysics simultaneously with the optical and CTD casts. The phytoplankton samples were preserved in liquid nitrogen and transported for postcruise processing of pigment concentrations by HPLC at two sites: PML and the Center for Hydro-Optics and Remote Sensing (CHORS). This was done to quicken the processing, as well as to provide an intercalibration of the results from the two systems. A summary of the parameters measured by the pigment extraction program, along with the sampling frequency, is given in Table 5. The filtering effort was split into two parts: the daily station and the underway sampling from the uncontaminated seawater supply.

In Case-1 water masses it is valid to say that the only constituents present above the dissolved fraction will be planktonic (including waste and breakdown products), of which the most optically significant are the autotrophs. By collecting representative samples (2 l from the mixed layer with profiles to resolve the lower reaches of the water column) and concentrating them on filters (Whatman GF/F 0.7 μm nominal pore size) it is possible to determine (by reference to standards) both the distribution and concentration of the range of pigments present in the sample by HPLC. When viewed in conjunction with the coincident light meter data (Section 2.2) it is possible to apply and calibrate CZCS-type band ratio algorithms to assess the blue-green component of the measured color, which correlates with chlorophyll *a*.

Table 5. Measured parameters for the filtration program. The numeric entries refer to the number of samples taken per session. Postcruise processing is indicated by the P symbol.

Measured	*Underway*		*Daily*	*Type of*
Parameter	*2 Hr*	*4 Hr*	*Profile*	*Processing*
Pigments		2	1	HPLC P
Chl. *a*	2			Fluorometer
Absorption (Filters)		1		HPLC P
SFP		1	2	HPLC P
DOC		1	2	Spectrophotometer
POC		2	5	CHN P

SFP is size-fractionated pigments.

CHN is carbon, hydrogen, and nitrogen analysis.

The high spatial, temporal, and spectral resolution of the SeaWiFS sensor, emulated by the profiling radiometers, should allow the determination of other pigments in addition to chlorophyll *a*. Of specific interest are phaeopigment concentrations (chlorophyll breakdown products) which should lead to an improved interpretation of satellite imagery. The improved sensor characteristics and range of wavelength sensitivities come at a time when the scientific community is moving from empirical models to the implementation of a more analytical approach. The goal of this effort is to increase the ability of investigators to gain more information from areas where traditional ground-truth methods only provide sparse coincident in-water data sets.

It is for these reasons that the coincident light and pigment information collected during AMT-1 is of such importance. The basin-scale coverage and diversity of biophysical regimes that have been (and in the future will be) encountered will provide a unique data set with which to build upon the extensive theoretical work already in progress. The launch of SeaWiFS and then the OCTS will give an added dimension to this work with calibrated satellite imagery available whilst the cruise is in progress. This type of study will allow the application of ground-truth technology that was not available during the operational lifetime of the CZCS, which ended in 1987.

2.5.1 Underway Pigment Sampling

The objective of the underway sampling was to characterize the principal part of the water column responsible for ocean color when viewed from space (down to about one optical depth or K_d^{-1}). In Case-1 waters, this was

split into total pigments (greater than 0.7 μm) and size-fractionated pigments (covering the fraction 0.7 > phytoplankton > 0.2 μm) to determine the optical significance of the smaller than 0.7 μm plant life. Two types of samples were collected: duplicate pigments, for subsequent HPLC analysis, and 2-hourly chlorophyll *a* samples to calibrate the underway loggers and the UOR. The 2-hourly chlorophyll fluorescence samples were processed approximately 2 days in arrears to allow a minimum of 15 hours for extraction. At each sampling, 500 ml of water was filtered through Whatman GF/F filters prior to extraction in 10 ml of 90% acetone. The samples were analyzed using a recently calibrated fluorometer built by PML.

Additional information was gained by observing the absorption spectrum of water samples taken from the uncontaminated supply collected on filter papers (again Whatman GF/F) to identify the spectral absorption characteristics of the filtered particulates. By bathing the sample in hot methanol (and removing the biological components) the sample can be rescanned to enable the determination of the absorption of the inorganic fraction. Spectrum reconstruction, from information gained by the HPLC, or by identifying absorption peaks directly from the trace, can identify the pigments present and the part they play in light attenuation at the identified concentrations. Spectrophotometric (350–480 nm) measurements were also made of samples of the uncontaminated supply that had been filtered through a Whatman 0.2 μm polyester membrane filter to analyze the optical effect of any DOC that may be present. This is a very important measurement as DOC absorption potentially competes with chlorophyll *a* at 443 nm, with the potential of significantly inhibiting primary productivity.

2.5.2 Daily Station Sampling

The samples collected during the daily stations will give valuable information about the water column that cannot be derived from surface measurements. One particular area of interest is the effect of high subsurface phytoplankton concentrations which may be shallow enough to effect the remotely sensed ocean color measurements. The range of regimes covered by the AMT-1 cruise will aid in further understanding the subsurface chlorophyll maxima which can degrade primary production estimates from satellite imagery. This can potentially distort the conclusions that may be made with regard to the carbon budget in the viewing area. A second particle absorption and DOC sample were analyzed within the lower mixed layer: first, to test the assumption that the mixed layer is just that; and, second, to go some way towards resolving the variation in absorption with depth of DOC and particulates. At the surface, a complete set of samples were collected so samples from the uncontaminated seawater supply and the CTD *surface* (7 m) bottle could be intercompared. This had the effect of examining the station 6–7 m pigment levels in triplicate. Particulate carbon samples were also taken: one for organic and one for inorganic analysis. Replication was not possible due to water budget constraints.

The methodology employed for the analysis of particle absorption and DOC was being used on a trial basis. The absence of a suitable dual path spectrophotometer meant a special system was developed using modern fiber-optic technology incorporated into a spectrophotometer designed and built by PML. The sampling and analysis of these parameters concentrated mostly in the area of the Mauritanian upwelling. The spectrophotometer used was an LKB Biochrome (now Pharmacia Biotech) single path unit that proved to be slow in operation. A significant batch of samples, again mostly from the area of the Mauritanian upwelling, were processed and the results will be analyzed in the near future. These measurements require special consideration due to the possibility of contamination by sample processing. Plans exist to develop a flow-through device that would be entirely sealed; it is intended that such a system be available for AMT-2.

2.6 Size-Fractionated Carbon

In order to fully characterize latitudinal changes in the community structure of plankton, a suite of sampling techniques were carried out on AMT-1. The primary aim was to characterize the plankton communities in terms of carbon, based on size fractions, and to supplement these data with traditional taxonomy and new automated technology for sizing zooplankton (OPC) in real time. The sampling strategy was, therefore, geared to define the various components of the planktonic carbon in a predetermined set of size classes between less than 1 μm to greater than 2 mm; this was done in accordance with JGOFS protocols (JGOFS 1991).

2.6.1 Particulates

Water from two of the five main depths at each station, 7 m and the chlorophyll maximum (Appendix C), was filtered in four batches through one of the following: membrane filters of 2, 5, 10, and 200 μm gauze. The filtrate from each prescreened batch was then filtered onto Whatman GF/F filters to produce a series of replicate samples for the following size fractions: less than 2, 2–5, 5–10, 10–200 μm, plus the total. Aliquots of 100 ml of water from these two depths were also taken for phytoplankton characterization and were preserved using lugol iodine and formaldehyde, both in 1% solutions. Samples were also taken at each of these depths (500 ml) for microzooplankton analysis by microscopy and image analysis.

2.6.2 Zooplankton Characterization

At each station, a WP2 plankton net (200 μm) was deployed and used to take a vertical, depth integrated haul from 200 m to the surface. The net was fitted with a

depth and temperature probe with self logging capability to record the actual depth reached by the net. The sample from this net haul was split into two halves: one half was analyzed for particle numbers using the OPC system, while the other half was used to subsample zooplankton biomass. The latter sample was size fractionated through 2,000, 1,000, and 500 μm sieves to produce sample fractions of the following sizes: 200–500, 500–1,000, 1,000–2,000, and greater than 2,000 μm. The remainder of the sample was preserved in borax buffered formaldehyde, with a final concentration of 4%, for taxonomic identification of community structure by microscopy.

2.6.3 Zooplankton Sizing

Zooplankton community size structure was investigated using an OPC (Focal Technologies, Inc., Dartmouth, Nova Scotia). This system sizes zooplankton (in the range approximately 250–11,000 μm) by light interference and expresses counts in terms of equivalent spherical diameters. OPC data is, therefore, capable of showing changes in community structure (size) and abundance (numbers) through contrasting biogeochemical provinces and over broad latitudinal scales.

The OPC instrument was used in two different ways during the cruise transect:

1. At each station, half the WP2 (200 μm mesh) net sample was circulated through the OPC using a small pump. Once a sample was analyzed by the OPC it was collected in a unit designed to recover the sample and ensure it only circulated through the OPC once. When all of the zooplankton samples were recovered, they were preserved for analysis in order to validate the OPC data.
2. The OPC was also operated in a *flow-through* mode in order to continuously sample along the cruise track during the underway sampling. This sampling strategy was only interrupted for the station work and regular (once a day) checking for background signals and computing housekeeping, i.e., file closure and backup.

While logging in the flow-through mode, the volume of seawater flowing through the sytem was recorded (typical flow rates were approximately 30 l/min and remained constant throughout the cruise). This ensured that all data was quantitative and also met the flow rate requirements specified by the manufacturer.

At regular intervals, the outlet from the OPC was connected to a custom-designed flow chamber with 200 μm gauze to allow the collection and preservation of material larger than 200 μm flowing through the OPC. By recording the time this took place, direct comparison between OPC counts and plankton retained at the outlet can be made back in the laboratory.

2.7 Circulation and Backscatter

The ADCP is an instrument primarily designed to measure the direction and speed of ocean currents. If a fixed frequency acoustic pulse is emitted at the surface, a component of the energy will be backscattered (reflected) off particles in the water column. The reflected pulse will have a different frequency due to the Doppler shift effect, with the change in frequency directly related to the particles' velocity component parallel to the direction of propogation of the pulse.

By emitting four acoustic pulses at 45° angles to one another, an ADCP can resolve the Doppler shifted reflected pulses into vector components, i.e., water velocity magnitude and direction (assuming the water is moving at the same velocity as the suspended particles). Depth resolution is achieved by measuring the time interval between emitting and receiving each pulse. The ADCP used during AMT-1, an RD Instruments (RDI) Type RD-VDM150, measures up to 128 depth locations, each 1–32 m in length. During the cruise, the number of depth bins was set to 128, each 2 m in length, giving a maximum depth range of 256 m.

The magnitude of the backscattered pulse from each depth location is also measured by the ADCP. This data provides information on the area of particulate scatterers, i.e., the greater the concentration of particulates, the greater the backscattered energy. At a specific frequency, there is a relationship between backscattered energy from a particle and the particle's size. The ADCP used during AMT-1 emits at 250 KHz, which is preferentially backscattered from particles of the approximate size of the zooplankton in the water column. The ADCP data can, therefore, be used to resolve a limited amount of qualitative biological information.

2.8 Inorganic Nutrients

The inorganic nutrients, nitrate, nitrite, phosphate, and silicate were determined in samples taken at approximately 4-hourly intervals from the ship's uncontaminated seawater supply whilst underway and in samples obtained during the daily CTD casts. The underway samples were taken coincident with samples for pigment and chlorophyll analysis. They were stored in the dark at less than 4°C in a laboratory refrigerator and were analyzed as a batch shortly after the CTD samples were obtained. Thus, the vertical profile samples were usually analyzed within one hour of collection and the underway samples were never more than 20 hours old at the time of analysis.

The determinations were made using a Technicon AAII Autoanalyser running conventional chemistries: phosphate and silicate as described by Kirkwood (1989), and nitrate and nitrite using a modified version of Grasshoff's method as described by Brewer and Riley (1965). The nitrate was determined as nitrite using a copper-cadmium reduction

column to reduce nitrate to nitrite and is, therefore, measured as nitrate plus nitrite. All results are presented as mmol m^{-3} (μmol l^{-1}) of the elements nitrogen, phosphorus, and silicon.

2.9 Dissolved Gases

The measurement of CO_2 partial pressure above and below the sea surface provides one major constraint on the instantaneous air-sea carbon flux. Coupled with knowledge of wind speed and models of exchange coefficients, the net carbon flux can be determined.

On the AMT-1 cruise, PML pCO_2 instruments measured the atmospheric partial pressure from air taken at bridge level through an 80 m, 0.25 inch (outer diameter) stainless steel tube and from an equilibrator system coupled to the uncontaminated seawater supply. The equilibrator consisted of a glass cylinder (6 mm in length and diameter) percolator bed packed into an acrylic tube. The equilibrator was supplied with air by short stainless steel tubes (5 m in length), and the temperature of water in the bed was monitored by a platinum resistance thermometer (PRT) coupled to high resolution measurement circuitry. The PRT temperature was calibrated by reference to a recently calibrated (June 1995) RTM (SIS).

The system detector was a Li-Cor model 6262 infrared CO_2/H_2O detector. The gas was passed through the detector via a series of miniature solenoid valves, which were use to select the marine air, air from the equilibrator headspace, and two tanks of standard gas. The standards bracketed the range of possible oceanic and atmospheric CO_2 concentration. Standards were blended at PML from commercial sources, and before the cruise, the standards were verified against primary standards which had been certified by reference to World Meteorological Organization (WMO) traceable standard mixtures.

The system control and data logging was carried out by an industrial, card-mounted PC coupled to an RS-485 data acquisition network. In conjunction with the CO_2 analysis functions, the computer recorded barometric pressure and geolocation from an independent global positioning system (GPS) receiver. The computer produced detailed log and data files which were downloaded for subsequent processing. The system is normally used in autonomous mode, mounted in the engine room space of merchant vessels. In the research mode, use was made of the data logging system from the JCR. The Ocean Logger provided the sea surface temperature (SST) from the inlet PRT in the transducer space; this data was merged with the pCO_2 system files prior to analysis.

2.10 Bridge Logs

A number of logs containing scientifically useful information were recorded by the bridge:

1) *Ship's Log* with hourly position and summary of ship's activities;
2) *Scientific Log* which details all activities with times and positions while on station or deploying towed equipment; and
3) *Meteorological Log* (or Met Log) which was completed every six hours and includes SST, wind and swell wave heights, wet bulb temperature, and any noteworthy remarks.

A summary of the information derived from these logs appears in Appendices G and H.

3. CRUISE TRACK

The normal course the JCR makes when in passage between the UK and Falkland Islands is a direct one: after leaving the English Channel and crossing the Bay of Biscay to Cape Finisterre, the ship sails close to Madeira and across the Atlantic outside the Cape Verde Islands. The course set for the AMT-1 cruise was altered to encompass more contrasting waters within the general direction of the normal passage. A summary of the major scheduling milestones is given in Table 6.

Table 6. Major scheduling milestones for AMT-1. Flights to the UK are operated by the Royal Air Force (RAF).

Date	*SDY*	*Activity*
18 September	261	Equipment to Grimsby.
19 September	262	Load ship and set up.
20 September	263	Complete loading.
21 September	264	Sail to Portsmouth and test instruments.
22 September	265	Load aviation fuel.
23 September	266	Sail for Montevideo.
19 October	292	Dock at Montevideo.
21 October	294	Sail for Stanley.
24 October	297	Dock at Stanley.
25 October	298	First flight to UK.
28 October	301	Last flight to UK.

On leaving the UK coastal shelf, the AMT-1 course headed more westerly than would normally be the case on passage, to carry out a station at 20°W,47°N; this is a well documented and repeatedly sampled area, forming part of a series of international JGOFS stations. The higher latitude stations are important for obtaining contrasting data with respect to the clearer, tropical waters.

From the 20°W,47°N station, the transect generally followed a southerly course down the 20°W meridian to 10°N (Fig. 4). Exceptions to this were relatively minor deviations to ensure sampling was carried out in international waters, and an unscheduled call into Madeira to allow one of the ship's crew to disembark for compassionate reasons. The part of the transect between about 10–20°N crossed the Mauritanian upwelling between the Cape Verde Islands

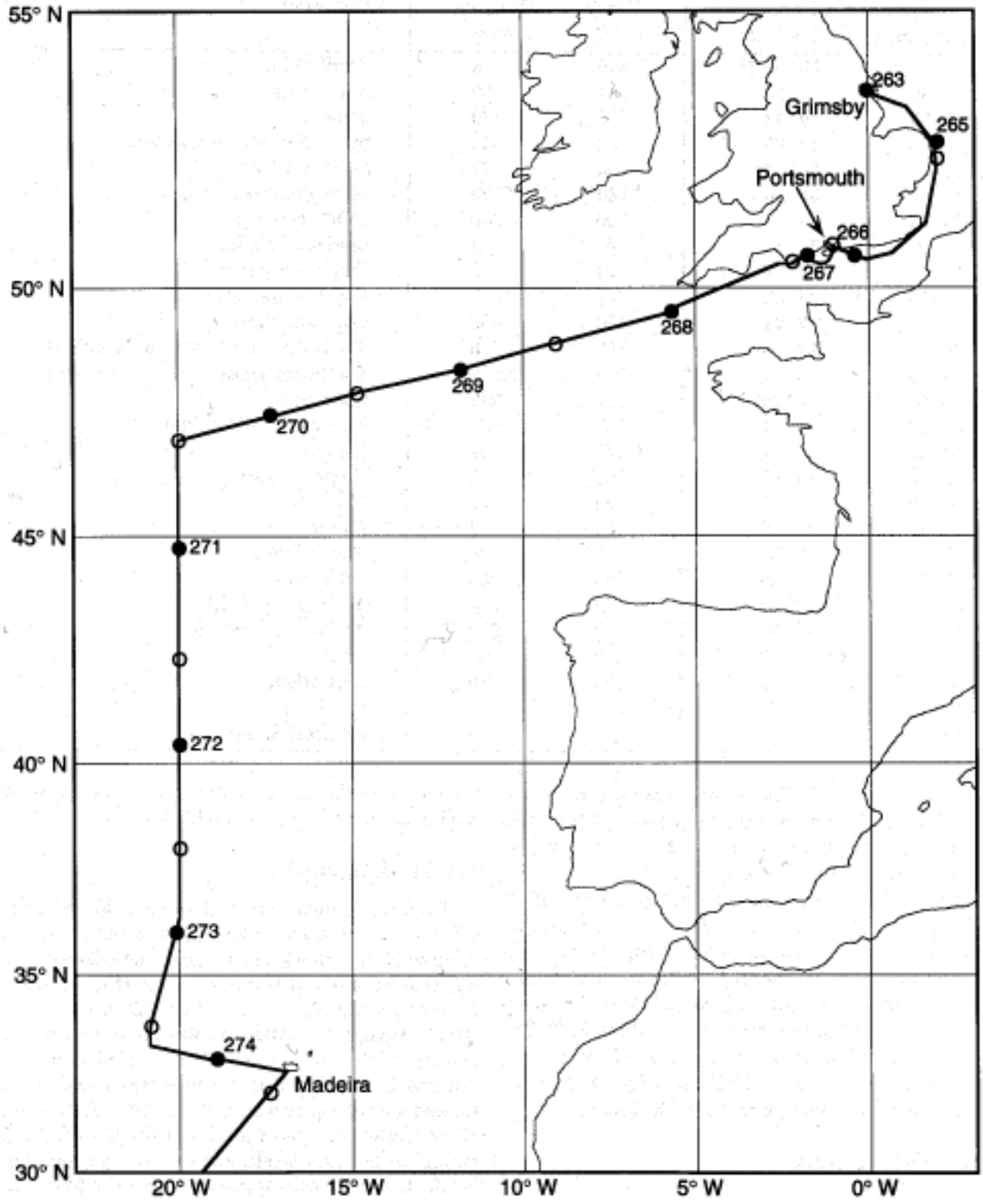

Fig. 4. AMT-1 cruise track for SDY 263–274. The solid and open circles denote the ship's position at 0000 and 1200 (GMT), respectively.

Table 7. The major navigational waypoints for AMT-1. The total distance traveled was approximately 8,708 nautical miles.

Waypoint Coordinate		*Course*	*Distance*	*Comment*
Longitude	*Latitude*	[°T]	[nmi]	
1° 57′ W	50° 40′ N	249	68	Anvil Point.
3 36	50 10	244	85	Start Point.
5 35	49 33	255	579	Scillies.
20 00	47 00	180	633	Start of southern transect.
20 00	36 27	194	177	Start of EEZ.
20 53	33 36	180	22	30 September station.
20 53	33 14	100	200	UOR recovery.
17 00	32 37	90	3	Madeira landfall.
16 56	32 37	73	2	Funchal approach.
16 53	32 38	219	416	Funchal pilot station.
21 51	27 23	170	490	Cape Bojador.
20 22	19 20	181	376	Territorial gap (start no sampling).
20 26	13 4	204	2,508	Southwest Dakar (end no sampling).
38° 00′ W	25° 00′ S	222	812	Cabo Frio.
46 38	33 21	255	424	East of the River Plate.
54 53	35 4	275	67	Lobos.
56 14	34 57	151	2	Calpean Star.
56 48	34 59	92	20	Channel.
55 12	35 0	135	42	Flores.
55 12	35 30	181	120	Banco Ingles.
55 16	37 30	186	858	Off Querandi.
55 38	40 10	159	50	To clear the EEZ.
55 15	40 57	188	653	22 October station.
57 38	51 42	235	21	Wolf Rock.
58 5	51 54	254	10	East Island.
58 20	51 57	270	5	Fox Point.
58 28	51 57		3	Choiseal Sound.

and West Africa (Fig. 5). The series of transect profiles illustrated within this report have been selected from this part of the cruise track, focusing on a 24 hour transect as the ship crossed into the upwelling.

From West Africa, the ship returned to a more direct course for Montevideo (Uruguay); the only course requirement was to stay in international waters (Fig. 6). On leaving Montevideo (Fig. 7), the JCR sailed a direct course for Stanley (Falkland Islands) which extended the latitudinal study an additional 1,000 nmi due south to 50°S. The AMT-1 cruise terminated in Stanley on 24 October 1995, having covered approximately 7,800 nmi (Fig. 8). The major navigational waypoints for are listed in Table 7.

4. STATION 273

Bottle samples were taken at seven discrete depths during the station 273 CTD cast. Depths were selected to better define the preliminary chlorophyll (fluorescence) profile obtained from the UOR (Fig. 9c) immediately before the CTD profile commenced. The water samples were placed into lightproof bottles and processed immediately to reduce thermal effects. After the CTD and UOR profiles, an XBT was taken (Figs. 10a and 10b).

4.1 Hydrography

Data for temperature and salinity, logged during the CTD profile at station 273, shows a surface mixed layer down to 50 m with a sharp thermocline followed by a gradual decrease in temperature to 200 m (Figs. 10c and 10d). The temperature recorded by the CTD was checked at each station against two high specifications (to three decimal places) RTMs. At station 273 the RTM temperature at 7 m was 23.360°C and at 150 m it was 15.357°C. Salinity showed a similar profile to temperature. The hydrography of the station, coupled with data from the UOR fluorometer and *in situ* light levels, was used to determine the water bottle depths for each station (two bottles were tripped at each depth). At station 273, the chlorophyll maximum was seen to be associated with the base of the thermocline and the change from warm surface water to cooler deep water. The main depths selected for station 273 were 7, 50, 70, 90, and 110 m; two additional bottles were used to sample water at 130 and 150 m.

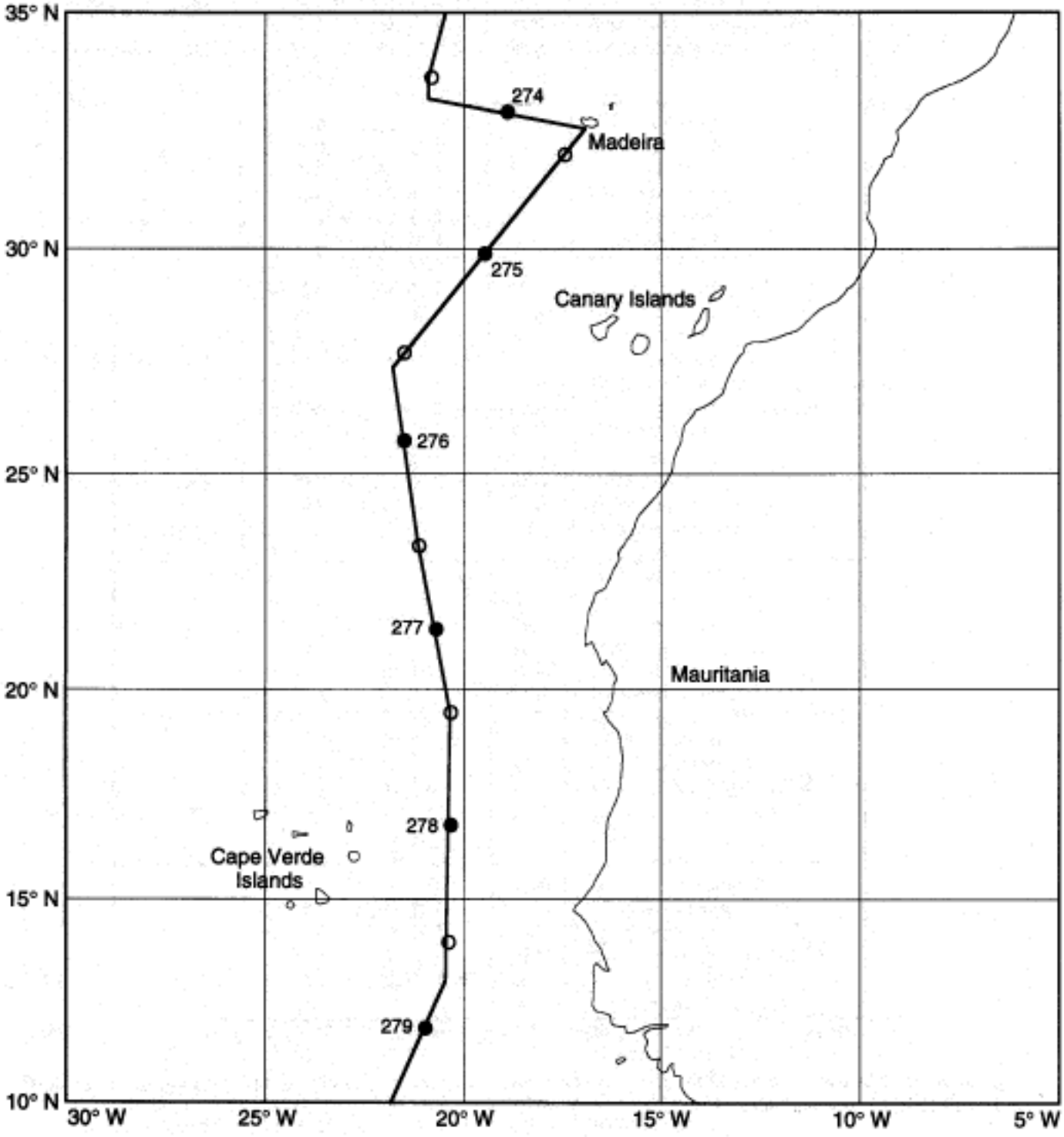

Fig. 5. AMT-1 cruise track for SDY 274–279. The solid and open circles denote the ship's position at 0000 and 1200 (GMT), respectively.

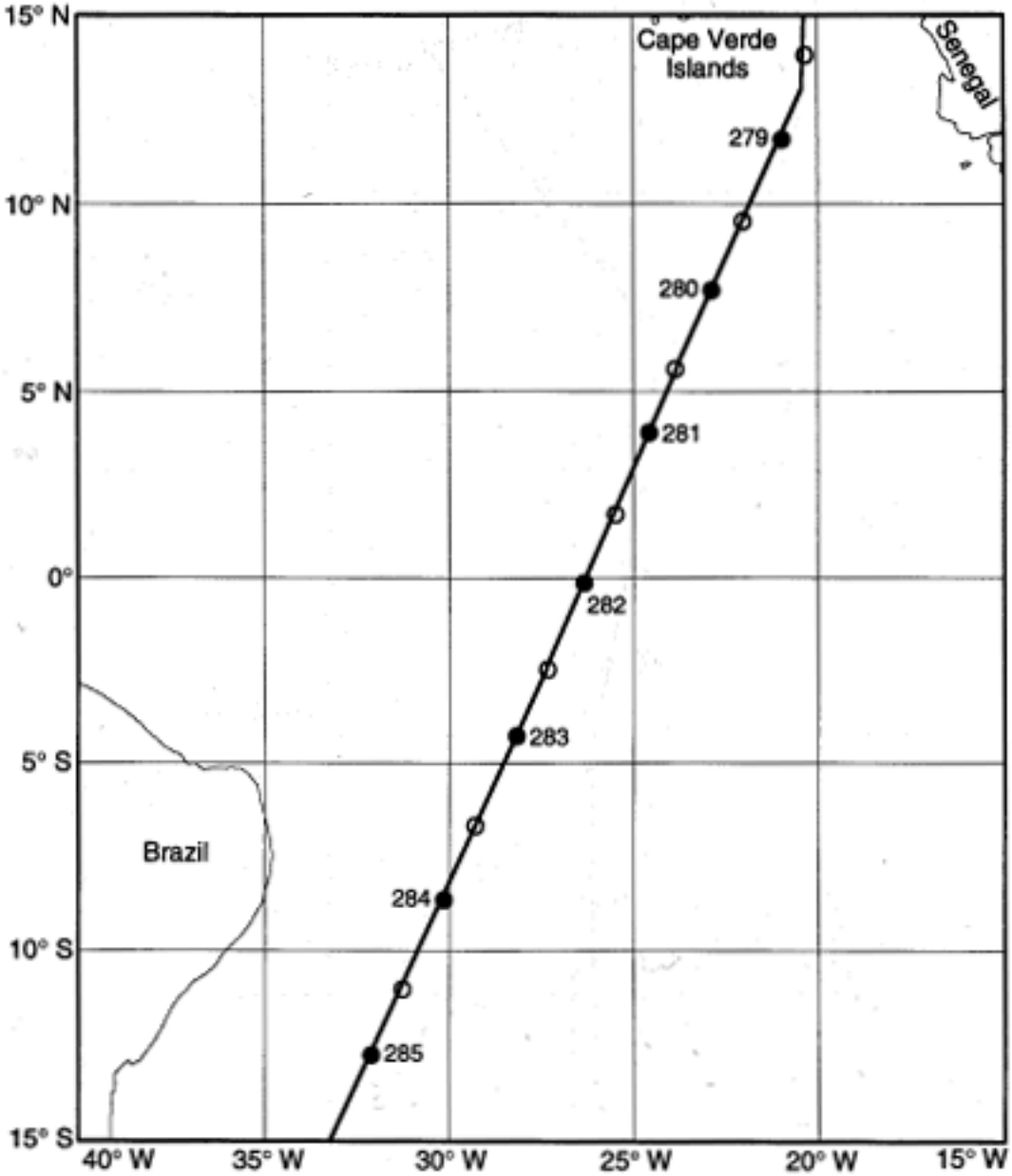

Fig. 6. AMT-1 cruise track for SDY 279–285. The solid and open circles denote the ship's position at 0000 and 1200 (GMT), respectively.

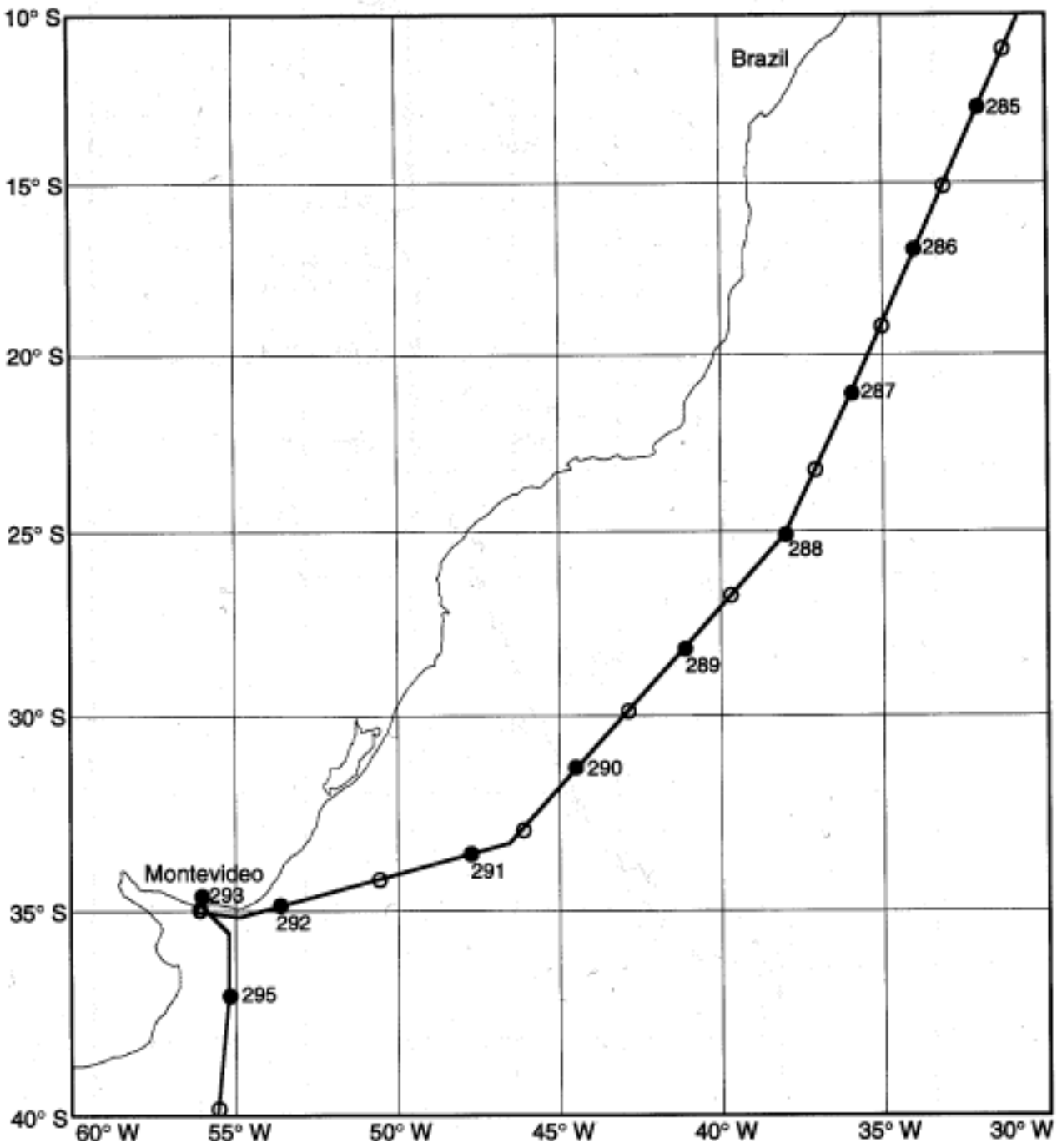

Fig. 7. AMT-1 cruise track for SDY 285–295. The solid and open circles denote the ship's position at 0000 and 1200 (GMT), respectively.

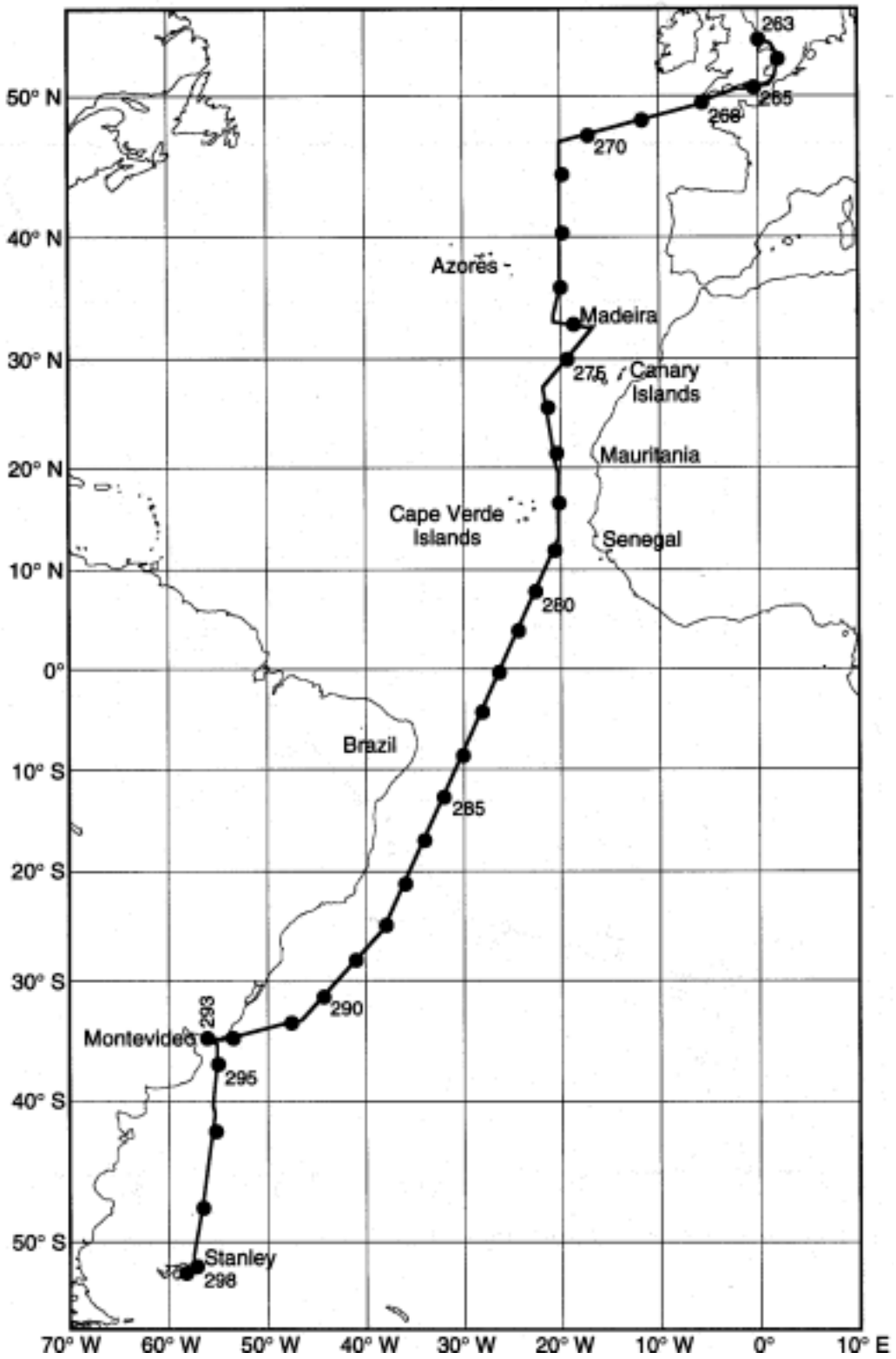

Fig. 8. AMT-1 cruise track for SDY 263–298. The solid circles denote the ship's position at 0000 (GMT).

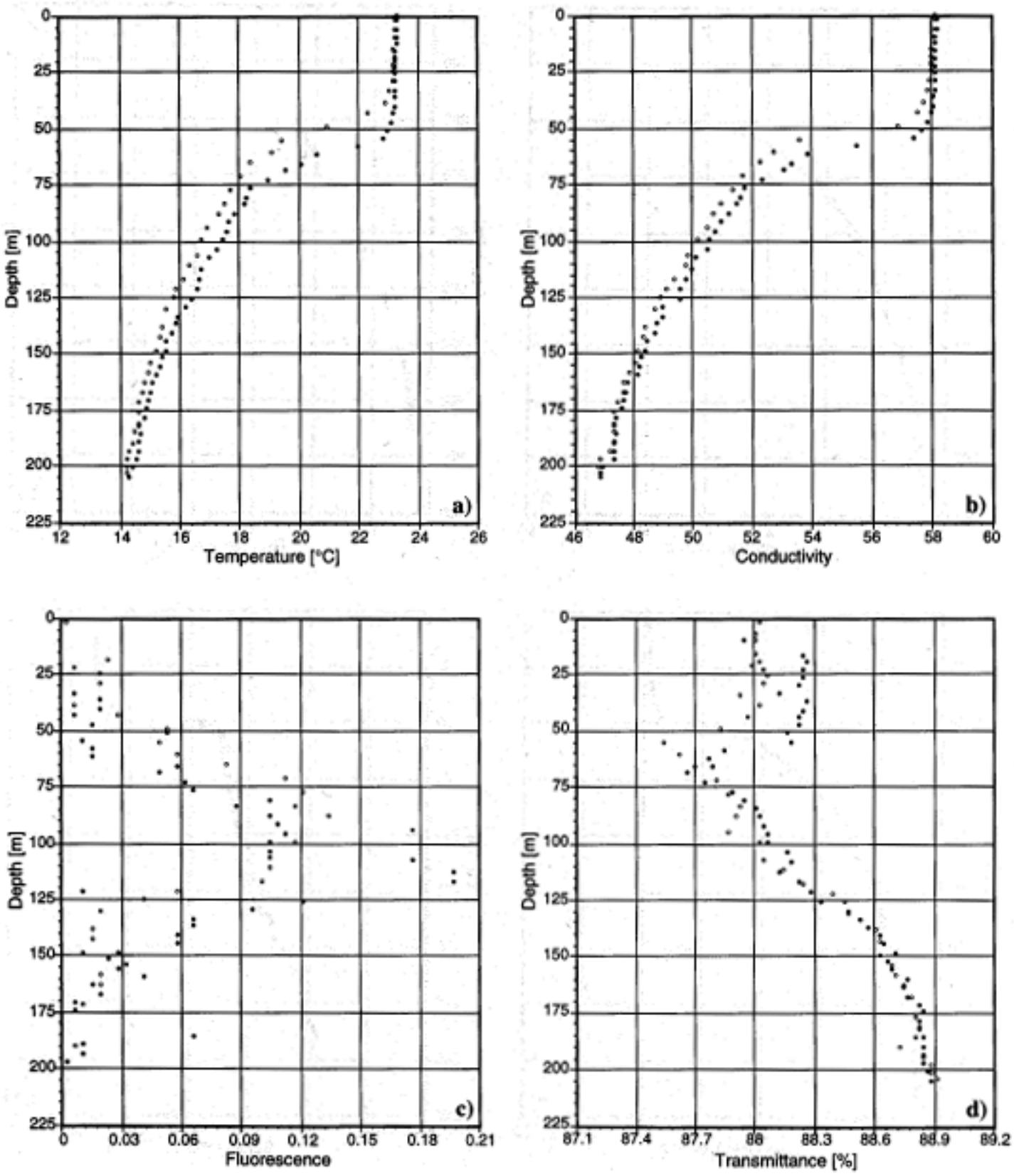

Fig. 9. UOR down (solid symbols) and up (open symbols) casts for station 273 (30 September): **a)** temperature, **b)** conductivity, **c)** fluorescence, and **d)** transmittance.

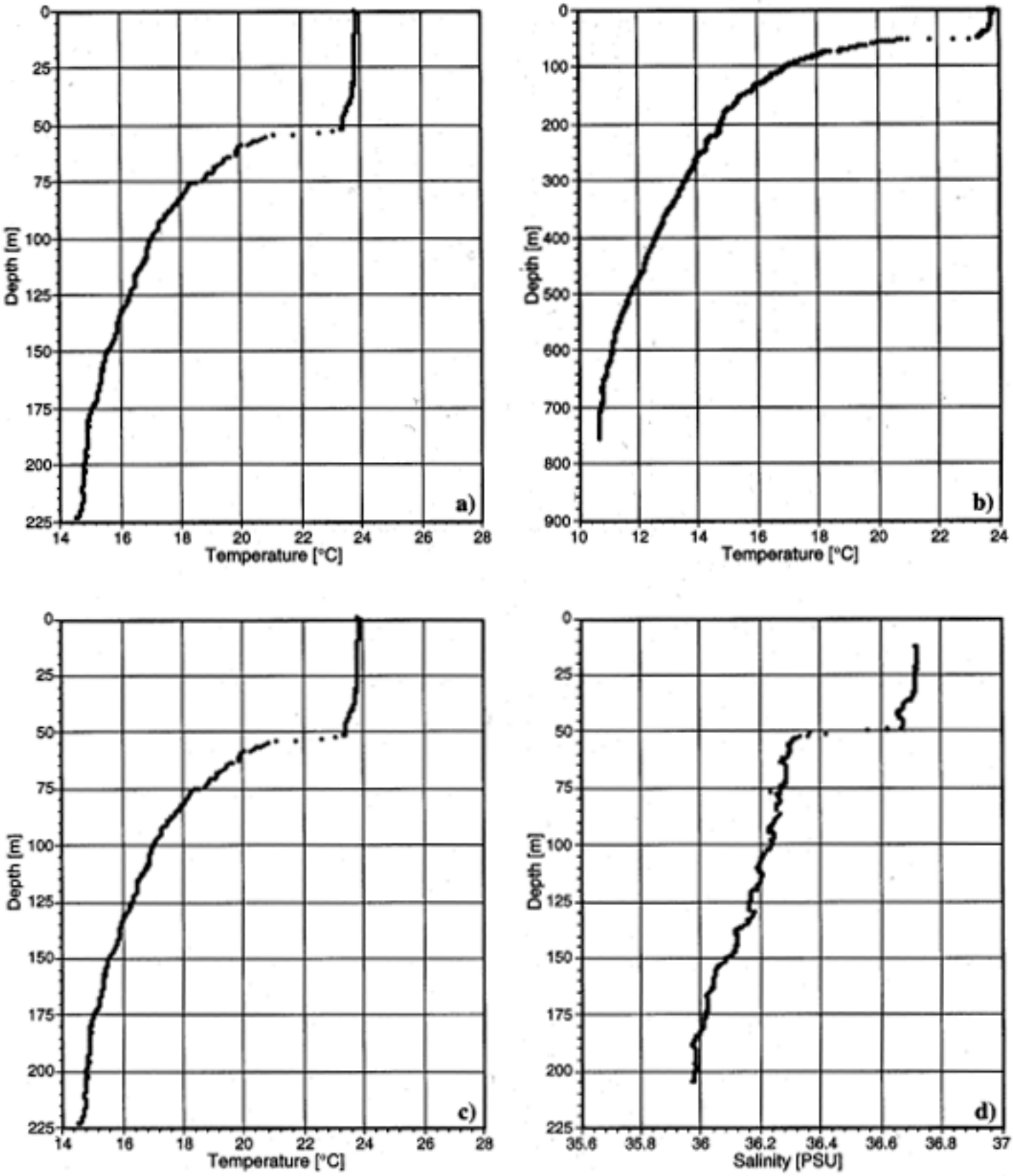

Fig. 10. Hydrographic profiles for station 273 (30 September): **a)** the upper 225 m of XBT 12, and **b)** the entire XBT 12 profile; **c)** temperature as a function of depth from CTD 273, and **d)** salinity as a function of depth from CTD 273.

Table 8. K_d determined by non-linear curve fitting for the upper part of the optics cast (1–50 m) in station 273.

Band No.	PRR-600 CWL	PRR-600 K_d	PRR-600 R^2	Satlantic CWL	Satlantic K_d	Satlantic R^2	Percent Difference
1	412	0.0292 ± 0.0008	87.8	413	0.0275 ± 0.0006	91.0	−6.2
2	443	0.0265 ± 0.0008	85.5	444	0.0257 ± 0.0006	87.6	−3.1
3	488	0.0276 ± 0.0008	85.1	489	0.0276 ± 0.0007	87.5	0.0
4	510	0.0427 ± 0.0010	91.7	509	0.0431 ± 0.0009	92.7	0.9
5	560	0.0743 ± 0.0060	98.6	555	0.0729 ± 0.0014	95.3	1.9
6	665	0.4469 ± 0.0097	98.6	664	0.4638 ± 0.0075	99.2	1.6

Table 9. K_d determined by non-linear curve fitting for the lower part of the optics cast (60–110 m) at station 273.

Band No.	PRR-600 CWL	PRR-600 K_d	PRR-600 R^2	Satlantic CWL	Satlantic K_d	Satlantic R^2	Percent Difference
1	412	0.0703 ± 0.0003	99.8	413	0.0723 ± 0.0002	99.8	2.7
2	443	0.0587 ± 0.0003	99.7	444	0.0582 ± 0.0002	99.7	0.9
3	488	0.0466 ± 0.0002	99.6	489	0.0469 ± 0.0002	99.7	0.6
4	510	0.0546 ± 0.0003	99.6	509	0.0556 ± 0.0002	99.7	1.8
5	560	0.0787 ± 0.0004	99.6	555	0.0794 ± 0.0004	99.7	0.9
6	665	0.0423 ± 0.0006	77.4	664			

Table 10. Satlantic K'_d ($K_d - K_w$), compared with K_{chl}.

CWL [nm]	K_w	K'_d (1–50 m)	K'_d/K_{chl}	K'_d (60–110 m)	K'_d/K_{chl}
413	0.021	0.007	0.03	0.051	0.24
443	0.017	0.009	0.04	0.041	0.23
489	0.026	0.002	0.02	0.021	0.17
509	0.035	0.008	0.07	0.021	0.20
555	0.064	0.008	0.09	0.014	0.20

4.2 Optics

Figure 11 shows the $L_u(443)$ and $L_u(555)$ data from both the PRR-600 and SeaOPS instruments. The profiles from the two are qualitatively similar, but the SeaOPS shows more noise in both channels below 120 m. Linear regression between the two sensors gave high R^2 values (99.5 and 99.1 for 443/444 nm and 555/560 nm, respectively), with no significant intercept and slopes of 1.06 (443/444nm) and 0.94 (555/560nm), for the PRR-600 and SeaOPS, respectively. The results for other bands are similar, and a full analysis will be prepared when a cross calibration of the pressure sensors is possible.

K_d is a quasi-inherent optical property, and was chosen as a test parameter because it is robust and well understood. The profiles (Fig. 11) show a light field typical of a DCM (Fig. 9c). The data was divided above and below the thermocline, 1–50 m and 60–110 m. The K_d values were calculated using a nonlinear curve fit of the form $E_d(z,\lambda) = E_d(0^-,\lambda)e^{(-zK_d)}$. The results of the comparison are shown in Tables 8 and 9. With the exception of the 412 nm band where calibration can be difficult (especially at high light levels), all the results agree to within better than 5%. One notable problem is the 665 nm band on the PRR-600, which continues to decrease below 60 m where there is no detectable light at this wavelength; this probably indicates some out-of-band response in this sensor.

The K_d values in the surface water are low, and an approximate value of chlorophyll may be derived by comparing K_d with K_{chl}. Table 10 shows that the value of chlorophyll in the surface water is in the region of $0.03\,\mathrm{mg\,m^{-3}}$. The apparently higher values for the 509 and 555 nm bands are probably due to Raman Scattering. The concentration values for the chlorophyll maximum are in the region of $0.20\,\mathrm{mg\,m^{-3}}$. These values are typical of this region and give some confidence in the optics results to date.

4.3 Fluorometry and Photochemistry

FRRF studies during AMT-1 were focused on obtaining information not only on fluorescence properties of phytoplankton, but also on monitoring the physiology of pho-

tosynthetic structures, and determining (if possible) how environmental factors such as irradiance, nutrients, and temperature affect photosynthesis. In general, most of the important changes in phytoplankton photosynthetic properties occur in the light-harvesting complexes of photosystem II (LHCII), where photons are individually trapped and their energy transferred to the photosynthetic electron transport chain. By examining the fluorescence characteristics of a phytoplankton population, it is possible to determine some of the environmental effects on LHCIIs, thereby establishing an index of environmental effects on photosynthetic rate processes.

Figure 12a compares maximal fluorescence, F_m, initial fluorescence, F_0, and their difference, F_v (variable fluorescence), versus depth to illustrate changes in population fluorescence characteristics throughout the water column. Fluorescence values are given in instrument units and are proportional to the fluorescence signal (λ=685 nm) observed at the detector.

F_m is a measure of total sample maximal fluorescence; it is directly comparable to values measured by standard active fluorometers, but with greater sensitivity. The F_m curve shows a fluorescence maximum around 110 m, generally symmetrical in shape with a six-fold increase from *surface* (7 m) readings. F_m is a sum of fluorescence photons emitted from active LHCIIs, damaged LHCIIs, and fluorescent detritus. Without other information about chlorophyll concentration (both photochemically competent and incompetent), it is difficult to assess the phytoplanktonic component of the total signal in F_m and F_0. However, by definition, fluorescence contributions to F_v are due solely to photochemically active LHCIIs. The F_v curve indicates bulk photochemistry follows the general trend of bulk fluorescence except at the fluorescence maximum. This may be due to variability in nonphotochemical sources of fluorescence over depth, or to variability in the proportion of active LHCIIs to inactive complexes. These variances are more readily illustrated in the second plot.

Figure 12b shows the trends in $\Delta\Phi_{\max}$ over depth for the same water samples shown in Fig. 12a. The parameter $\Delta\Phi_{\max}$ is defined to be the ratio of F_v to F_m, and corresponds to the (normalized) maximum number of reaction centers in the chlorophyll population which are capable of photosynthesis. The factors affecting $\Delta\Phi_{\max}$ include nutrient availability, toxic substances in the environment, photodestructive effect (primarily photo-oxidation), and other nonphotochemical quenching processes.

Analysis of $\Delta\Phi_{\max}$ trends can be difficult without corresponding data sets of environmental factors (e.g., nutrients, irradiance, mixing processes, etc.). One general trend which is often observed, however, is apparent in the 273 profile: photodestructive effects of supraoptimal irradiance at the surface. Phytoplankton living near the surface are more likely to be exposed to damaging levels of sunlight; such levels cause damage to reaction centers and require many hours (approximately 2–4) to repair. The low level of $\Delta\Phi_{\max}$ near the surface, with values increasing with depth, are likely due to light damage. An analysis of this data versus the *in situ* light field might better illustrate this effect; however, most noon stations on bright days showed this trend.

4.4 Photosynthesis and Calcification

Carbon fixation by phytoplankton was very low at station 273, taking values in the range 0.02–0.05 $\mathrm{mgC\,m^{-3}\,h^{-1}}$ throughout the upper 130 m (Fig. 13). It is likely that these low productivity values were due to nutrient limitation, as both nitrate and phosphate were depleted in the upper mixed layer (Section 4.9). A photosynthesis irradiance experiment was carried out with seawater from 110 m in order to determine the photosynthetic parameters of the phytoplankton assemblages inhabiting the DCM. Microalgae in the DCM were adapted to low irradiance levels, as shown by the fact that the maximum photosynthetic rate per unit biomass ($PB_{\max}$) was attained at only 75 $\mu\mathrm{E\,m^{-2}\,s^{-1}}$ (Fig. 13b). Photoinhibition of photosynthesis occurred at irradiances above approximately 100 $\mu\mathrm{E\,m^{-2}\,s^{-1}}$, probably as a result of light-induced damages to the reaction centers (see Section 4.1.3). The low $PB_{\max}$ (approximately 0.45 $\mathrm{mgC\,mgChl^{-1}\,h^{-1}}$) suggests phytoplankton cells in the DCM had a reduced potential for growth in response to increased light conditions.

4.5 Pigment Extractions

No preliminary results for pigment extractions are presented, since all of the samples will be analyzed after the cruise in the laboratory. A summary of the samples taken, however, is presented in Appendix J.

4.6 Zooplankton Characterization

In order for biological oceanographers to fully characterize ocean provinces and the biogeochemical processes that prevail within them, they must first characterize the planktonic assemblages they contain. Work on AMT-1 focused on some of the key issues in characterizing biological parameters in a way that reflects the current resolution of physical and chemical processes and enables the data to be compatible with these in terms of future modeling. Zooplankton, often key components in terms of biological processes and carbon flux, are usually poorly defined for large-scale processes. The data obtained from AMT-1 are aimed at bringing zooplankton characterization into line with other biological and physical parameters. The data presented in Fig. 14 show zooplankton characterized in terms of abundance and size distribution (based on size classes) obtained in real time and with similar resolution to other parameters useful in modeling processes in biological oceanography.

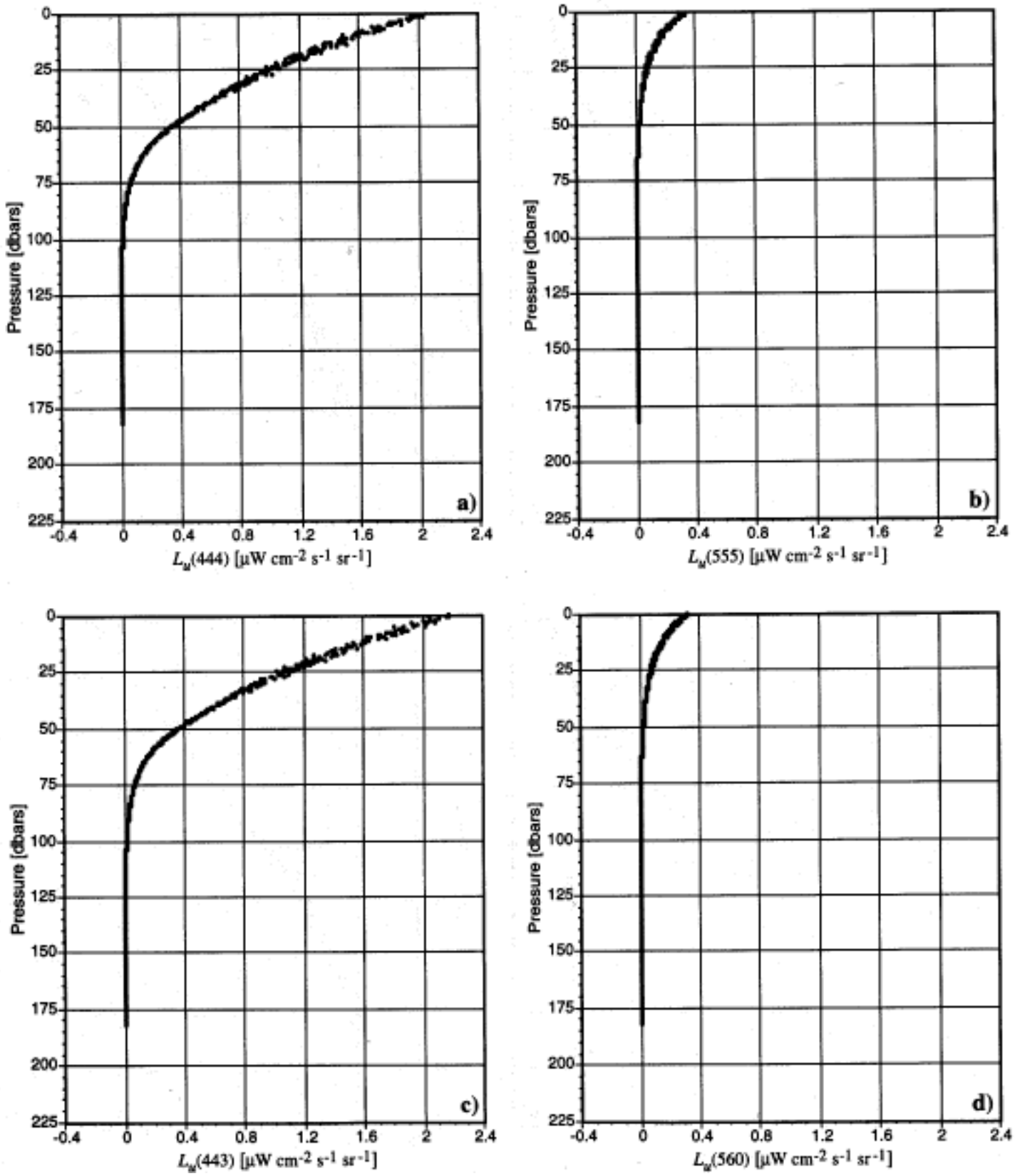

Fig. 11. In-water radiance profiles for station 273 (30 September): **a)** $L_u(444)$ from SeaOPS, **b)** $L_u(555)$ from SeaOPS, **c)** $L_u(443)$ from the PRR-600, and **d)** $L_u(560)$ from the PRR-600.

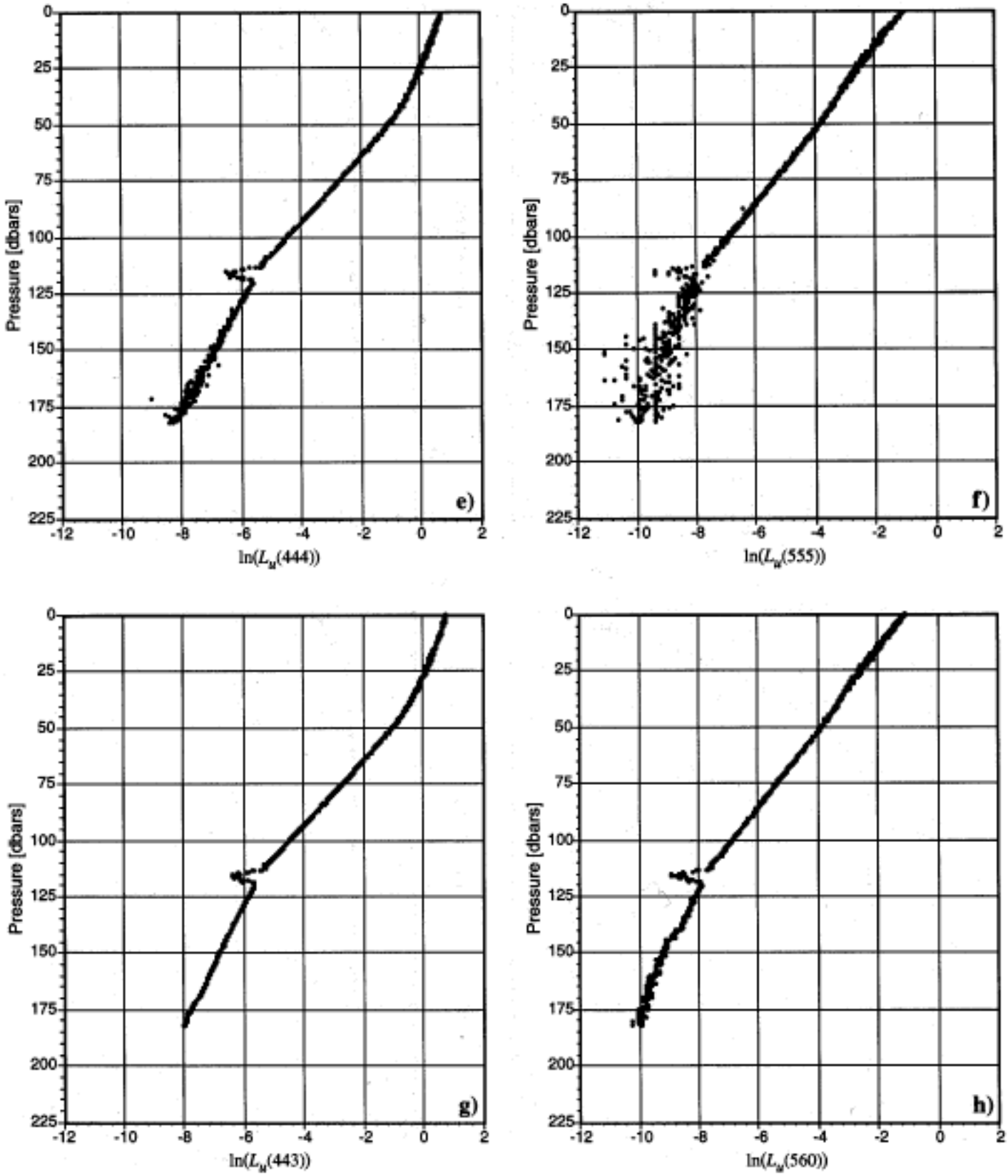

Fig. 11. (cont.) Log-transformed in-water radiance profiles for station 273 (30 September): **e)** $L_u(444)$ from SeaOPS, **f)** $L_u(555)$ from SeaOPS, **g)** $L_u(443)$ from the PRR-600, and **h)** $L_u(560)$ from the PRR-600.

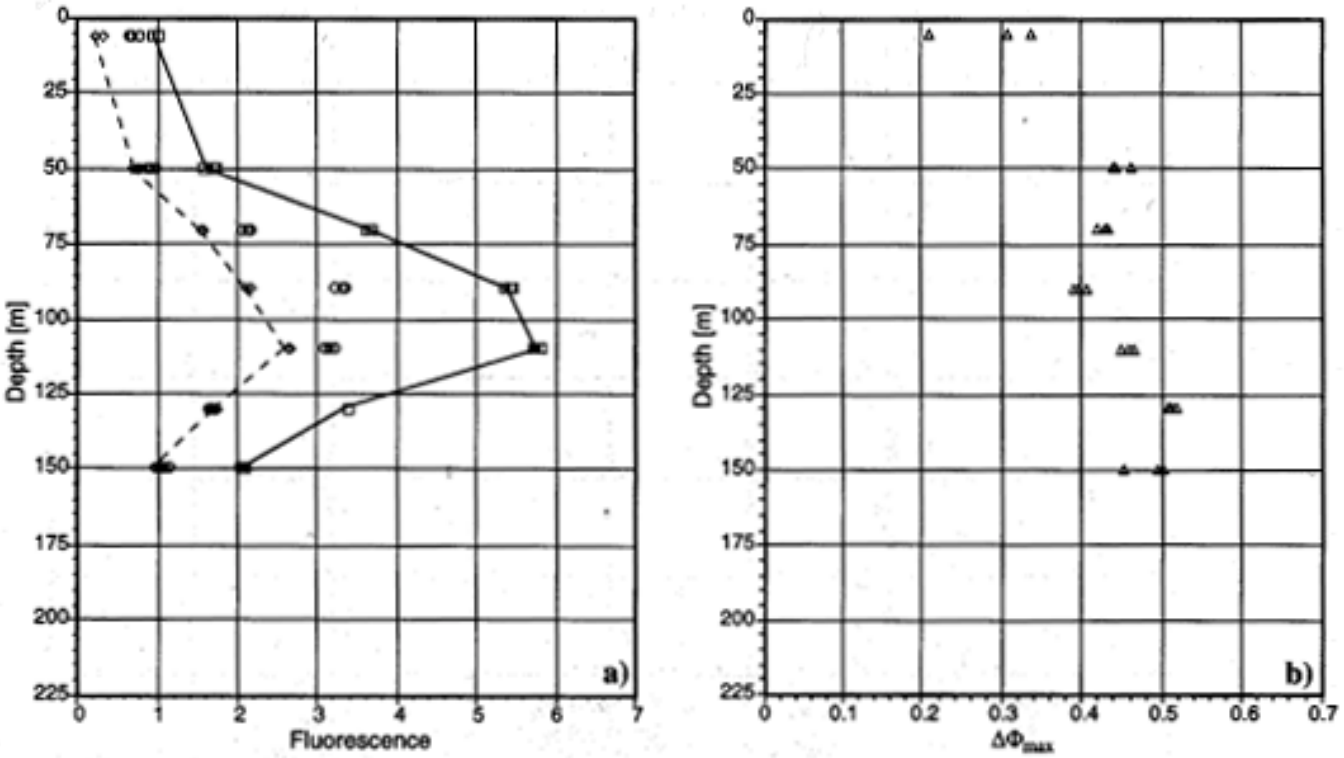

Fig. 12. Fluorescence and photochemistry derived from FRRF samples during CTD 273: **a)** F_0 (diamonds and dashed line), F_v (circles), and F_m (squares and solid line); and **b)** $\Delta\Phi_{\max}$.

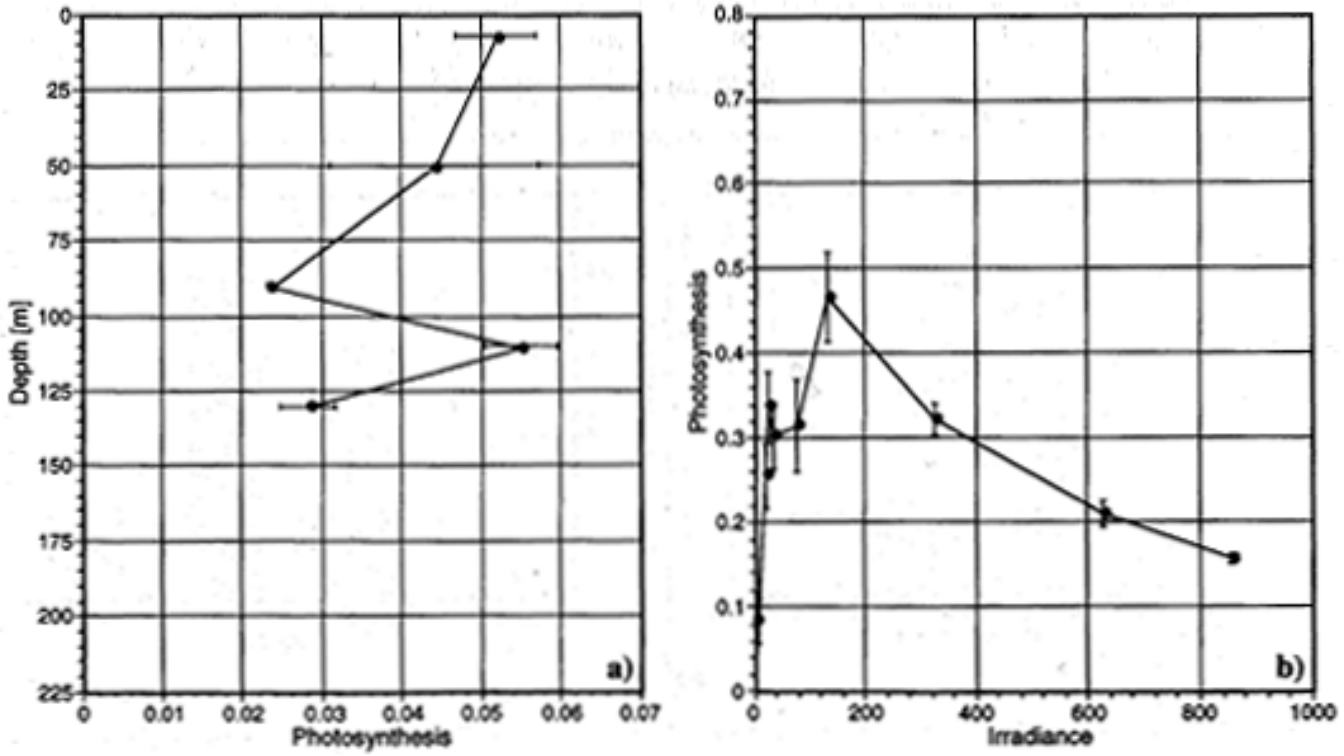

Fig. 13. Photosynthesis results for station 273: **a)** vertical profile of photosynthetic rate ($\mathrm{mgC\,m^{-3}\,h^{-1}}$); and **b)** the relationship between chlorophyll normalized photosynthesis ($\mathrm{mgC\,mgChl^{-1}\,h^{-1}}$) and irradiance for phytoplankton from 110 m. The error bars represent ± 1 standard error of the estimate ($n = 2$).

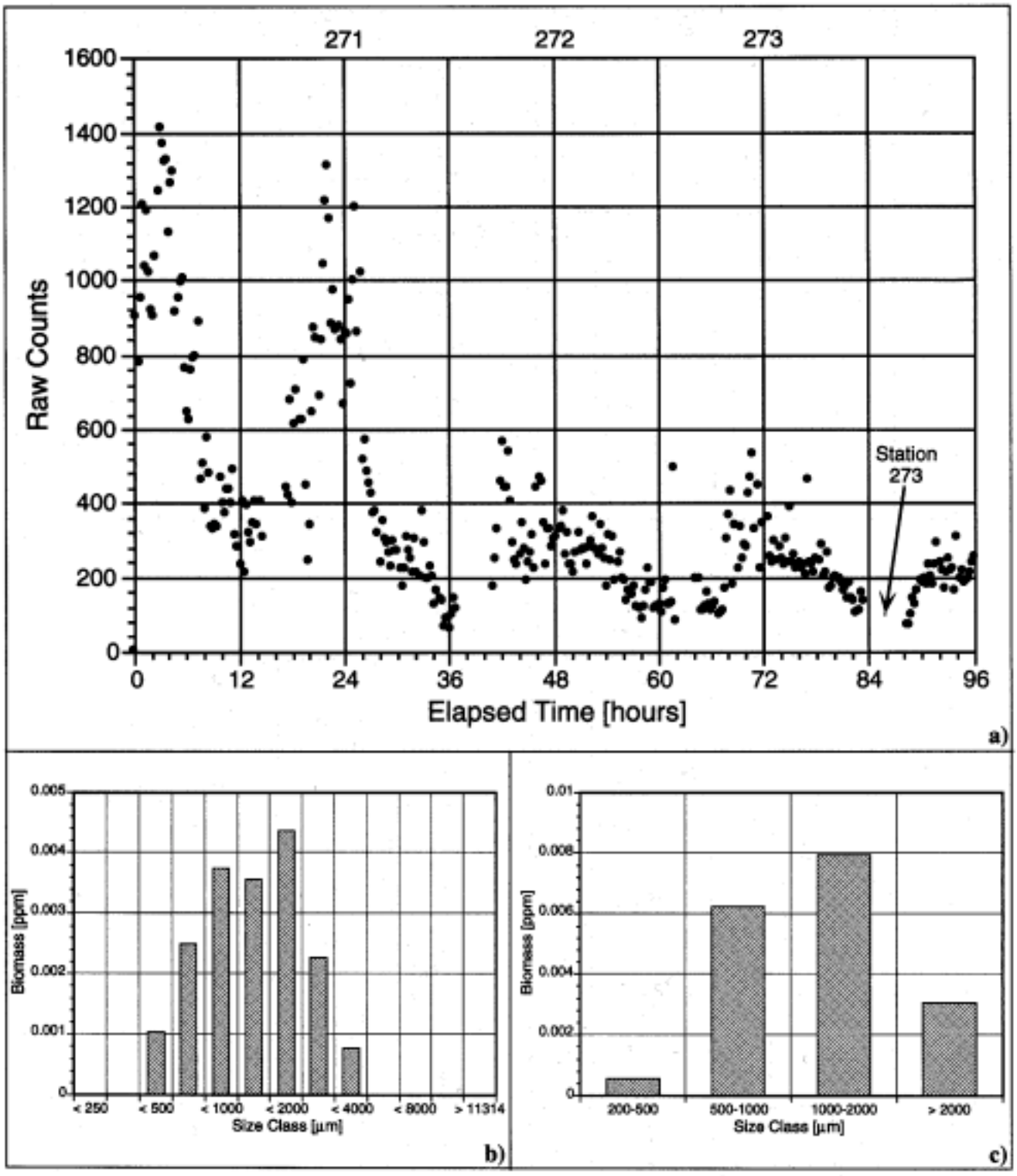

Fig. 14. Underway and net cast sampling results in association with station 273: **a)** raw counts of plankton (0.20–11 mm) from underway *surface* sampling (7 m) counted on the OPC for the four days beginning on SDY 270 up to, and including, station 273 (SDY 270–273 as indicated along the top of the graph); **b)** data from half an integrated (0–200 m) plankton net haul run through the OPC and expressed in 13 size classes from less than 250 to greater than 11,314 μm; and **c)** the same OPC data expressed in 4 size classes to match the JGOFS carbon size fractions for zooplankton biomass.

Figure 14a shows the abundance of zooplankton over the four days up to and including the day for station 273. The first day of this sequence was station 270 at 20°W,47°N and the remaining stations are approximately 24 hours apart (roughly every 260 nmi) in a southerly transect. The data clearly show a transition from higher productivity waters in the north to lower productivity in the south. There are also clear trends (particularly during the first two days) showing increased numbers of animals in the *surface* waters (7 m) at night. The data from station 273 (Figs. 14b and 14c) presented in this report shows most zooplankton in the range 0.5–2 mm, with approximately 80% of biomass in these two categories; biomass data for this figure are presented as parts per million (ppm).

4.7 Size Fractionation

Preliminary results for size fractionation are not presented, since all of the samples will be analyzed after the cruise in the laboratory. However, a summary of the size-fractionated particulate and zooplankton carbon samples taken are presented in Appendix D.

4.8 Circulation and Backscatter

A summary of the current velocities for station 273 is given in Fig. 15. The current magnitude is at a minimum ($15\mathrm{cm\,s^{-1}}$) at about 25 m depth (Fig. 15a). Below this, the current increases rapidly to about 100 m depth, where it becomes approximately constant (at 30–35 $\mathrm{cm\,s^{-1}}$). Above 25 m there is a single point increase in magnitude, but this is possibly an artifact.

Throughout the water column, the bulk of the current is flowing in a southwesterly direction: 220–240° (Fig. 15b). At a depth of 10 m, however, the current is flowing in a more westerly direction (from 253°). This is possibly due to the prevailing wind direction over the collecting period. The directional changes within this narrow band do not correlate with features on the current magnitude profile (Fig. 15c). This suggests the variation in current magnitude is not due to water motion factors such as current shear, but probably due to thermal factors.

The relative backscatter profile (Fig. 15d) shows a surface maxima (95%), decreasing with depth to a minima at 115 m (68%). The backscatter increases below 115 m, reaching 83% by 250 m. Two submaxima occur between the surface and 115 m, at 50 m (83%) and 85 m (75%).

4.9 Inorganic Nutrients

The analytical results for the nutrient analyses at station 273 are given in Fig. 16. As of 2 October, having not yet reached the upwelling region off the West African coast, the inorganic nutrient values in surface waters, except for silicate, were typically below detection at less than $0.1\,\mathrm{mmol\,m^{-3}}$ for nitrate, less than $0.01\,\mathrm{mmol\,m^{-3}}$ for nitrite, and less than $0.05\,\mathrm{mmol\,m^{-3}}$ for phosphate. Silicate concentrations were uniformly low but measurable with typical values in the region of $1\,\mathrm{mmol\,m^{-3}}$.

Higher surface values of all nutrient levels were found in the Western Approaches, before leaving the continental shelf, and here, nitrate values at the start of the transect were measured at $4\,\mathrm{mmol\,m^{-3}}$ falling to below detection after the first 16 hours steaming towards 20°W,47°N. The vertical profiles allowed samples to be collected from the base of the mixed layer below the thermocline where, as would be expected, nutrient values were higher.

5. SDY 276–277 TOW

Following on from the preliminary data gathered and illustrated for station 273, this section reviews preliminary data for the region of transition from the northern open ocean waters, into the upwelling off Mauritania, West Africa. The surface profiling parameters (temperature, salinity, and chlorophyll) showed a marked change (lower temperature and higher fluorescence) during the late afternoon, after the station on SDY 276. The reduced temperature and high fluorescence remained throughout the night of SDY 276 and into the following day (SDY 277). The station for SDY 277 was earlier than was normally the case, and the UOR tow after the station was only of one hour duration. These were both caused by the near proximity of territorial waters.

The station on SDY 277 was selected after the ship sailed through a patch of high chlorophyll water (see various figures within this section). Some of the contributions within this section include data on broader latitudinal scales than the transect between the two stations (276 and 277). There are also some vertical profiles for these two stations which help illustrate the contrast between the more dynamic upwelling waters and the open ocean water farther north.

5.1 Hydrography

Figures 17 and 18 show contoured temperature and chlorophyll sections on either side of the SDY 276 and 277 stations, respectively, in an area of upwelling water. In each figure, the UOR tow into, and out of, the daily station has been combined to give an overview of the oceanographic properties spanning the station. The distance covered by the ship was recorded from the ships log and interpolated onto the data.

Both the temperature and the chlorophyll measurements on SDY 276, Figs. 17a and 17b, respectively, clearly show a marked frontal feature as the upwelling region was encountered at approximately 230 km. At the upwelling region, the depth of the thermocline decreased from 60 to 30 m and the surface water temperature decreased as colder

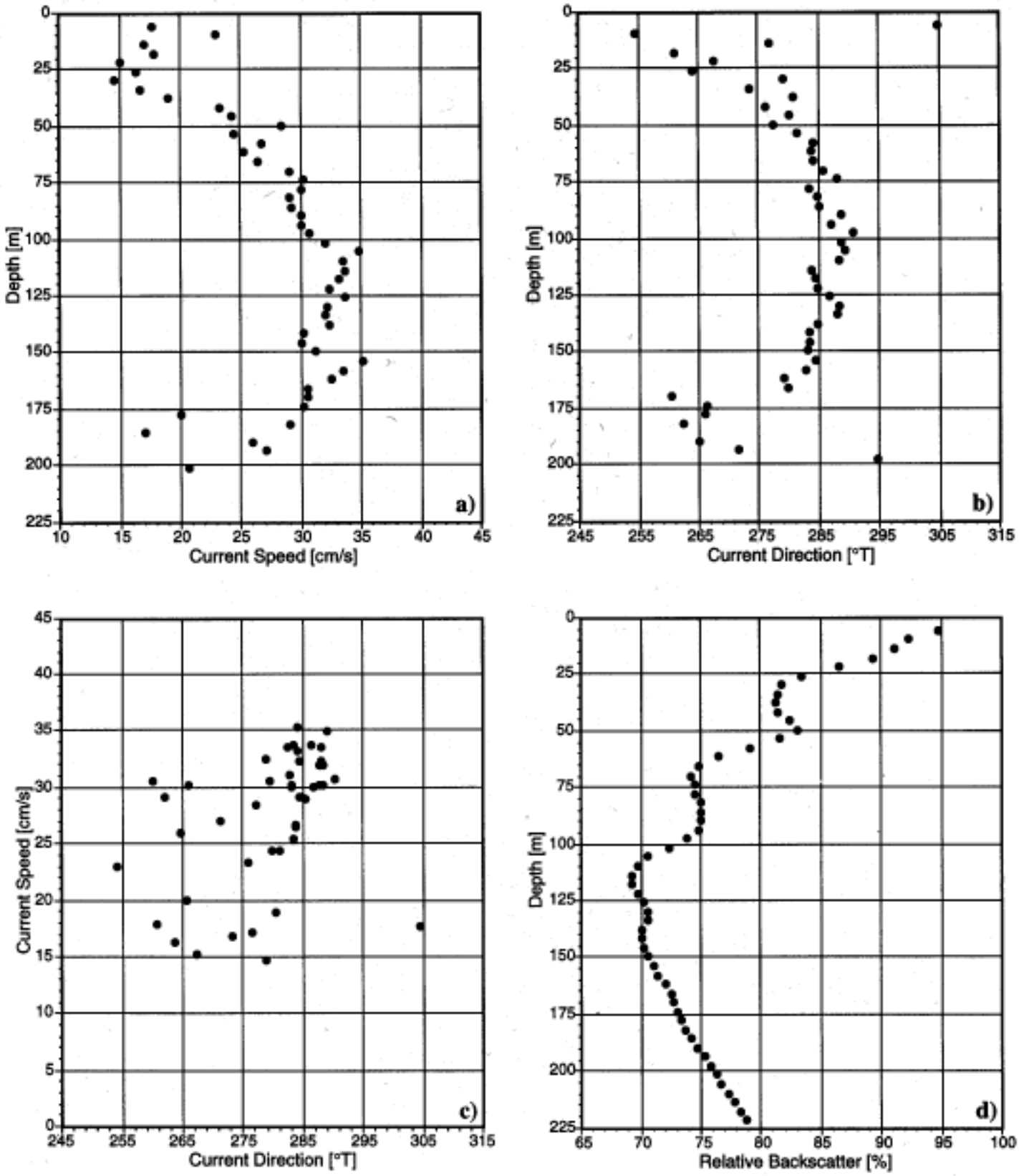

Fig. 15. Station 273 ADCP data: **a)** current speed as a function of depth, **b)** current direction as a function of depth, **c)** current speed as a function of current direction, and **d)** relative backscatter as a function of depth.

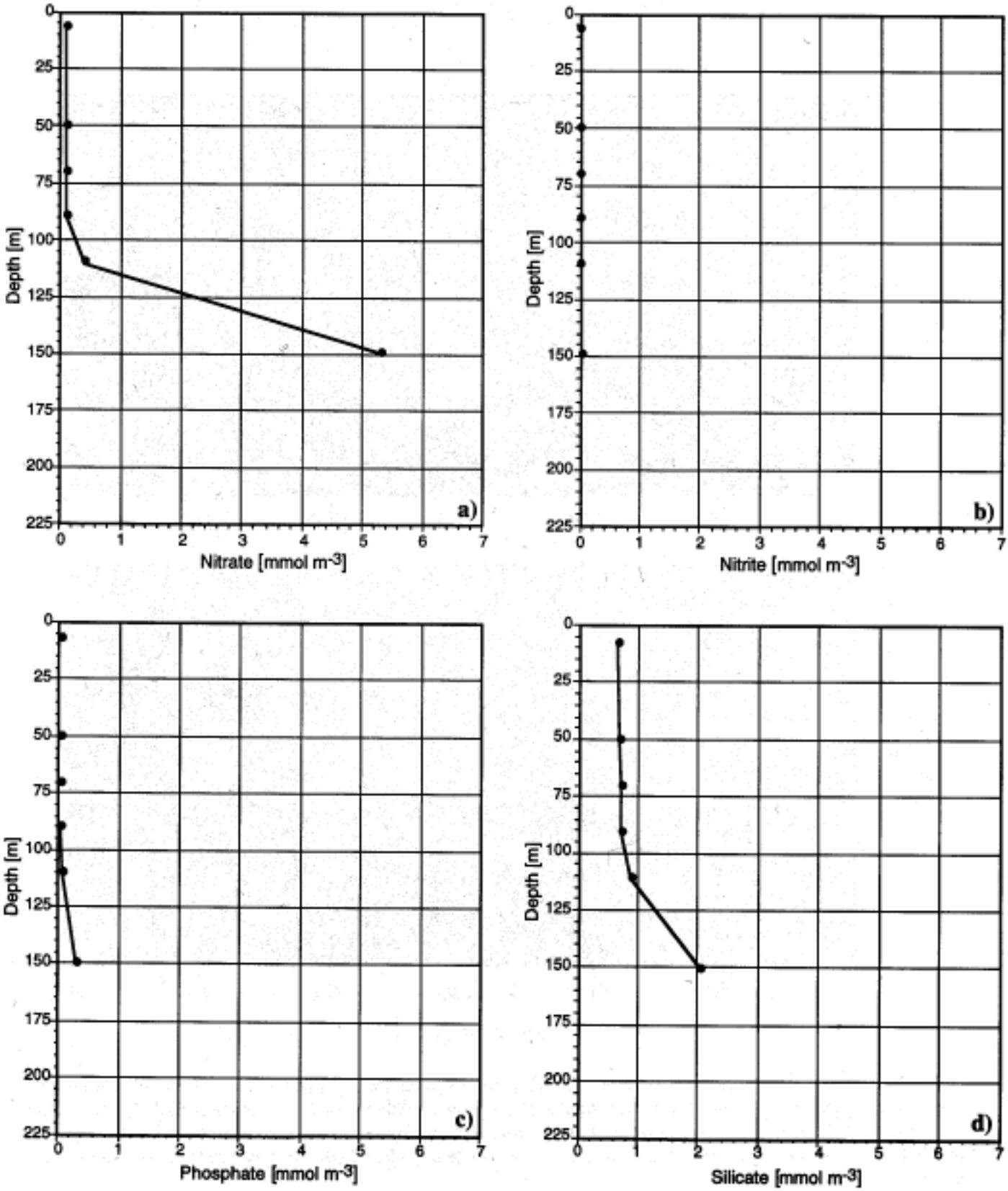

Fig. 16. Nutrient profiles for station 273 (30 September): **a)** nitrate, **b)** nitrite, **c)** phosphate, and **d)** silicate.

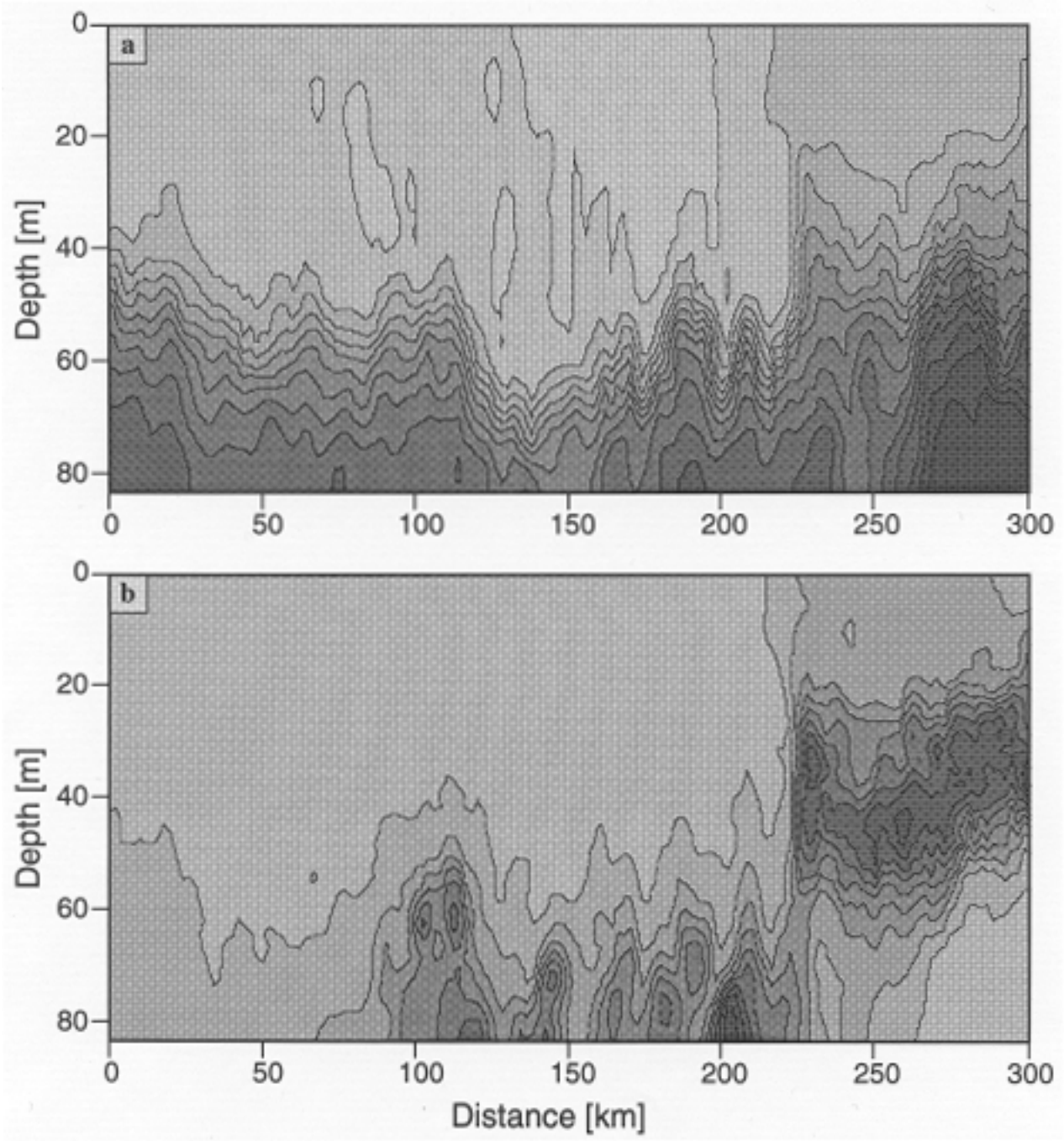

Fig. 17. Contour plots from UOR tows on SDY 276: **a)** temperature (°C), and **b)** (uncalibrated) chlorophyll concentration ($\mathrm{mg\,m^{-3}}$). For the former, lighter greys denote higher water temperature (25°C) and darker greys lower (16°C and less); for the latter, darker greys denote higher chlorophyll concentration ($1.5\,\mathrm{mg\,m^{-3}}$) and lighter greys lower ($0\,\mathrm{mg\,m^{-3}}$). The contouring intervals are 0.5 and 0.05 for temperature and chlorophyll, respectively.

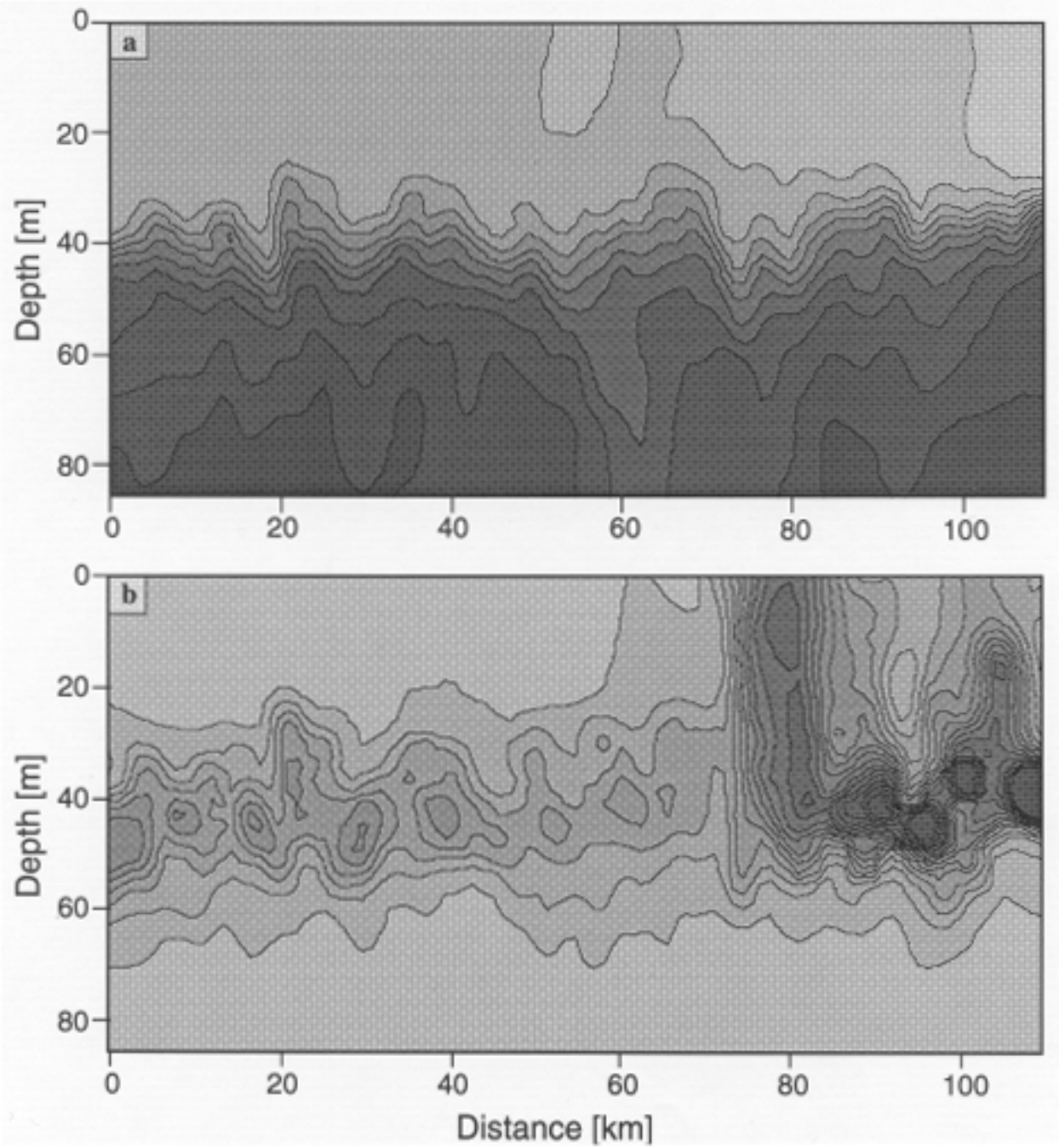

Fig. 18. Contour plots from UOR tows on SDY 277: **a)** temperature (°C), and **b)** (uncalibrated) chlorophyll concentration ($mg\,m^{-3}$). For the former, lighter greys denote higher water temperature (24.5°C) and darker greys lower (18°C and less); for the latter, darker greys denote higher chlorophyll concentration ($0.5\,mg\,m^{-3}$) and lighter greys lower ($0\,mg\,m^{-3}$). The contouring intervals are 1.0 and 0.1 for temperature and chlorophyll, respectively.

water moved higher into the water column. The depth of the chlorophyll maximum similarly decreased from 75 to 30 m as the more biologically productive deeper water upwelled through the water column.

During SDY 277, the most significant feature encountered was the high concentration of chlorophyll (Fig. 18a) between 75–100 km. It should be noted that the chlorophyll scale on this plot is five times greater than in the SDY 276 plot. The temperature structure (Fig. 18b) remained relatively stable throughout the day with a constant mixed layer depth around 30 m.

At the SDY 277 station, the UOR was deployed vertically to a depth of 200 m, and the temperature profile obtained on the down cast shows a mixed layer depth of 30 m (Fig. 19a) and a chlorophyll maximum of 1.9 at the same depth (Fig. 19b), which is consistent with the results from the towed data set.

5.2 Optics

During the transect, bio-optical information was collected from the PRR-600 and SeaOPS profiles, the UOR sensors, and the AC-9. The UOR, PRR-600, and SeaOPS light sensors measured optical properties at SeaWiFS wavelengths. The underway AC-9 meter also measured optical properties at the SeaWiFS wavelengths, and three extra wavelengths designed to interpret biogeochemical parameters.

These three sources of data provide complimentary bio-optical information:

1. The PRR-600 and SeaOPS provided discrete optical profiles. These were used for extrapolation of the light field to the surface, for the development and validation of satellite algorithms.
2. The UOR provided synoptic measurements of surface optical properties, both the light field and beam attenuation. These data provided essential information for understanding local bio-optical variability.
3. The AC-9 meter provided underway measurements of the underlying inherent optical properties of absorption and attenuation.

These measurements will be used to further develop bio-optical models that relate the observed radiance and irradiance measurements to the underlying biogeochemistry. The bio-optical data from the transect when used in conjunction with the FRRF fluorometry, the primary production measurements, and the HPLC pigment analyses will be used to develop models that relate satellite observations of ocean color and temperature to integrated water column production. Such production models can be coupled to satellite physical observations, such as wind speed, to provide estimates of air-sea gas exchange also observed on the cruise.

5.2.1 UOR Light Sensors

The UOR light sensors consist of SeaWiFS wavelength compatible sensors fitted to the tail of the UOR. The UOR is fitted with both upwelling radiance and upwelling irradiance sensors, as well as downwelling irradiance sensors (Table 2). Although these were deployed during the transect over the upwelling region, unfortunately the 444, 490, and 555 nm downwelling irradiance sensors failed. As a test wavelength for comparison with the fluorescence and SeaOPS data, the 514 nm downwelling sensor was used; this wavelength, although not ideal, has a robust response to pigment.

The data from both the UOR and the SeaOPS profiler were depth averaged in 2 m bins. Although this binning was rather course, it matched the data rate of the UOR (one data point every 4 s at a dive rate of 0.25–0.5 m s^{-1}). The UOR data was selected for a tilt and roll of less than $\pm 10°$. K_d values were calculated by nonlinear fitting of the equation $E_d(z,\lambda) = E_d(0^-,\lambda)e^{(-zK_d)}$, where z is the depth and $E_d(0^-,\lambda)$ is the surface irradiance.

Figure 19a shows the underway calibrated fluorescence and $K_d(514)$ for the UOR for three tows: the tow prior to the upwelling region, the tow leading up the chlorophyll maximum, and the tow out of the upwelling region. The UOR $K_d(514)$ agrees well with fluorescence levels, increasing from 0.05 prior to the upwelling, to a maximum of 0.125. The maximum is compatible with pigment in the region of 2–3 mg m^{-3} chlorophyll. Figure 19a also shows the $K_d(509)$ derived from the SeaOPS instruments between tows. The $K_d(509)$ from SeaOPS was 0.102 ($\pm$0.008) compared with $K_d(514)$ from the UOR of 0.129 ($\pm$0.008) and 0.112 ($\pm$0.004) for the last undulation of the tow into the station and the first undulation of the tow out of the station, respectively. The K_d values show remarkable agreement given the dynamics of the area and difference in timing of the three profiles: 0940 for the tow into station, 1050 for the SeaOPS cast, and 1210 for the tow out of the station (GMT).

Figures 19b and 19c show the downwelling log and linear irradiance plots for the three profiles. The irradiance was normalized using the mean irradiance from the SeaOPS deck cell for the two UOR tows, compared to the SeaOPS cast. The SeaOPS cast is, thus, calibrated uncorrected data. The poststation profile required the least normalization and the prestation profile the most. Prior to the station, the sky conditions were patchy cloud. The best agreement was with the poststation UOR profile, where sky conditions were similar to the SeaOPS cast. Figure 19d shows the comparison between the SeaOPS light levels and the UOR light levels, with the majority of the poststation profile falling near the 1:1 line. Given the disparate data, these profiles show remarkable agreement which, in part, is due to the efforts in referencing the sensors to common irradiance scales during SeaWiFS Intercalibration Round-Robin Experiments (SIRREXs).

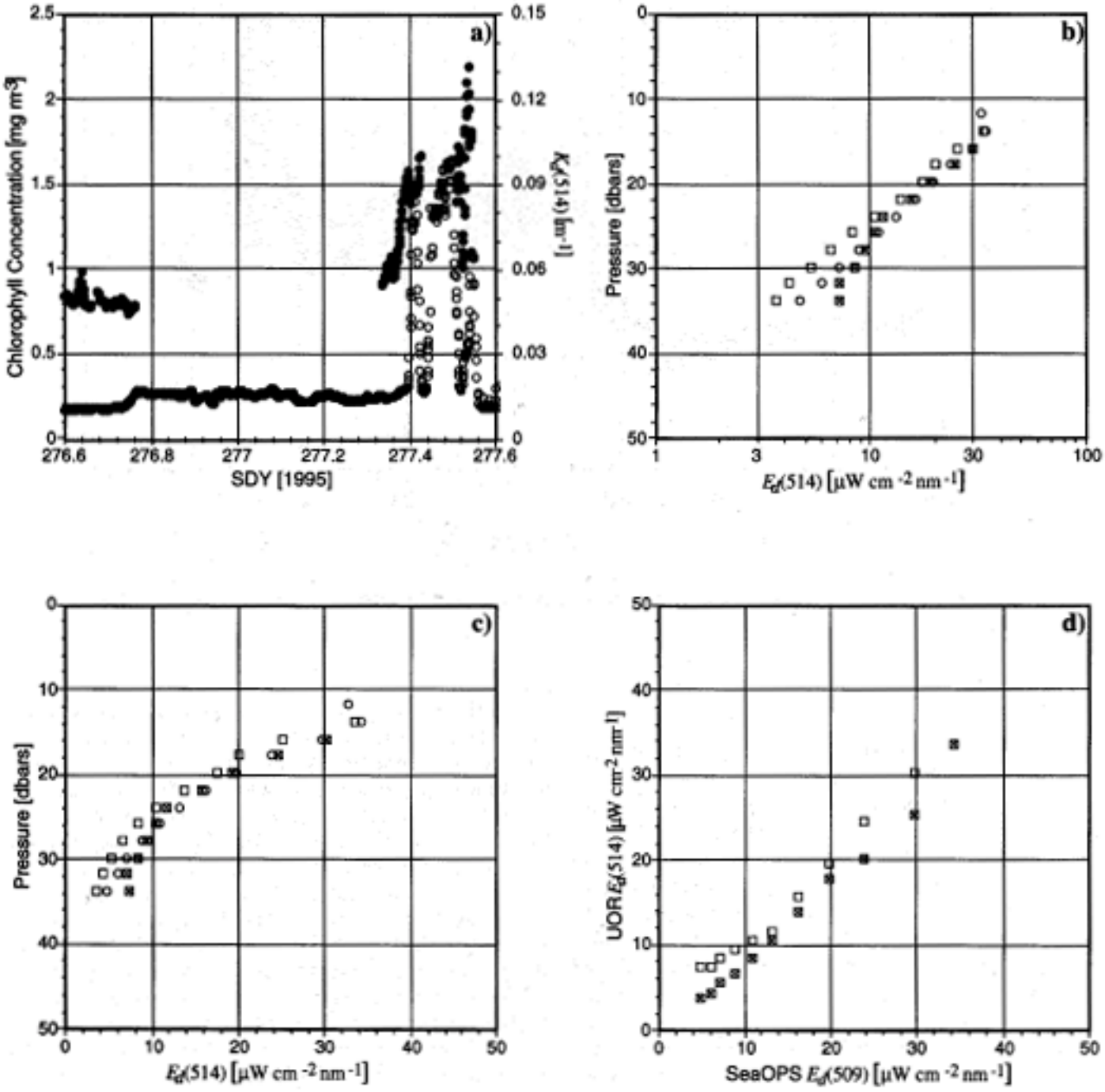

Fig. 19. Preliminary optical results for the upwelling region: **a)** chlorophyll concentration (open circles) and (SeaOPS) $K_d(514)$ (solid circles) during the passage through the upwelling region; **b)** UOR prestation (open squares) and poststation (crossed squares) irradiance profiles compared to the SeaOPS cast (circles); **c)** the same information in Fig. 19b presented with a linear irradiance axis; and **d)** UOR prestation (open squares) and poststation (crossed squares) irradiance as a function of the SeaOPS irradiance.

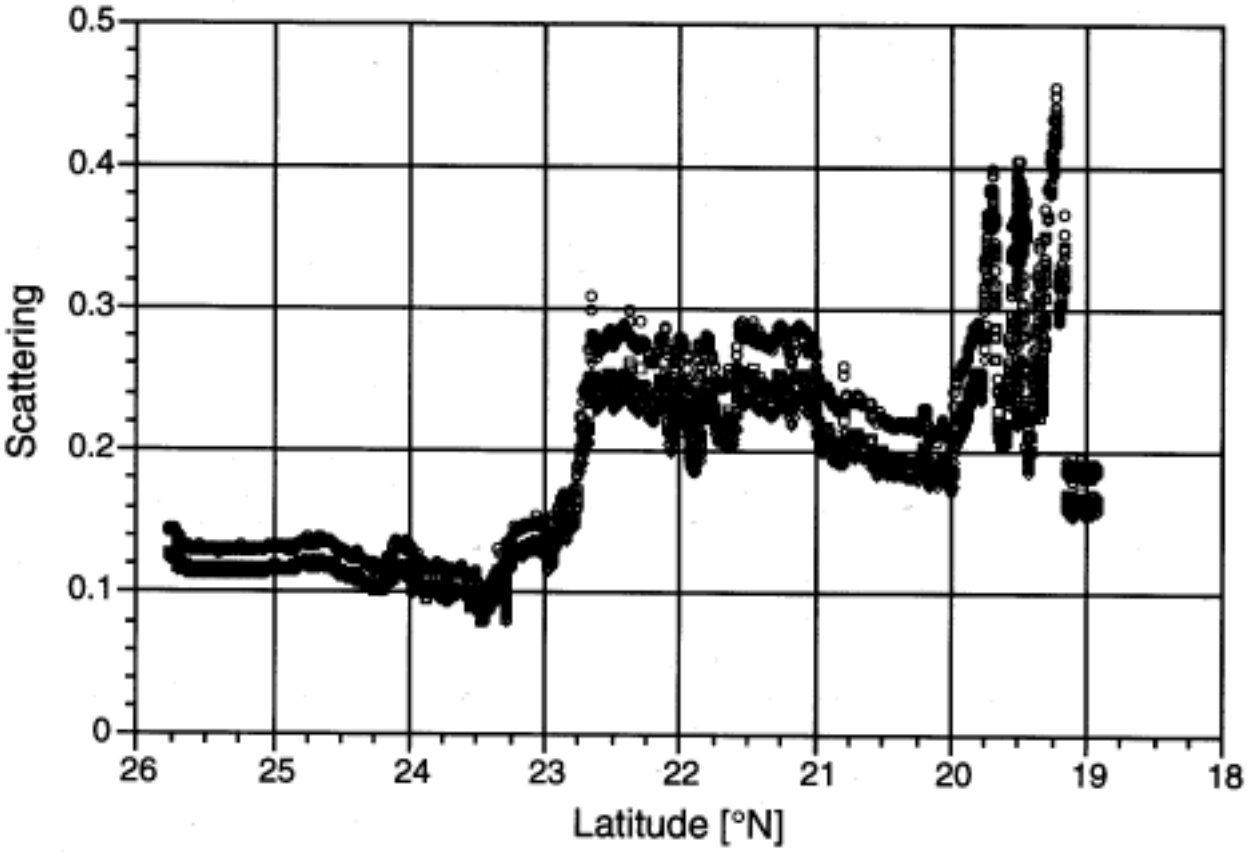

Fig. 20. AC-9 scattering measurements for three wavelengths, 412 (circles), 488 (squares), and 555 nm (diamonds).

5.2.2 AC-9

One of the main science criteria for deploying the AC-9 was to achieve closure between optics profile observations and the biogeochemical parameters. As such, the AC-9 data, which produces 27 parameters, will be subject to detailed modeling. To verify the functionality of the AC-9, three wavelenghts have been chosen to display example data: 412 nm, whose absorption is dominated by chlorophylls and Gelbstoff; 488 nm, where the absorption is influenced by both carotenoids and by chlorophyll; and 555 nm, which represents the absorption minimum of phytoplankton pigments.

Figure 20 shows the data for the scattering coefficients, showing a significant increase below 23°N. All three wavelengths show similar patterns, with the scattering increasing with decreasing wavelength. Figure 21a shows the absorption coefficients; there is an expected increase in the absorption at 412 and 488 nm, with increasing chlorophyll in the region 19–22°N with the strongest response at 19.5°N. The 555 nm band shows the least response to increasing chlorophyll. In the region before the chlorophyll maximum, the 412 nm band shows a greater proportional response than the 488 nm band. This difference in response may indicate DOC is higher in the region 20–22°N.

All three absorption measures show an increase at 23–24°N. This increase seems to be uncorrelated with chlorophyll as determined by fluorescence, but seems to reflect sea surface temperature. Comparision with the normalized absorption coefficients (Fig. 21b), shows that the normalization removes this peak. The 555 nm band, however, now produces a negative value for the absorption. Given the low chlorophyll values of these waters, it seems that the assumption that backsactter from water is less that backscatter from chlorophyll has been violated and that the method overcompensates for temperature effects.

Despite the problems, the instrument produced a valuable data stream that is available for the complete transect. It is envisaged that the problems with the sample data set will be corrected with more sophisticated processing.

5.2.5 PAR

Data from the SeaOPS deck cell and the JCR PAR sensor were compared for the mornings of SDY 276 and 277. PAR was calculated from the SeaOPS deck cell by integrating the data in 20 nm bands, from 400–700 nm. Irradiance was estimated by linear interpolation for regions of the spectrum with no SeaWiFS band. PAR was calculated in terms of $\mathrm{W\,m^{-2}}$ and μE ($\mu\mathrm{mol\,quanta\,s^{-1}\,m^{-2}}$). Figure 22 shows the comparison between the two sensors,

and shows the majority of the data lies on the 1:1 region of the plot (the dashed line). The JCR PAR sensor is noisier, but this is expected, since the SeaOPS data is the sum of seven sensors. The mean peak irradiance from SeaOPS was $390.2\,\mathrm{W\,m^{-2}}$ and $371.9\,\mathrm{W\,m^{-2}}$ for the JCR PAR, giving a possible underestimate of 5% from the JCR sensor. Given the different positions of the sensors, and the patchy cloud distributions during the two days considered, it is reasonable to assume the calibration of the JCR sensor is adequate.

In terms of quantal irradiance, the SeaOPS sensor gave a mean peak irradiance of $1{,}761\mu\mathrm{mol\,quanta\,s^{-1}\,m^{-2}}$, giving a conversion factor of 4.74 from irradiance to quantal irradiance for the JCR PAR sensor. This figure compares favorably with the conventional figure of 4.6.

5.3 Fluorometry and Photochemistry

5.3.1 Underway Fluorometry

For the upwelling region, an ad hoc calibration of the underway (Turner) fluorometry was produced using the underway fluorometric discrete samples. Figure 23 shows the calibrated trace (open circles) with the sample values (solid circles) overlaid. The calibration equation was $C = -0.046 + 0.064F$ (R^2=87.4%), where C is chlorophyll concentration ($\mathrm{mg\,m^{-3}}$) and F is fluorescence. A full calibration will be applied with adjustment for quenching to the final (postcruise) data set.

As mentioned earlier (Section 2.3.1), the data logged by the underway system and the fluorometer showed initial problems with auto-ranging, and it was decided to fix the range at a level consistent with the anticipated levels in the Mauritian upwelling. The data in Fig. 23 show that this approach produced a clean signal with no level shifts.

5.3.2 UOR Fluorometer

5.3.3 FRRF

The FRRF data collected for SDY 276–277 illustrate photosynthetic trends (Fig. 24a) and productivity estimates (Fig. 24a) during this part of the transect. Temperature is plotted as a marker to indicate the boundary of the upwelling region, as well as to indicate the effect of temperature on photosynthetic parameters. PAR is plotted to indicate general light-dark cycles and periods of intermittent cloud cover, which can have very rapid (approximately 5–10 minutes) effects on photochemistry. F_m is the maximum fluorescence observed; $\Delta\Phi_{\max}$ is the maximum quantum yield of Photosystem II (PSII).

The most significant fluorescence related structure encountered within the upwelling was the peak at approximately 19.5°N, which was subsequently used for profile studies on SDY 277. Such an anomaly is difficult to interpret during a surface transect with the FRRF, since the magnitude of the peak tends to obscure the surrounding photochemical events. Consequently, analysis of this structure will be left for discussion of the profile for day 277 and the discussion here will concentrate on the general trends of the upwelling region.

5.3.3.1 Fluorescence Trends

F_m, the maximum fluorescence signal, increases significantly as the upwelling region is encountered (Fig. 24a); it rises from a background level of approximately 1.0 (FRRF units) to a maximum of about 12.9. The sharp drop in F_m at 22.4°N coincides with two significant physical events: the edge of the temperature gradient and sunset. F_m continues to follow a locally low, but generally high, trend with a noticeable dropoff at 20.8°N, which corresponds to the first encounter of a significant temperature gradient and the edge of the upwelling region.

Compared to before the upwelling, the average level of F_m within the region increased. Because most of the upwelling region was sampled at night, irradiance effects on fluorescence are virtually nonexistent. Very short spikes in the F_m signal at night might be attributable to zooplankton coming to the surface, concentrating phytoplankton in their digestive tract, and thus being recorded in the FRRF as significant (momentary) fluorescence sources.

The sharp drop in F_m at 22.4°N is difficult to assess because of the two significant physical events with which it coincides. Temperature changes could affect the composition of the phytoplankton population and, thus, the drop could be attributed to a different population. However, sharp changes in irradiance can trigger the recovery from daytime short-term nonphotochemical quenching, and, thus, for the short time in which phytoplankton are adjusting to low (i.e., night) light levels, fluorescence quenching is still in effect until this mechanism is shut off biologically. Analysis of this event with nutrient and pigment data will give better insight into this drop in fluorescence.

Although the short-term component of nonphotochemical quenching can be seen in the F_m signal during periods of high irradiance (note F_m perturbations at 22.8°N). The general night F_m trends closely follow physical characteristics, such as, temperature. Daytime F_m trends, however, are a more complex convolution of physical influence, nonphotochemical quenching mechanisms, and photodamage.

5.3.3.2 Photosynthesis Trends

Of special interest between SDY 276–277 are the changes in $\Delta\Phi_{\max}$ over the day/night cycle while passing through the upwelling region. Values of $\Delta\Phi_{\max}$ increase upon entering the upwelling, rising from 0.42 to 0.50 between 22°N and 20.8°N, respectively. A step occurs in the $\Delta\Phi_{\max}$ signal when the first significant increase in temperature is reached; the average $\Delta\Phi_{\max}$ falls from 0.50 to 0.45.

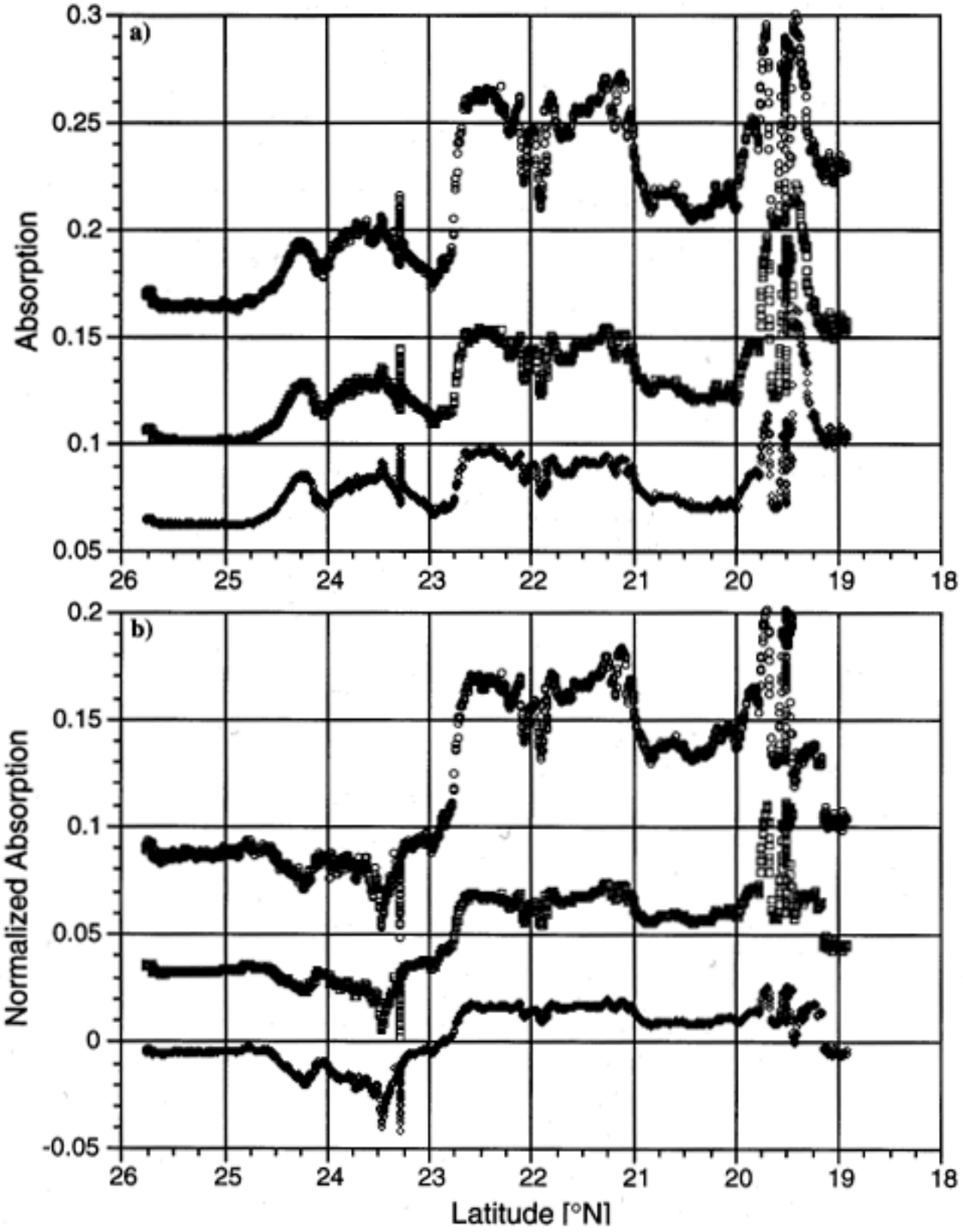

Fig. 21. AC-9 measurements for three wavelengths, 412 (circles), 488 (squares), and 555 nm (diamonds): **a)** absorption (a), and **b)** normalized absorption (a_N). All measurements are in units of m^{-1}.

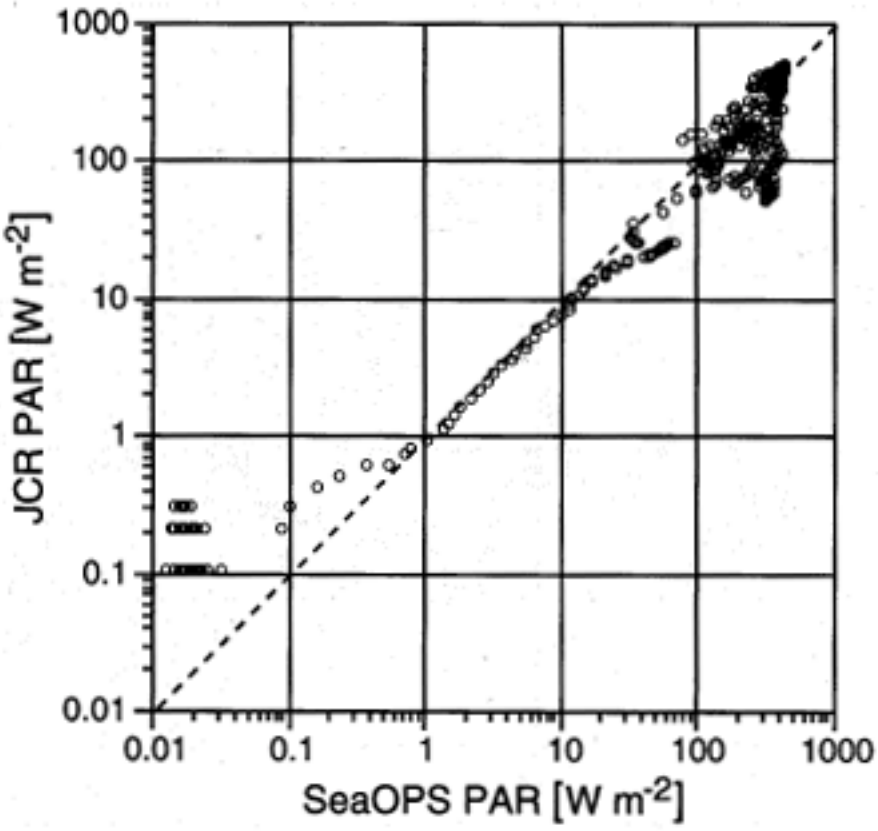

Fig. 22. A comparison of the SeaOPS calculated PAR with the JCR PAR sensor. The dashed line is the 1:1 line.

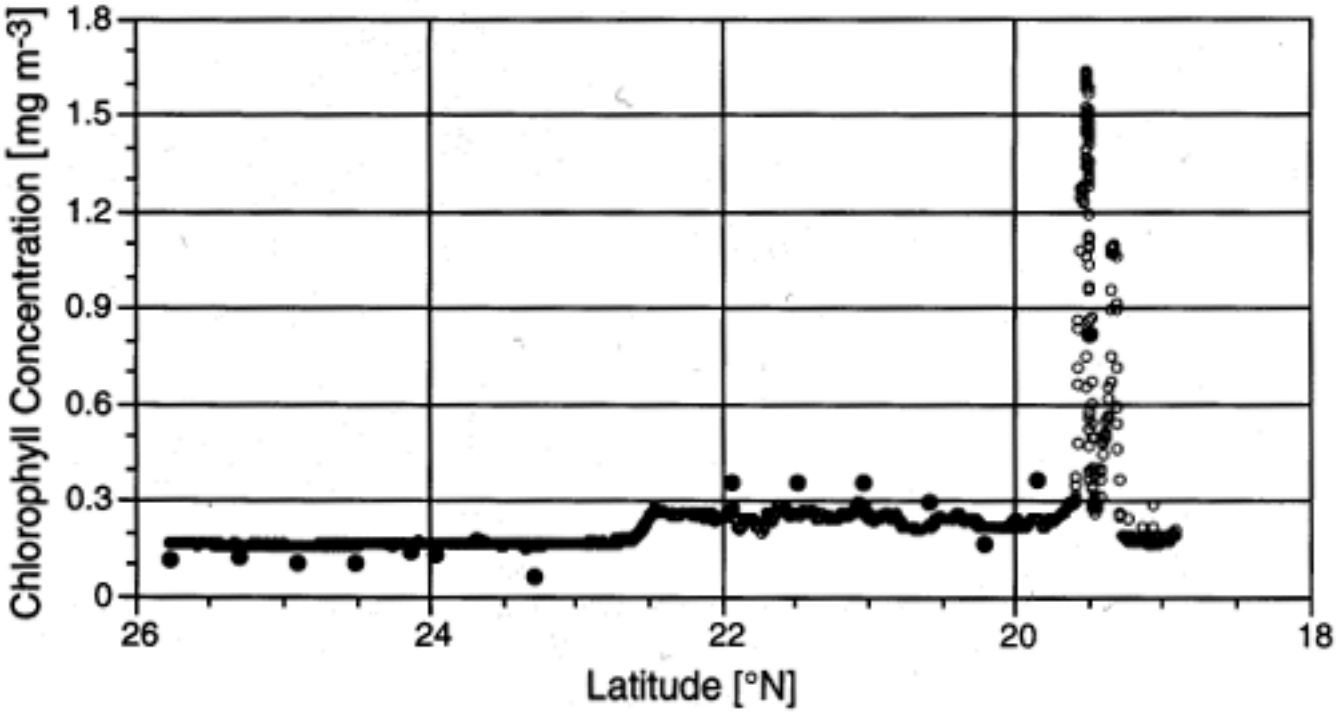

Fig. 23. Calibrated Turner fluorometer (open circles) plotted with underway discrete samples (solid circles).

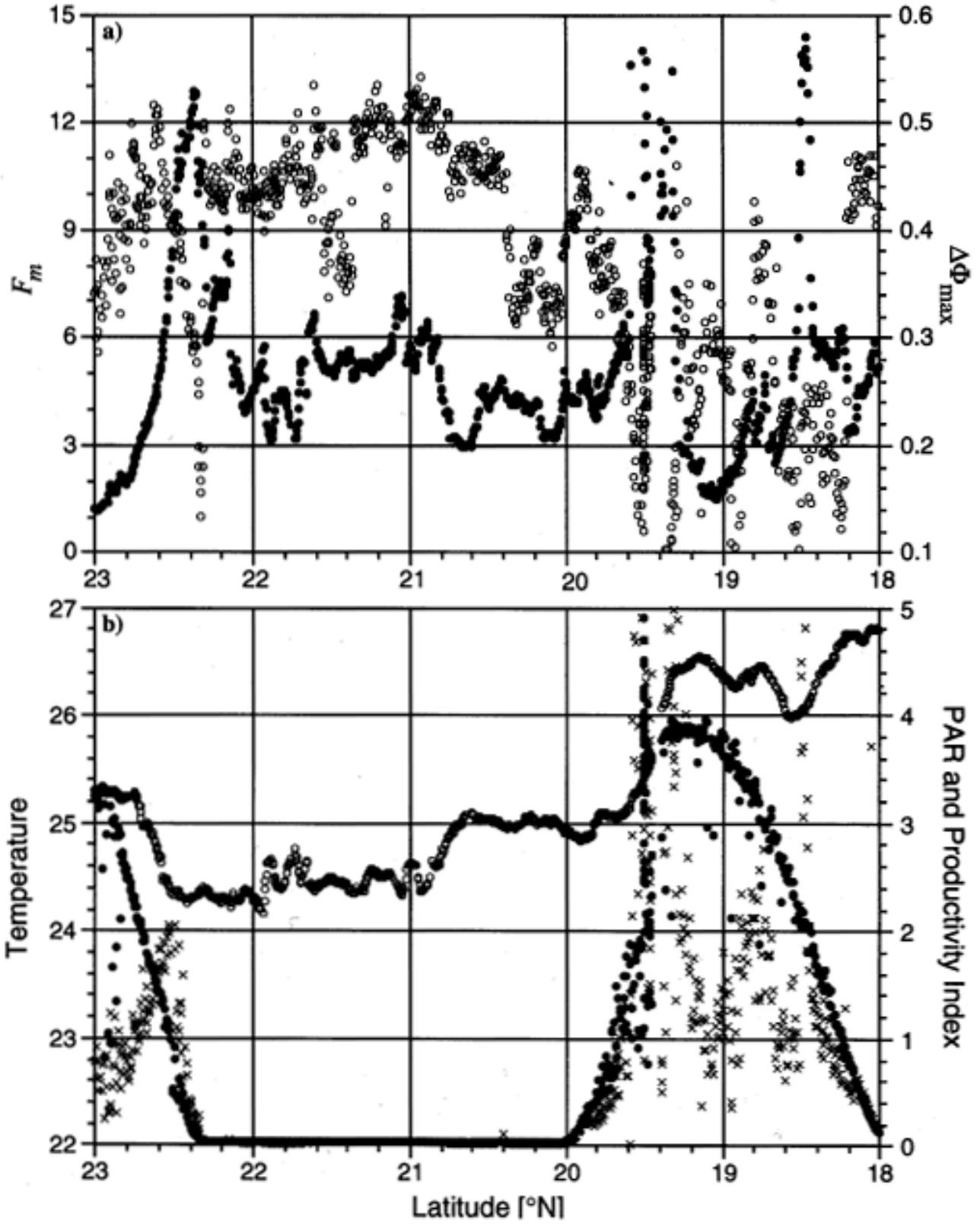

Fig. 24. FRRF data for SDY 276–277: **a)** F_m (solid circles) and $\Delta\Phi_{\max}$ (open circles), and **b)** temperature (open circles), PAR (solid circles), and productivity index (crosses). Temperature has units of °C, PAR has been scaled by 10^2 and productivity by 10^5; the latter two have arbitrary units.

Another significant drop in $\Delta\Phi_{max}$ occurs between 20.5–19.8°N, at an average level of 0.35. Values of $\Delta\Phi_{max}$ recover from this drop at dawn, and then falls gradually as ambient irradiance increases.

At night (22.4–20°N), when the phytoplankton are repairing their photosynthetic structures, $\Delta\Phi_{max}$ rises as the number of competent reaction centers increases. Evidence of this can be seen from around 22–21°N. The sharp decrease at 20.8°N coincides with a sharp rise in water temperature, which may be either population or temperature driven.

The fall and recovery between 20.4–20°N is significant, with an average value of 0.34. This coincides with a feature in the temperature curve, but beyond that, no real correlation can be made without nutrient data. When daylight arrives and irradiance levels increase, the rapid fall in $\Delta\Phi_{max}$ can be attributed to short-term nonphotochemcial quenching. This trend continues until nightfall.

5.3.3.3 Productivity Trends

Although values of photochemical quenching are not available from the benchtop FRRF instrument, a crude estimate of phytoplankton productivity can be produced by calculating the product of F_v, the cross-sectional area (not plotted), and PAR. These three measurements represent the three major limiting factors in PSII photosynthetic rate. The resulting productivity index is plotted in Fig. 24b, against PAR and temperature to indicate both the boundary of the upwelling region and ambient irradiance. Productivity is zero for most of the upwelling, obviously due to the lack of solar irradiance at night.

It is interesting to note that such a rough estimate of productivity shows a sharp increase entering the upwelling, even though FRRF data were being acquired during a period of relatively low irradiance. At dawn on day 277, the productivity index again rose with irradiance, and fell off sharply upon finally crossing into the warmest water mass.

5.4 Photosynthesis and Calcification

A series of underway primary productivity measurements were carried out from 23–13°N along approximately 21°W (Fig. 5) during the period SDY 276–278. Figure 25a shows a dramatic increase in the surface photosynthetic rate at around 19°N, coinciding with the existence of deep water upwelling nutrients to subsurface layers (see Figs. 17 and 18 for a vertical distribution of temperature along the transect). Maximum values of primary production were approximately $1.5\,\mathrm{mgC\,m^{-3}\,h^{-1}}$ and persisted in the southern part of the front down to 13°N.

Photosynthesis and irradiance experiments reflected the differences in the photoacclimation state of the microalgae at the DCM along the transect (Fig. 25b–d). Phytoplankton at the DCM on SDY 278 showed the highest maximum photosynthetic efficiency measured during the early part of the cruise, approximately $3\,\mathrm{mgC\,mgChl^{-1}\,h^{-1}}$ (Fig. 25d). Phytoplankton at the chlorophyll maximum on SDY 277 showed no sign of photoinhibition (Fig. 25c), whereas microalgae from the DCM on SDY 276 and SDY 278 became photoinhibited at irradiance levels above $400\,\mu\mathrm{E\,m^{-2}\,s^{-1}}$ (Figs. 25b and 25d). The lack of photoinhibition on SDY 277 indicates subsurface phytoplankton in the upwelling area were adapted to relatively high irradiance levels. This suggests the subsurface chlorophyll maximum at 13°N was a relatively stable structure, and that residence time of phytoplankton at optimum light levels was high in relation to their turnover rate.

Marked differences were found between SDY 277 and 278 in the relative contribution of each size fraction to total phytoplankton biomass and production at the chlorophyll maximum (Fig. 26). Cells larger than $20\,\mu$m were responsible for more than 80% of total chlorophyll and 60% of production, respectively, on SDY 277. By contrast, the phytoplankton biomass and productivity were dominated by the less than $2\,\mu$m size fraction on SDY 278. At this station, the relative contribution of the smaller cells to total chlorophyll concentration and photosynthesis was above 60%. These results illustrate how physical forcing, in this case upwelling, brings about not only a change in algal biomass and productivity, but also a shift in the taxonomic composition of the phytoplankton assemblages. As a result, the importance of the classical food chain and export production would be higher in the upwelling area, whereas recycling and the microbial loop would dominate in the oligotrophic regions.

Calcification experiments were conducted throughout the cruise in order to evaluate the basin-scale significance of inorganic carbon production by coccolithophores. Although the results obtained are still in a very preliminary form, they suggest that the incorporation of carbon into calcium carbonate had only a minor quantitative importance as compared with the rates of organic carbon production. In most cases, calcification was undetectable with the methodology used. Positive values of calcification rates, however, were measured at some restricted locations. Further detailed analyses of the obtained data will be necessary to assess if these calcification rates were significant.

5.5 Pigment Extractions

Figure 27 shows the change in along-track chlorophyll *a* concentration during SDY 276–278, while the ship passed into the upwelling region. A clear area of increased biological activity can be seen, coincident with a drop in temperature brought about by the colder deep upwelling water mass. This information, in conjunction with the daily station assessments of ocean color and biology (using the profiling radiometers and CTD), are the fundamental products required to enable the calibration and validation of satellite imagery. The development of key mathematical relationships between ocean color and pigment concentration is also a key goal.

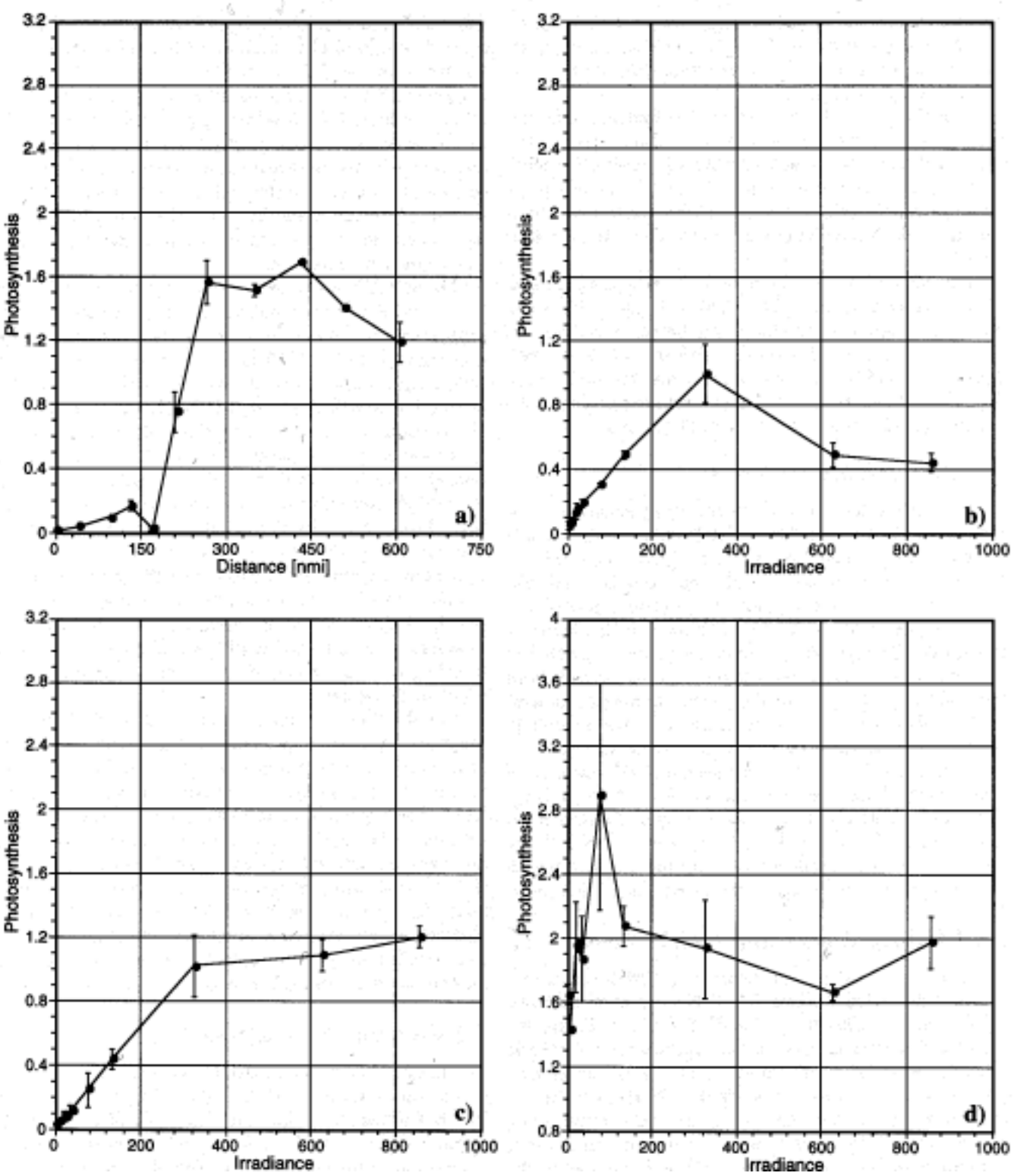

Fig. 25. Photosynthesis results for the SDY 276–277 tow: **a)** *surface* (7 m) photosynthetic rate ($\mathrm{mgC\,m^{-3}\,h^{-1}}$); and the relationship between chlorophyll-normalized photosynthesis ($\mathrm{mgC\,mgChl^{-1}\,h^{-1}}$) and irradiance for phytoplankton from **b)** 80 m on SDY 276, **c)** 30 m on SDY 277, and **d)** 70 m on SDY 277. The error bars represent ± 1 standard error of the estimate ($n = 2$).

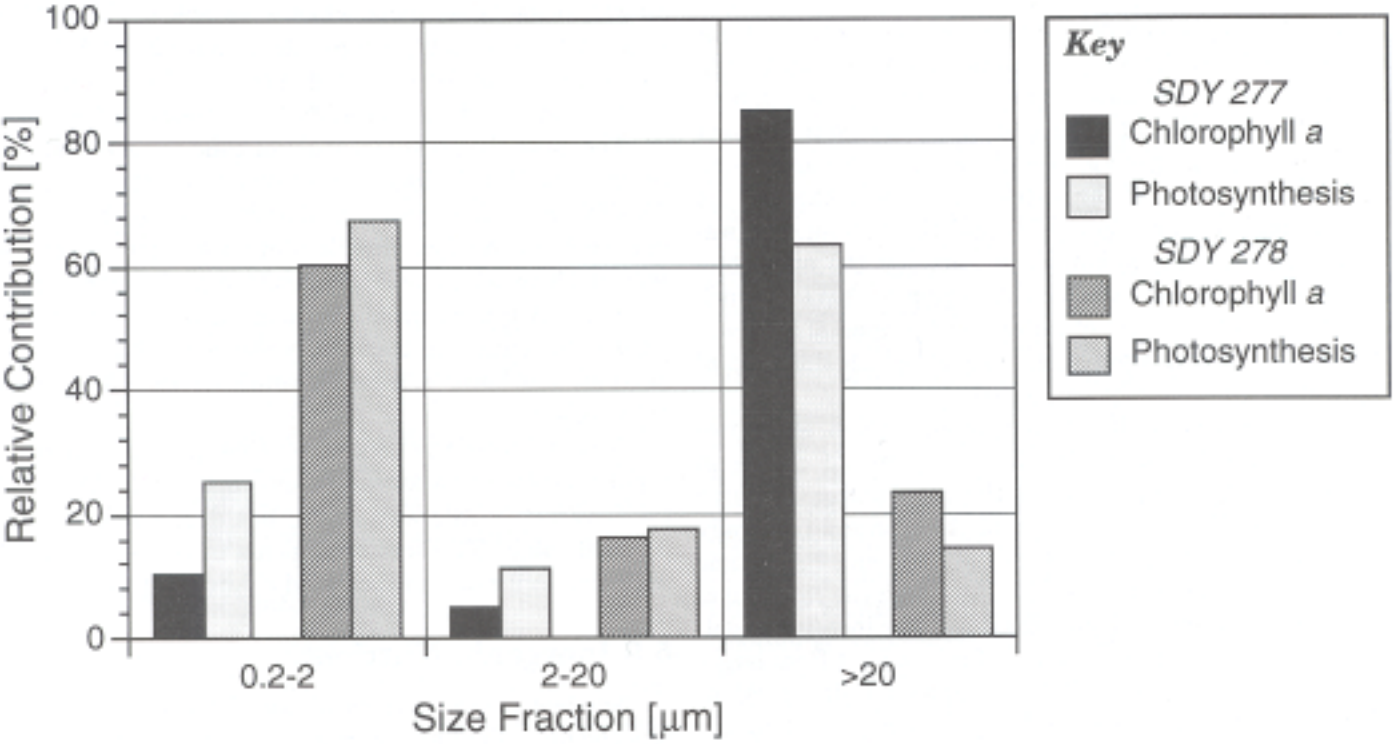

Fig. 26. Relative contribution (%) of each size fraction to total phytoplankton chlorophyll concentration and primary production at the deep chlorophyll maximum on SDY 277 (left two bars) and 278 (right two bars): 0.2–2 μm; 2–20 μm, and greater than 20 μm.

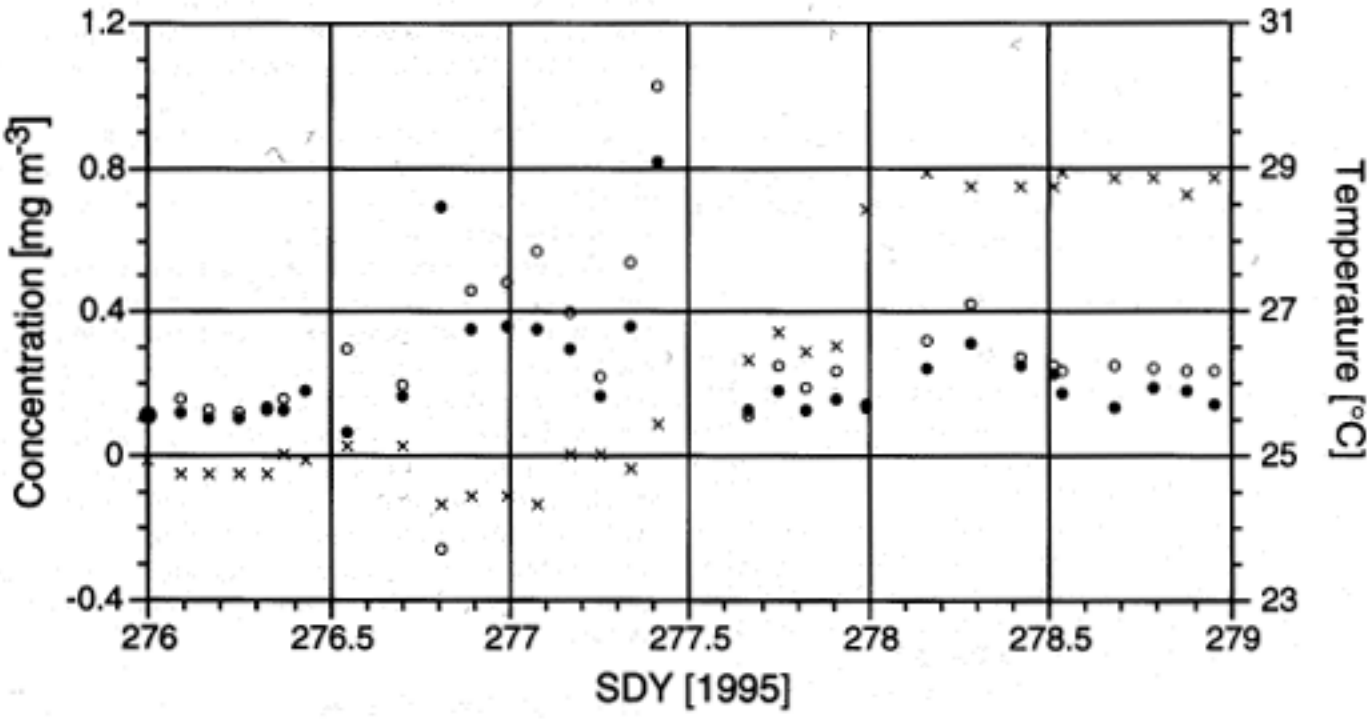

Fig. 27. Chlorophyll *a* (solid circles) and phaeopigment (open circles) concentration as a function of time during the tow through the upwelling region. SST (7 m) is also shown (crosses) for the same time period. The latitudinal range for this time period is approximately 21.8–11.8°N for SDY 276–279, respectively.

5.6 Zooplankton Characterization

The zooplankton data presented for the specimen transect shows both the surface profile of raw counts (abundance) between the stations (Fig. 28a) in conjunction with the station profiles at each end of the 24 hour transect (Figs. 28b–e). In general, zooplankton were more abundant in the period of the specimen transect than at the first example of a station (273) and the surrounding waters. This can be explained, in part, by the other biological and physical data for this region of AMT-1 which clearly shows the effects of fronts and the general influence of the Mauritanian upwelling, through which this part of the transect was closely associated.

Vertical net hauls, integrated through 200 m, at the two stations (Figs. 27b and 27c) show a significant change in the community composition of the zooplankton in terms of size class. The northern end of the transect (generally believed to be outside frontal effects) had twice the volume of zooplankton than station 277. Although the raw counts at the two stations were not dissimilar, the increase in volume of material can be accounted for by a shift from larger to smaller animals (Fig. 27d). Samples for size fractionated particulate and zooplankton (corresponding to the size classes in Figs. 14c, 27d, and 27e) were taken for subsequent analysis and validation against biomass (volume) estimates from the OPC. Samples preserved in formaldehyde, which correspond to all the data sets presented here, are available for analysis after the cruise to validate OPC results.

5.7 Size Fractionation

No preliminary results for size fractionation are presented, since all of the samples will be analyzed after the cruise in the laboratory. A summary of the samples taken, however, is presented in Appendix D.

5.8 Circulation and Backscatter

Figure 29a shows a contour plot of the ADCP relative backscatter for the time between stations on SDY 276–277. This image was compiled by contouring 10 minute averages of ADCP data. The figure can be described by considering it as four seperate zones. Zone 1, 1500–1900, is characterized by a surface backscatter maxima (up to 90 units) which decreases rapidly to 53 units at a depth of 100 m. A slight increase in backscatter is observed between 40–250 m, with a maximum at 250 m of 57 units. A typical profile for this region is given in Fig. 29b.

Zone 2 covers the 1900–0300 time period. At 1900, the contour plot shows a rapid increase of backscatter across the entire depth range, with the bulk of the increase taking place over only 1 hour. After this rapid change in backscatter, there are three areas of increased activity, centered on 2300, 0030, and 0200. The contrast with the surrounding water for these areas is the greatest between 20–40 m. There does, however, appear to be a backscatter increase directly below these areas, which is notable to about 200 m. Figure 29c shows a typical profile for zone 2. At 100 m the backscatter is at 70 units (an increase of over 30% from zone 1), and at 250 m, 60 units (an increase of 5%).

The most remarkable feature of zone 3, 0300–0800, is a region of intense backscatter between the surface and 40 m. This feature differs from the areas of enhanced backscatter in zone 2 in two ways: first, it is of far greater extent; and, second, there is no obvious increase in backscatter directly below it. A typical profile is included in Fig. 29d. Comparing this with Fig. 29c clearly shows the higher surface maxima and lower mid-depth values of zone 3 compared with zone 2.

Zone 4 covers the 0800–1100 time period. There is a rapid decrease in backscatter from 0800–0930. After 0930, the backscatter increases again, but does not quite reach its 0800 value. This feature appears to correlate spatially with the occurrence of increased chlorophyll values.

5.9 Inorganic Nutrients

Nutrient concentrations obtained for station 276 (before the upwelling) and station 277 (within the upwelling), clearly demonstrate the source of the verdant primary production, assayed as chlorophyll, within the upwelling region transected by 276–277 (Fig. 18).

The cold water upwelling in this region was rich in the nutrients that fuel active photosynthetic activity in the photic zone. Figure 30a shows nitrate profiles for stations 276 and 277. At station 276, nitrate was depleted (below detection at 0.1 μmol) down to 80 m rising only to 2 μmol at 110 m. This is approximately consistent with the DCM which was centered at about 80 m. Station 277 was depleted in nitrate at the surface, but values of greater than the 10 μmol were found at 50 m.

The relative chlorophyll levels at the two stations almost exactly mirrored the nutrient levels (Fig. 30b). The DCM in the upwelling region was centered at 40 m depth and reached five times the concentration observed at station 276. The phytoplankton at 96 m on station 276, however, experienced only 1 μmol nitrate compared with 6 μmol at the same light level in the upwelling region. The 1% light levels at stations 276 and 277 were deduced from the *in situ* light profiles to be 96 and 45 m, respectively, and are consistent with the locations of the DCM. At both stations, the 1% light levels were slightly below the chlorophyll maxima.

5.10 Dissolved Gases

Figure 31 shows the ΔpCO_2, temperature, and (Turner) fluorescence-derived chlorophyll for the transect over the upwelling area. The data has been corrected for the temperature effects; however, it must be considered preliminary, since the final calibrations of the PRT in the Ocean

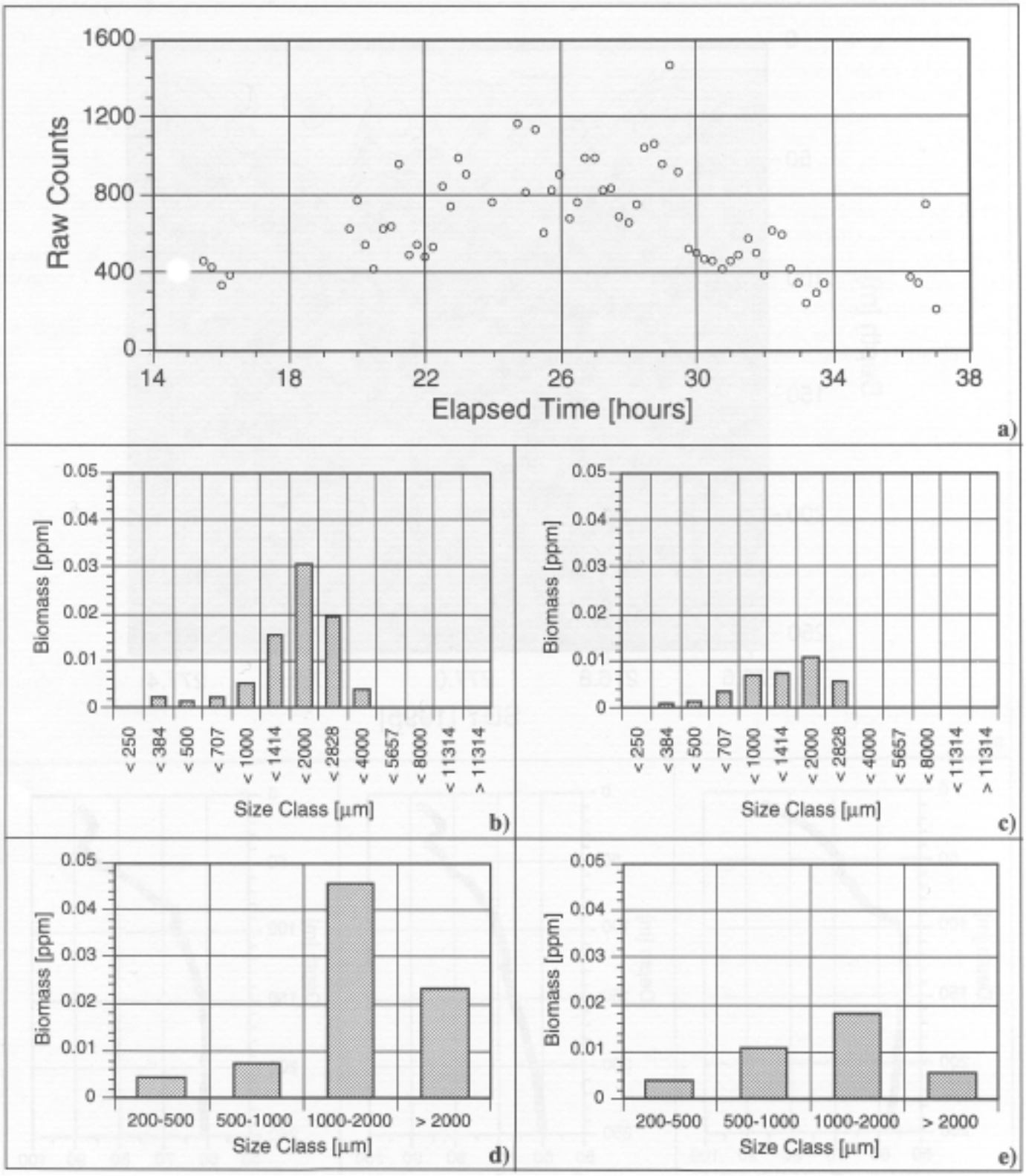

Fig. 28. Underway and net cast sampling results for SDY 276–277: **a)** raw counts of plankton (0.20–11 mm) from underway *surface* sampling (7 m) counted on the OPC beginning on SDY 276 at 1400; data from half an integrated (0–200 m) plankton net haul run through the OPC for **b)** station 276 and **c)** station 277; and OPC data expressed in JGOFS carbon size fractions for zooplankton biomass for **d)** station 276 and **e)** station 277.

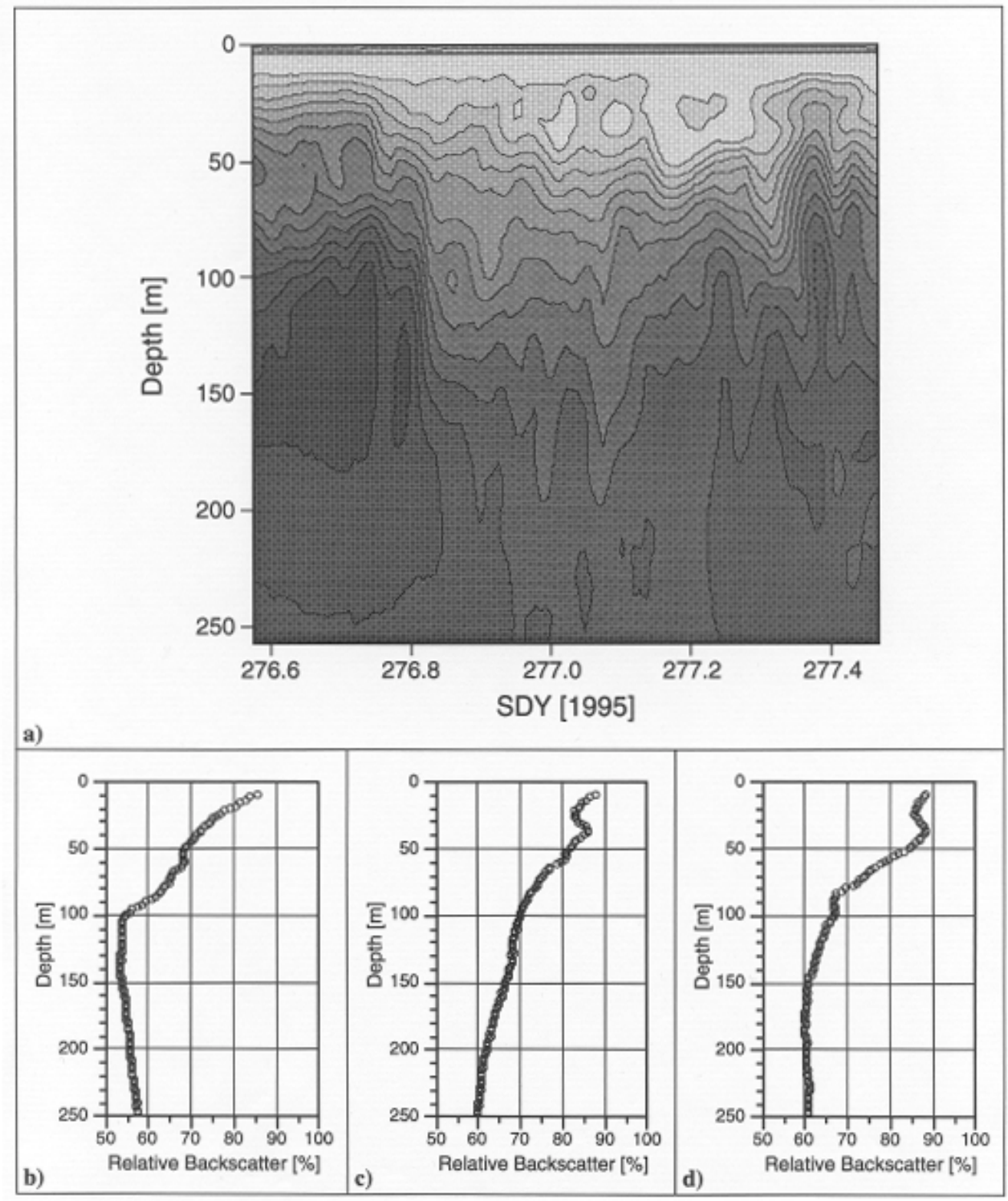

Fig. 29. ADCP relative backscatter profiles from SDY 276–277 (all times are in GMT): **a)** the entire time period, **b)** 1600 SDY 276, **c)** 0000 SDY 277, and **d)** 0400 SDY 277.

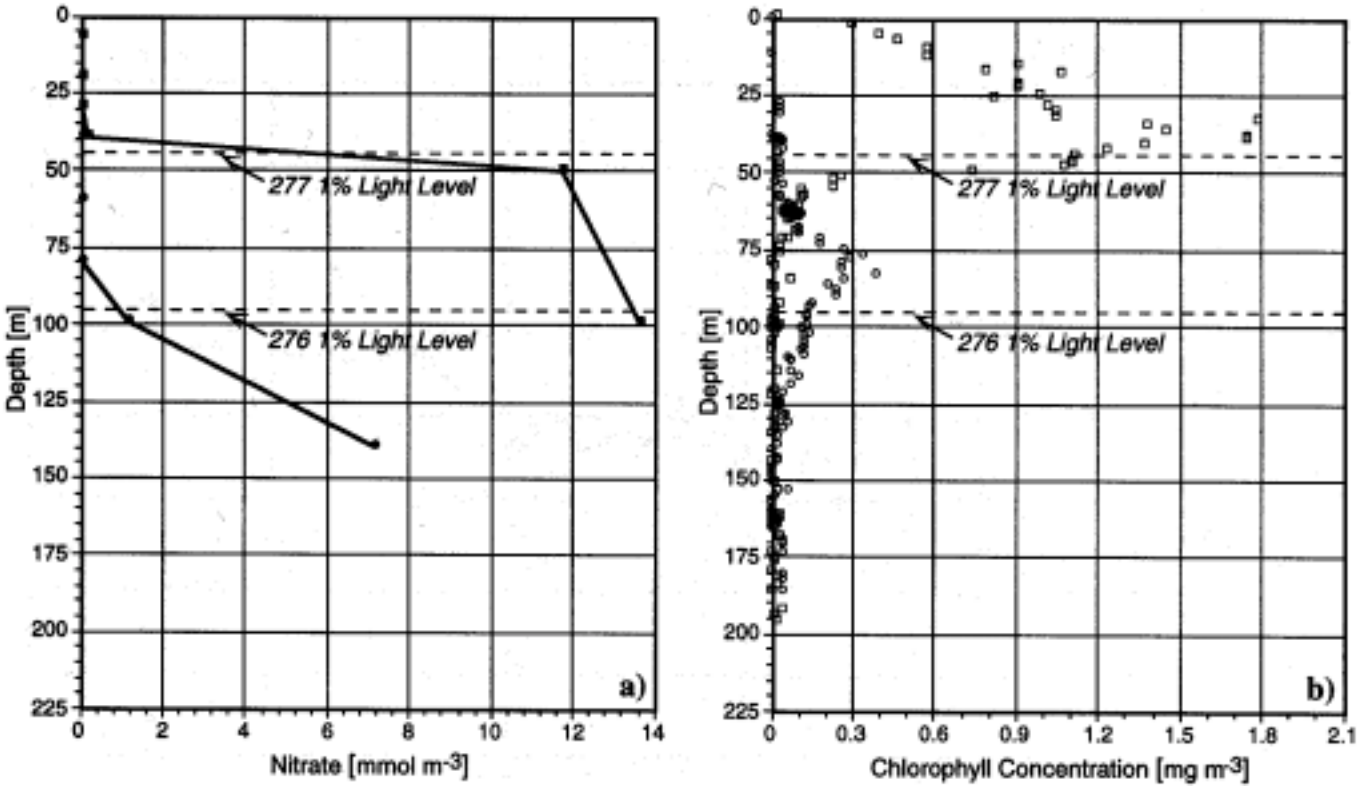

Fig. 30. Vertical profiles outside, station 276 (circles), and inside, station 277 (squares), the Mauritanian upwelling: **a)** nitrate, and **b)** chlorophyll. The 1% light levels for each station are given by the labeled dashed lines. The chlorophyll fluorescence sensor is only nominally calibrated, although, relative changes from day to day and through the water column are representative. Chlorophyll quenching is not significant at the 1% light level.

Logger system and the PRT in the pCO_2 system are not yet available. Temperature errors lead to a 4% pCO_2 rise per °C. Since it is unlikely that the combined error of the Ocean Logger and pCO_2 system is greater than 1°C, the overall error in the ΔpCO_2 is around $\pm 20\,\mu$Atm, given the prevailing air pCO_2. The ΔpCO_2 shows no change in the early part of the transect, despite the increase in chlorophyll at 23.5°N.

It is encouraging to note there is no change associated with the increased SST around 23°N. The ΔpCO_2 shows a marked change at 19.5°N associated with the upwelling and increased chlorophyll fluorescence. The change shows a significant rise in the air-sea pCO_2 difference, which is greater than the possible instrument temperature error. This would indicate that in this region, there is a significant instantaneous net air-to-sea CO_2 transport. Depending on the subsequent rate of primary production, this could lead to a net carbon flux.

6. CRUISE SYNOPSIS

This section reviews preliminary results for the data compiled to illustrate the hydrography, biology, and chemistry of most, if not the whole transect. Many of the figures within this section give an immediate *flavor* of the contrasting water masses and regions of productivity which the JCR passed through during the approximately 8,000 nmi transect.

The cooler, more productive waters of the North Atlantic (around 47°N) soon gave way to warmer, clearer (less productive) waters north of the upwelling off Mauritania. The 24 hour transect discussed earlier between stations 276 and 277 (i.e., between 23°N and 19°N) can be put into the context of the upwelling as a whole when related to this section. South of the Mauritanian upwelling, there is clear evidence of the equatorial upwelling; this is the least well described feature in this region, however, because sampling was mostly carried out on each side of it.

The *clear blue* waters of the first southern latitudes provided increasingly clear waters with increasing light penetration, resulting in a deepening chlorophyll maximum. The latitudinal trend developed as the transect headed south and productivity increased as the transect sampled towards the confluence of the Brazil and Falkland Currents. Other preliminary results within this section show clear changes on productivity and population structure, since the transect crossed so many oceanic provinces.

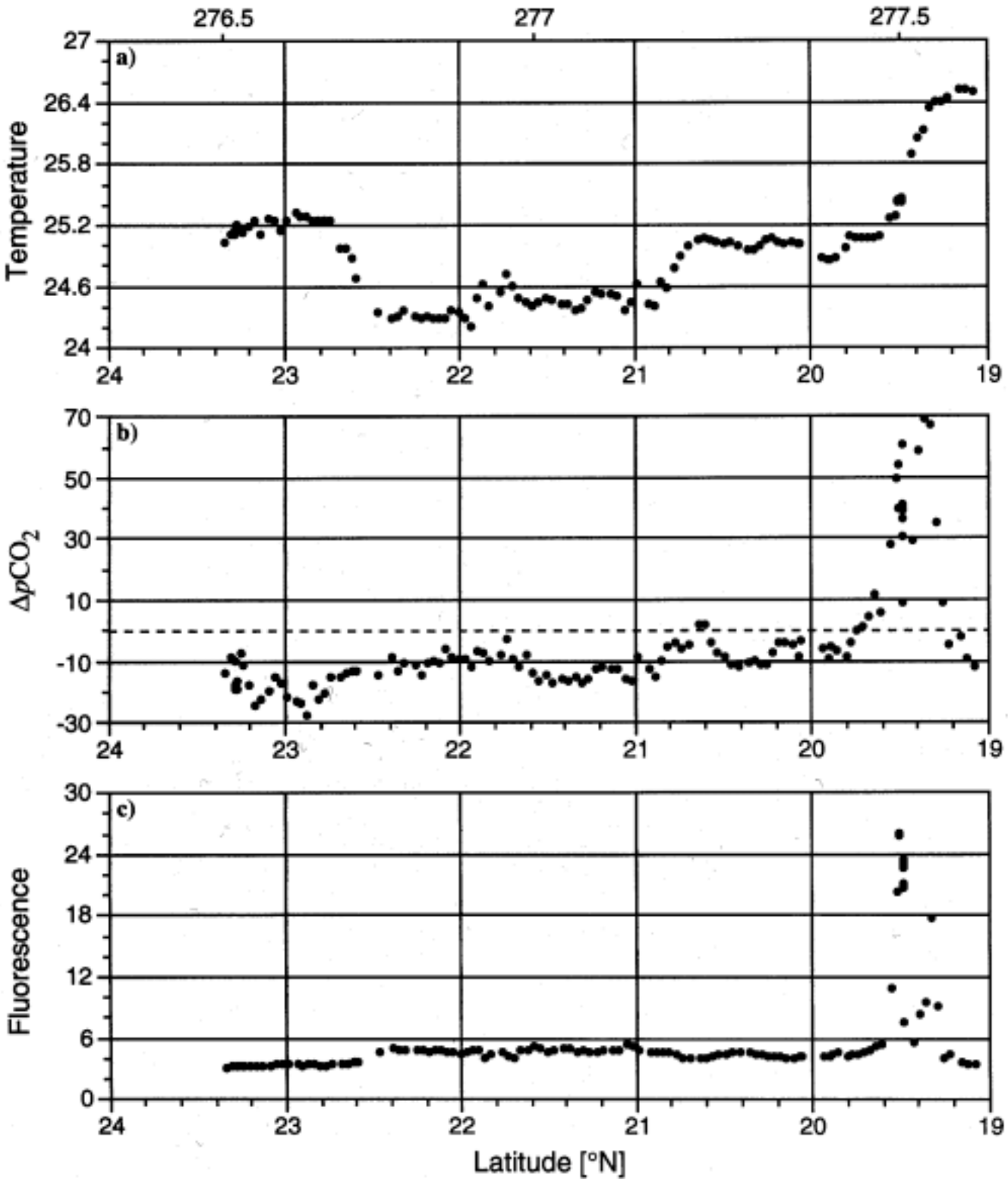

Fig. 31. Dissolved gases results for along-track tow 276–277, inclusive: **a)** SST (°C), **b)** ΔpCO_2 (provisional μAtm), and **c)** fluorescence (relative units).

6.1 At-Sea Calibrations

The measurements of temperature and salinity obtained from the CTD, SBE thermosalinograph, and underway SST sensors were compared with the calibration values. The CTD temperature value is not easy to compare accurately without taking careful precautions because of the thermal mass of the CTD rosette package and the large thermocline gradients encountered in some oceanic regions. Nevertheless, with the exception of a few outliers, which may be associated with less than optimum temperature equilibration times, the mean of CTD temperature error relative to thermometer values (Fig. 32a) imply that the CTD reads high by +0.016°C ($1\sigma = 0.038$). The error for the salinity value derived from temperature and conductivity sensors on the CTD throughout AMT-1 are shown in Fig. 32b. Apart from one or two outliers, which can be attributed to the motion of the CTD rosette package near the sea surface, the mean error in salinity determined for this instrument is +0.001 ppt ($1\sigma = 0.004$) of the value determined by the Autosal instrument throughout the survey.

Precise calibration of the underway temperature sensor is not completely reliable using comparisons with reversing thermometers on the CTD, as adopted here. This is because the underway data became noisy when the vessel was stopped and maneuvering on station, which may be related to mixing of surface water with deeper waters as a result of propeller and thruster action or, possibly, to the incorporation of engine cooling water into the uncontaminated seawater supply. Nevertheless, discounting obvious outliers in Fig. 32c, the temperatures recorded by the underway system can be seen to be only very slightly higher than the thermometer readings. The majority of values being scattered between 0.02–0.06°C higher than those measured by thermometer at a depth of 7 m (similar to the pumped supply inlet). There was no trend with time over 22 days and the mean error was +0.034°C ($\sigma = 0.035$). The relationship between salinity, temperature, and conductivity used to compute salinity for the uncontaminated seawater thermosalinometer was the standard RVS, `SAL83` equation after Culkin and Smith (1980). The salinity errors measured in this way are consistently scattered close to zero error (relative to the salinity bottle values), as shown in Fig. 32d, with a mean of −0.005 ppt ($\sigma = 0.012$).

6.2 Transect Overview

The preliminary (mostly uncalibrated) data in this section reviews the transect as a whole from the temperate North Atlantic waters of 47°N to the spring conditions of the South Atlantic (down to 50°S). The temperature structure for the transect from 47°N to 50°S is illustrated in Figs. 33–34. The data in Fig. 33 is from XBT profiles (to a depth of 760 m) and show the extent and depth of stratification along the transect, with the strongest thermocline being found around the equator, particularly to the south of it. The importance of sampling high variability regions with a higher frequency of instrument deployments is shown in Fig. 33b, which clearly shows the presence of a warm core ring. In comparison, the coarser (basically daily) sampling in Fig. 33a does not adequately resolve the ring. The temperature of the entrapped core water of the ring was 5°C higher than the surrounding water of the Falklands Current. Figure 34 shows another latitudinal temperature summary, only this time the data is derived from the UOR casts (for the top 200 m). The contoured data clearly shows the cooler, less structured waters of the higher latitudes and is compatible with the other data sets which sampled the top 200 m.

The hydrographic summaries (Figs. 33–34) clearly show the upwelling region between 20°N and 10°S, which is also well represented in the chlorophyll and nitrate data given in Figs. 35a and 35b, respectively. The underway (towed) UOR data for chlorophyll fluorescence were only of value in the extreme northern and southern latitudes, and in the upwelling region. This was because the maximum depth achieved with the towed body was generally not sufficient to define the DCM in the central oceanic basins; however, fluorescence profiles were obtained to depths of 200 m using the UOR deployed as a profiling instrument on each daily station.

When contoured, the chlorophyll *a* concentration data (Fig. 35a) clearly show a latitudinal trend which is consistent with the nitrate distribution shown in Fig. 35b. From 50°N to the center of the mid-Atlantic basin (approximately 30°N), the depth of the DCM decreased from around 40 to 90 m as productivity fell in response to low nutrient levels (Fig. 35b). This trend was reversed in the Mauritanian upwelling region (20°N) where enhanced nutrient supplies gave rise to high chlorophyll fluorescence levels between 10–50 m. In this situation, productivity was inhibited at greater depths even though the nutrient supplies were in excess because of the degree of light attenuation caused by the concentrated phytoplankton population. From the upwelling region to the center of the Brazilian basin, the depth of the DCM increased, reaching a maximum depth of 150 m at 18°S before decreasing with increasing southerly latitude.

From 30°S, productivity was greatly enhanced by the nutrient-rich waters of the Falklands Current and in these conditions, as in the upwelling region, the depth of the DCM decreased (10–80 m). The high chlorophyll fluorescence at the southern end of the transect is also associated with high levels of nutrients, but these result from the over-wintering mixing processes associated with the dynamics of the temperate Southern Ocean. Samples for phytoplankton taxonomy were taken and experiments for primary production were carried out along the whole of the transect. When fully analyzed, these data will help expand the chlorophyll fluorescence data profiles. Preliminary data from both the FRRF and primary production

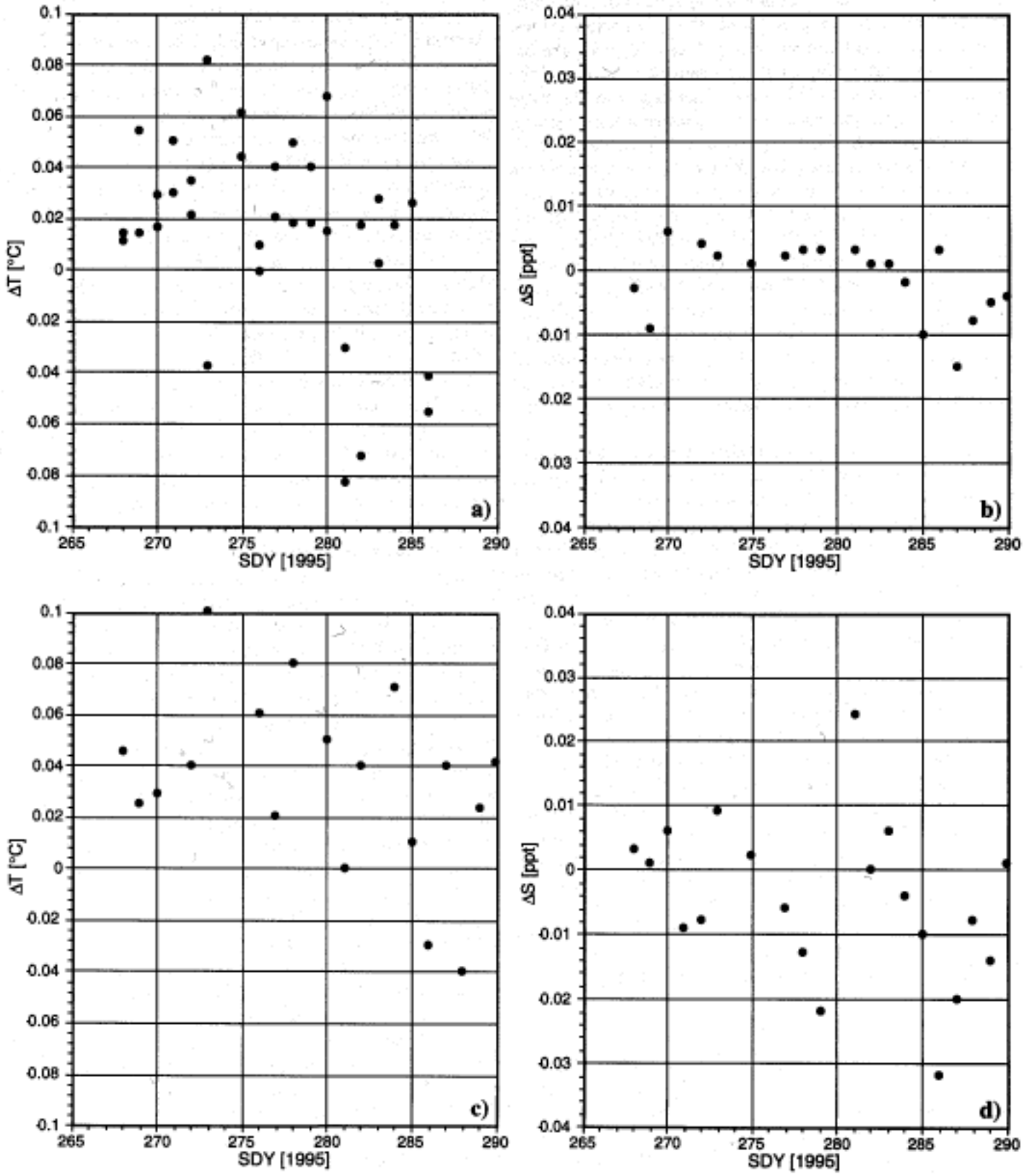

Fig. 32. a) CTD temperature, **b)** CTD salinity, **c)** Ocean Logger temperature, and **d)** Ocean Logger salinity.

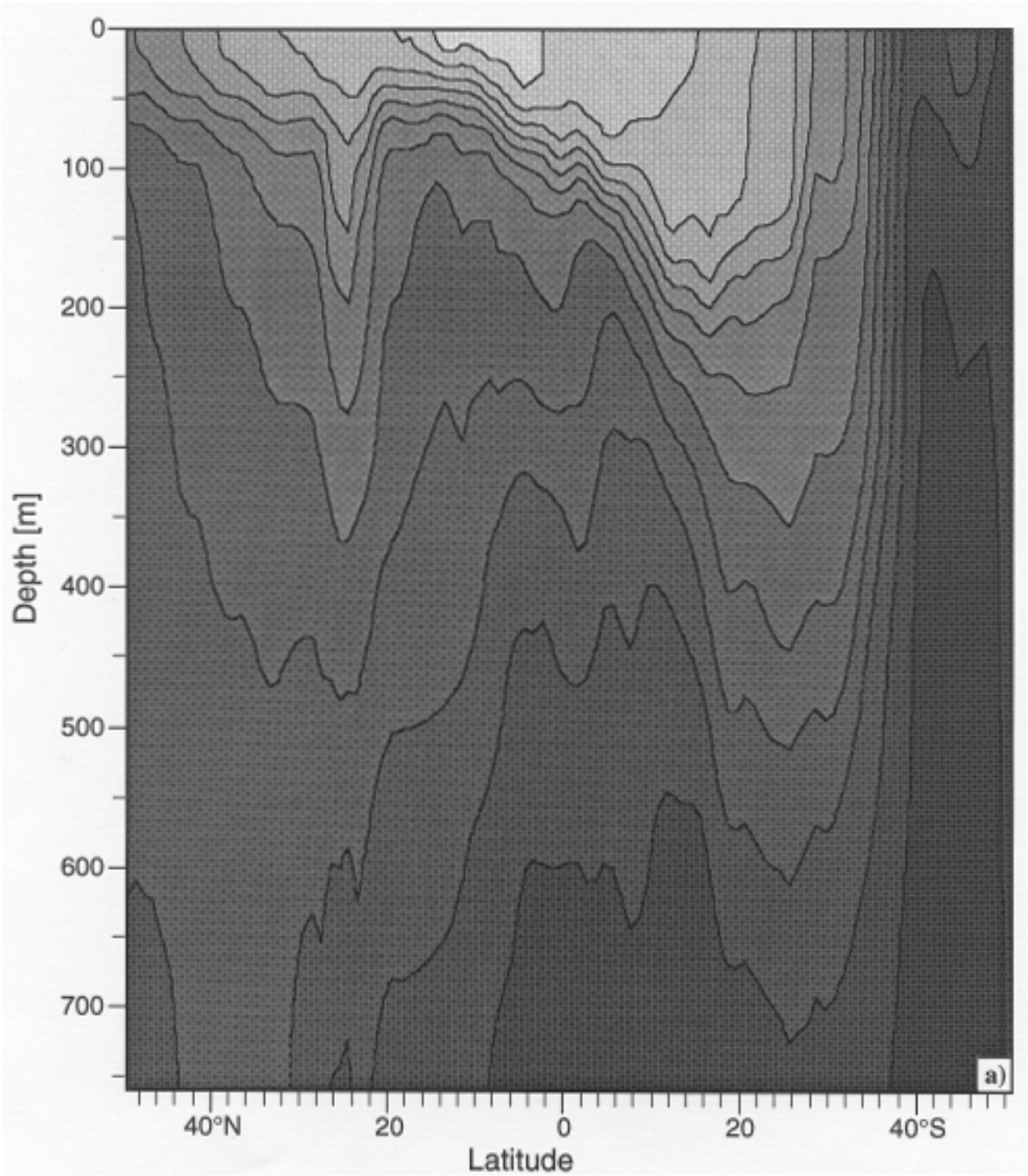

Fig. 33a. The temperature structure along the AMT-1 cruise track as determined by XBT data.

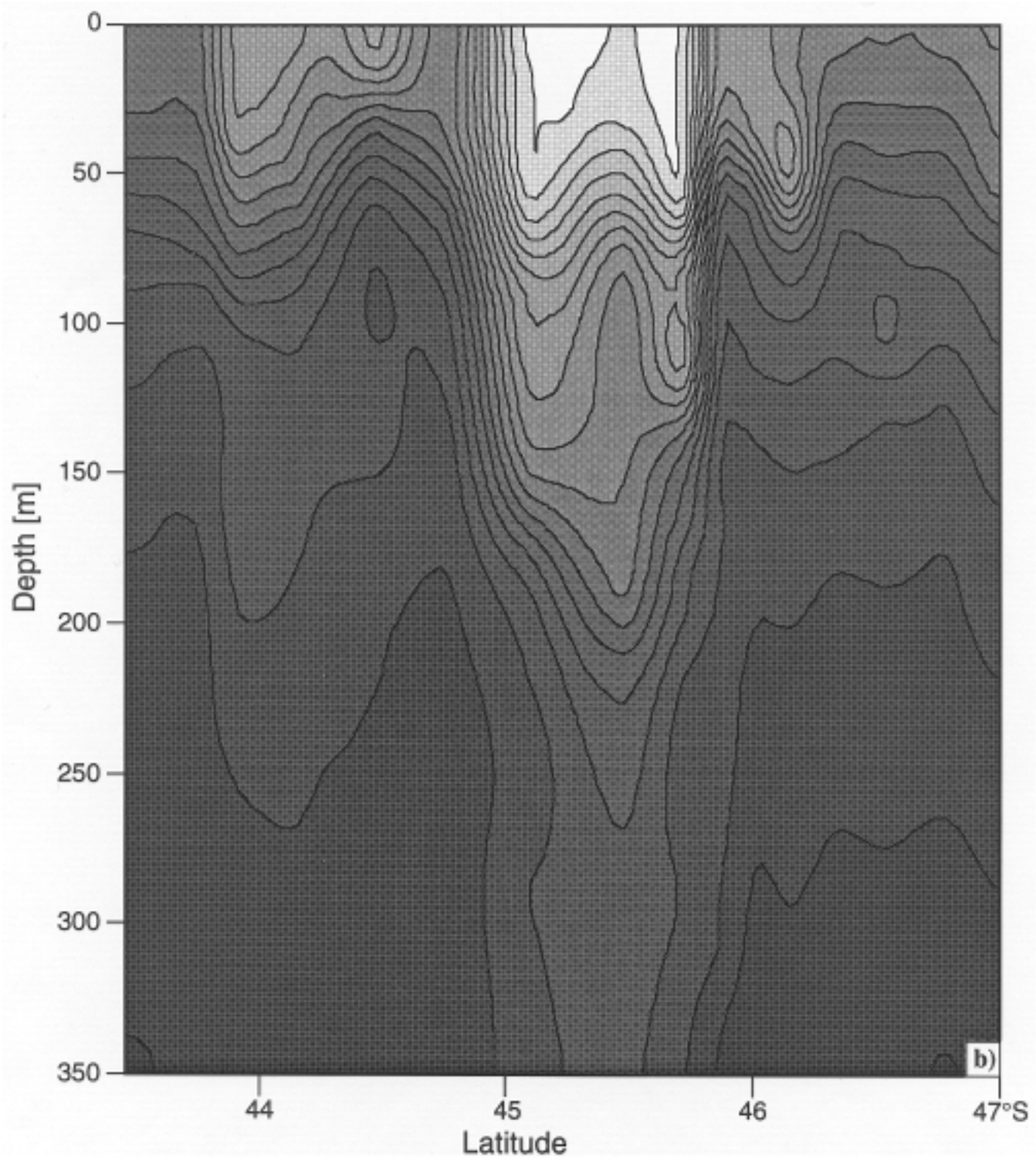

Fig. 33b. A higher spatial resolution of part of the data presented in Fig. 33a. The data shown corresponds to when the JCR was transiting a Brazil Current warm core ring.

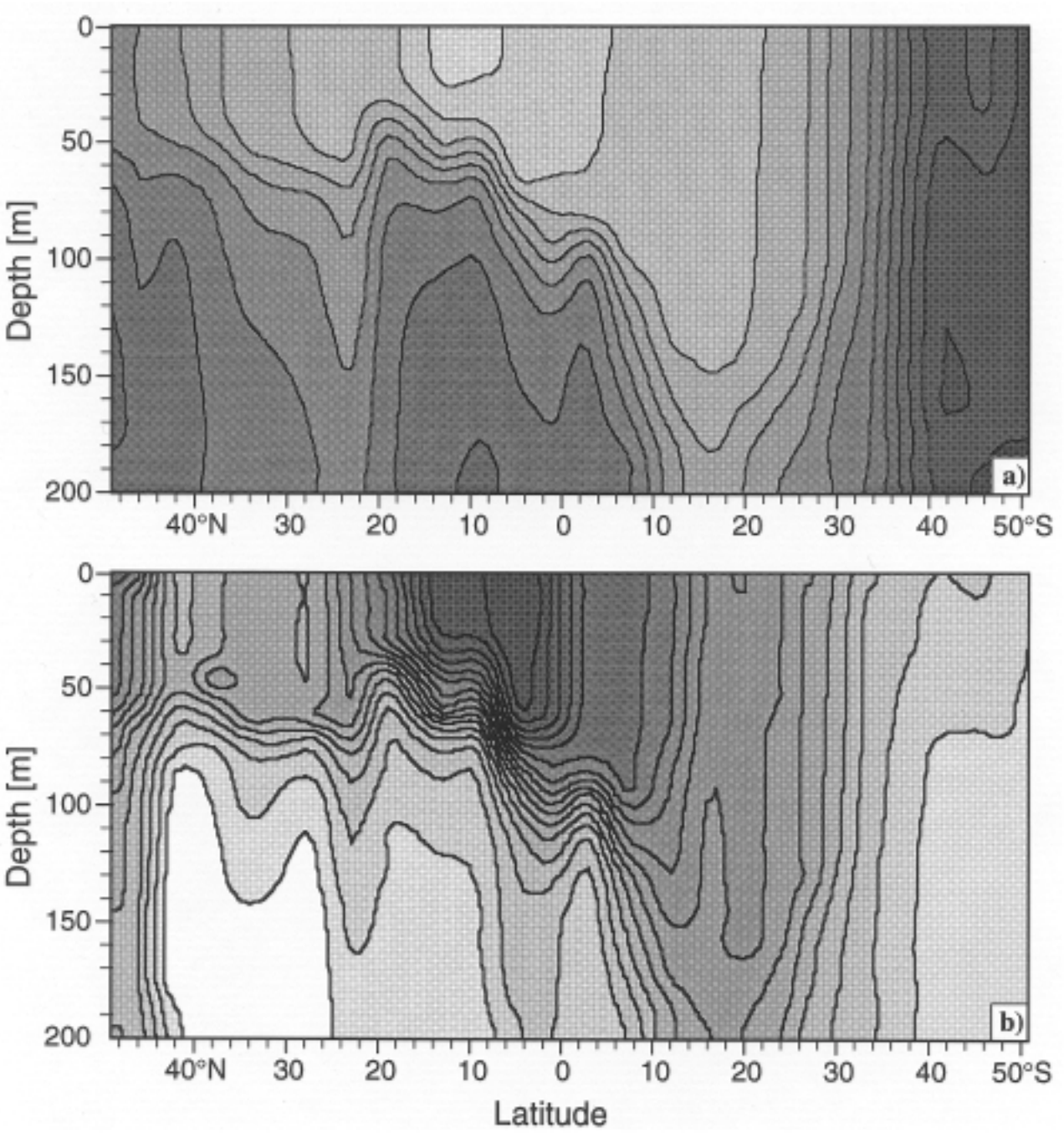

Fig. 34. UOR casts: **a)** temperature (°C), and **b)** density. The contour interval for the former is 2°C with light tones corresponding to high temperatures (white is 30°C and above) and dark tones to low (dark gray is 4°C and below); the contour interval for the latter is 0.25 with light tones corresponding to high density (white is $\sigma_t = 27$ and above) and dark tones to low (dark gray is $\sigma_t = 23$ and below).

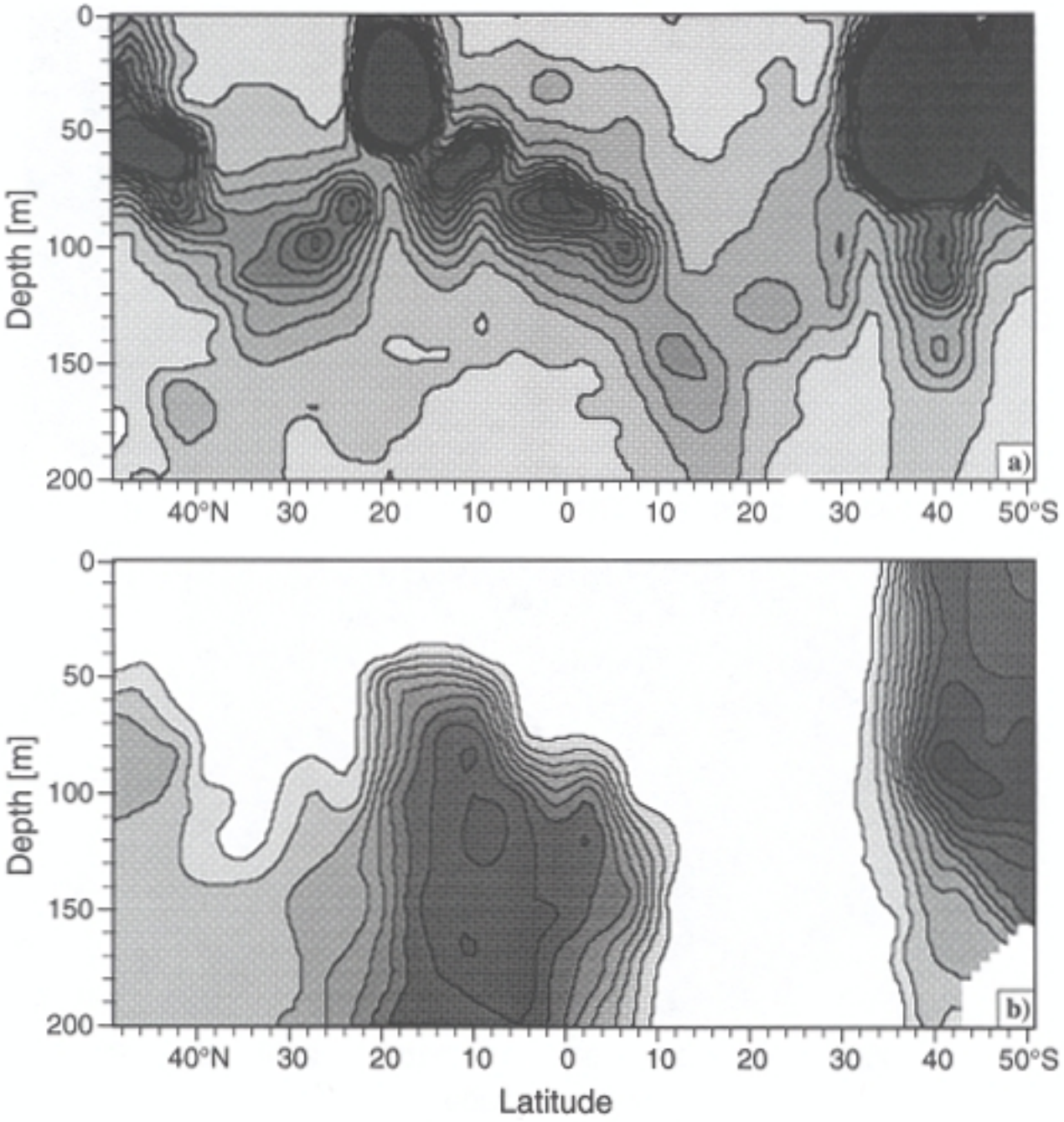

Fig. 35. Transect overviews of **a)** chlorophyll *a* concentration, and **b)** nitrate concentration. The contour interval for the former is 0.05 with light tones corresponding to low concentrations (white is 0.00 and below) and dark tones to high (dark gray is 0.50 and above); the contour interval for the latter is 2 with light tones corresponding to low concentrations (white is 2 and below) and dark tones to high (dark gray is 22 and above).

were analyzed on board and are included here to give additional detail to the production regimes that were sampled during the transect.

Figure 36 shows F_m and quantum yield plotted versus depth and station (Figs. 36a and 36b, respectively). Both plots are compilations of data taken during profile casts, and it should be noted that since both F_m and $\Delta\Phi_{\max}$ are affected by ambient irradiance, the structures shown in these plots to some extent contain artifacts of the light regime in the water column for each individual cast.

FRRF maximum fluorescence (F_m) is presented here as an indication of phytoplankton biomass versus depth for the rosette profiling operations. The FRRF was one of three different fluorometer designs used during AMT-1 to profile the water column in terms of fluorescence for each daily station, and although each fluorometer is designed to measure a different aspect of phytoplankton fluorescence, a certain amount of correlation may be seen in all of the data sets. One pattern, however, which has been observed in the FRRF data set is the structure of the phytoplankton beneath the upwelling feature of stations 276–280 at depths of 150–200 m.

Coinciding with the F_m feature described above, a formation may be observed injecting into the upwelling region directly underneath the surface-defined *location* of the Mauritanian upwelling (center is at station 277) in the plot of quantum yield. At the base, this physiological feature is roughly twice as wide as the surface of the upwelling. In essence, the injection is an extremely low $\Delta\Phi_{\max}$ mass of water being brought up from depth in the transport of the upwelling. The cusp of this structure falls directly beneath the upwelling, and the southern *shoulder* of this injection correlates well to the thermocline characteristics of the water (as seen in temperature contour plots elsewhere) as well as the station chlorophyll contours provided by the UOR. In the previous analysis of the upwelling station, it was noted that the station was conducted on an anomaly inside the upwelling, and, thus, might not be a good representation of its photosynthetic characteristics. Analysis of the entire transect in the manner presented here shows a very definite trend underneath the upwelling on a much larger scale than would be indicated by smaller scale upwelling studies.

As mentioned, a major factor affecting quantum yield values produced by FRRF measurements is high-level ambient irradiance. Midday stations, planned to coincide with solar noon, best illustrate the effects of long-term nonphotochemical quenching (i.e., photoinhibition) throughout the transect. The general trend for the midday samples is typical: quantum yield increases with depth, due to the fact that photoinhibition is a surface phenomenon. Throughout the transect, however, it can be noted that at no station was quantum yield close to the theoretical 0.65 dimensionless maximum. This would suggest that even though various upwellings and coastal regions might provide phytoplankton with an excess of nutrients, in no area throughout the transect were optimal quantum yields observed in daytime. Maximum observed daytime $\Delta\Phi_{\max}$ reached approximately 0.55 in a few places; surface $\Delta\Phi_{\max}$ generally ranged from 0.20–0.40 over the transect. A more detailed analysis of nighttime recovery trends will be completed in order to better understand the surface (7 m) characteristics and their implications for the midday samples.

Integrated chlorophyll *a* concentration ranged between 20–70 $\mathrm{mg\,m^{-2}}$ during most of the transect, reaching higher values (greater than 100 $\mathrm{mg\,m^{-2}}$) in the Mauritanian upwelling region at approximately 20°N(Fig. 37a). Higher variability was observed in the distribution of the integrated primary productivity (Fig. 37b). Carbon fixation rates reached extremely low values (less than 5 $\mathrm{mgC\,m^{-2}\,h^{-1}}$) in the 25–35°N region. Maximum primary production took place at 20°N and 33°S, where values around 70 $\mathrm{mgC\,m^{-2}\,h^{-1}}$ were measured. An increase in primary productivity was observed in the southern part of the transect, which was due to an increase in both phytoplankton biomass and photosynthetic efficiency. The average photosynthetic rate for the whole transect was 20.5±4.0 $\mathrm{mgC\,m^{-2}\,h^{-1}}$, which yields a rough estimate of primary production for the area covered by this transect of about 0.2 $\mathrm{gC\,m^{-2}\,d^{-1}}$.

Interestingly, the relationship between photosynthesis and chlorophyll concentration was not constant and showed a remarkable variability ranging from less than 0.2 $\mathrm{mgC\,mgChl^{-2}\,h^{-1}}$ at 25–35°N to 1.5 $\mathrm{mgC\,mgChl^{-2}\,h^{-1}}$ at 33°S. Very low values of photosynthesis were measured at 25–35°N without a significant decrease in chlorophyll levels. It is difficult to explain this observation at this preliminary stage. Differences in the taxonomic composition of the phytoplankton assemblages, however, could account for the observed uncoupling, given that both chlorophyll content and photosynthetic efficiency are strongly size dependent. Maximum chlorophyll concentration was found at 20°N, coinciding with the upwelling of nutrient-rich waters. The photosynthesis-to-chlorophyll ratio was higher at 13°N than at 20°N, however, which suggests phytoplankton to the south of the upwelling area had a better physiological state. It could be argued that phytoplankton in the upwelling region had been brought to the surface recently, so microalgae were not acclimated to high irradiance conditions. The results from a P-I experiment, however, showed subsurface phytoplankton in the upwelling region were well adapted to high light conditions, showing no photoinhibition at an irradiance as high as 900 μE m−2 $\mathrm{s^{-1}}$ (Fig. 25c).

Alternatively, the differences in the photosynthetic performance of phytoplankton between 13–20°N could be a result of a change in the taxonomic composition of the phytoplankton assemblage. In fact, the size distribution of chlorophyll concentration changed dramatically from a dominance of large cells at 20°N towards a dominance of small cells at 13°N (Fig. 26). A higher photosynthetic efficiency by smaller phytoplankton could, therefore, account for the increased photosynthesis-to-chlorophyll ratio observed at 13°N.

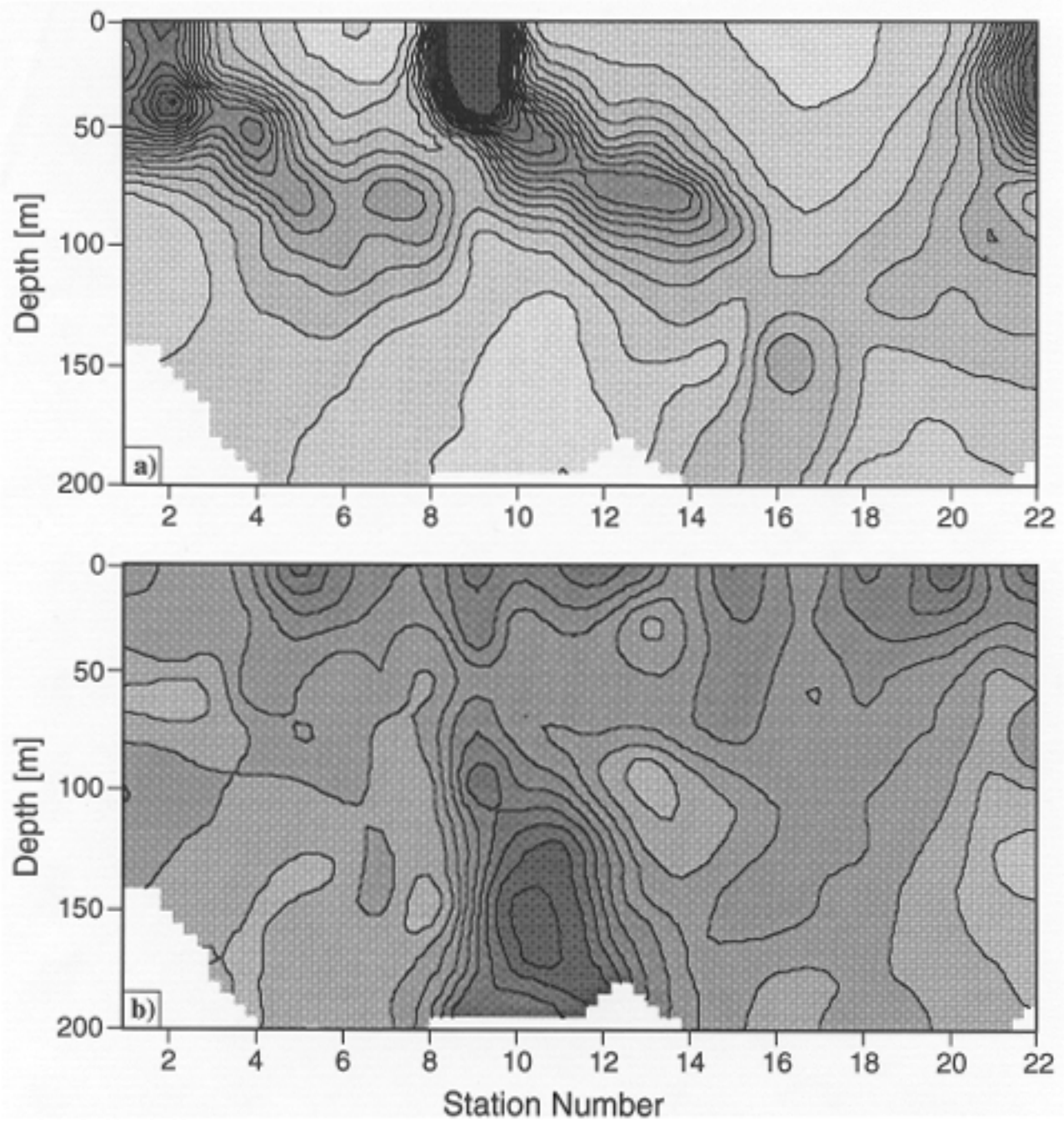

Fig. 36. Latitudinal compilations of **a)** F_m, and **b)** quantum yield as a function of depth. Both plots are derived from FRRF measurements.

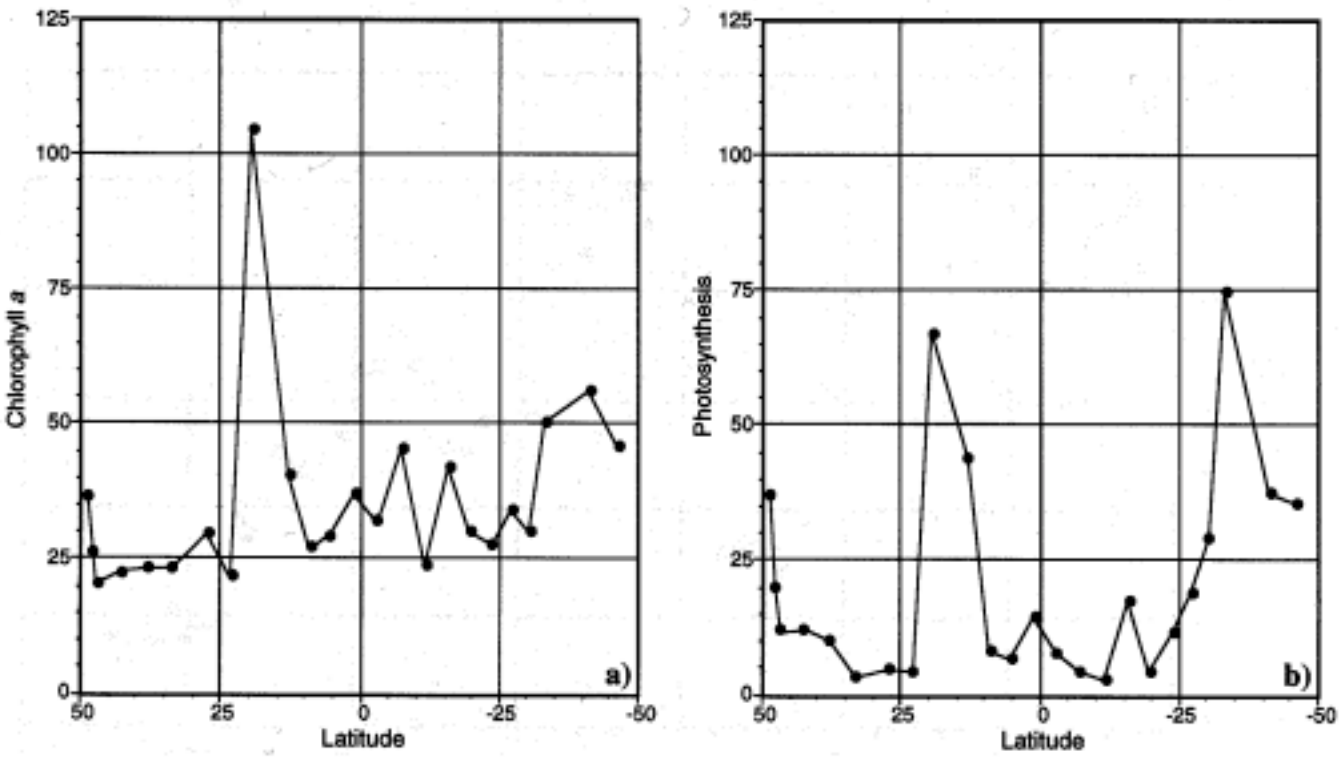

Fig. 37. Latitudinal distribution of **a)** integrated chlorophyll *a* concentration ($\mathrm{mg\,m^{-2}}$) and photosynthetic rate ($\mathrm{mg\,m^{-2}\,h^{-1}}$) along the cruise track.

Further processing of the obtained data, including determination of the phytoplankton species composition, will be necessary in order to fully understand the differences between chlorophyll and primary production distribution. Evaluation of this uncoupling at a basin scale will hopefully provide a tool to improve primary production estimates through remotely sensed ocean color.

Data on the surface dynamics of pCO_2 are shown in Fig. 38a. Surface data for pCO_2 shows the feature examined in Section 5 at 20°N and puts this into the context of the transect as a whole. The data highlights the areas of *drawdown* as opposed to net release of CO_2, and it can be seen that although the area examined in Section 5 showed substantial local drawdown, the major net CO_2 drawdown takes place between 10°N and the equator and with increasing chlorophyll levels at the southern end of the transect.

The transect will yield new and important data on the size-fractionated carbon of particulate and zooplankton biomass over latitudinal scales, i.e., along the transect. This will be important in understanding biogeochemical processes in relation to production regimes along the transect. Preliminary data from the OPC presented in Fig. 38b shows the total biovolume for the zooplankton in the top 200 m of the water column along the transect. These uncalibrated data have been divided into the standard size classes for JGOFS studies. In the future, these data will be compared to carbon values taken from each station in order to fully characterize the zooplankton community structure.

During the transect south of Montevideo, the waters were considerably cooler than the water on the southern end of the Brazil Current. This cooler Falklands Current water forms a dynamic boundary when it swings east after meeting the Brazil Current. Occasionally, in areas of frontal activity where there are many forces at work creating eddies and gyres, water from one origin becomes entrapped in that of another.

The data presented here and in conjunction with samples to be analyzed back in the laboratory represent a unique description of both the biogeochemical provinces of the Atlantic Ocean and the production regimes over nearly 8,000 nmi. Much of the background data included in this report will be used to interpret and understand the various dynamic processes at work in the contrasting waters of both the North and South Atlantic Oceans.

7. DISCUSSION

Initial discussions between PML and BAS about the concept of using the JCR for a translatitudinal study during her passage through the Atlantic Ocean were endorsed by approval for NERC funding in the summer of 1995. Although it was good news that the first AMT cruise was going to be sooner rather than later, there were both scientific and logistic hurdles to overcome in a very short amount of

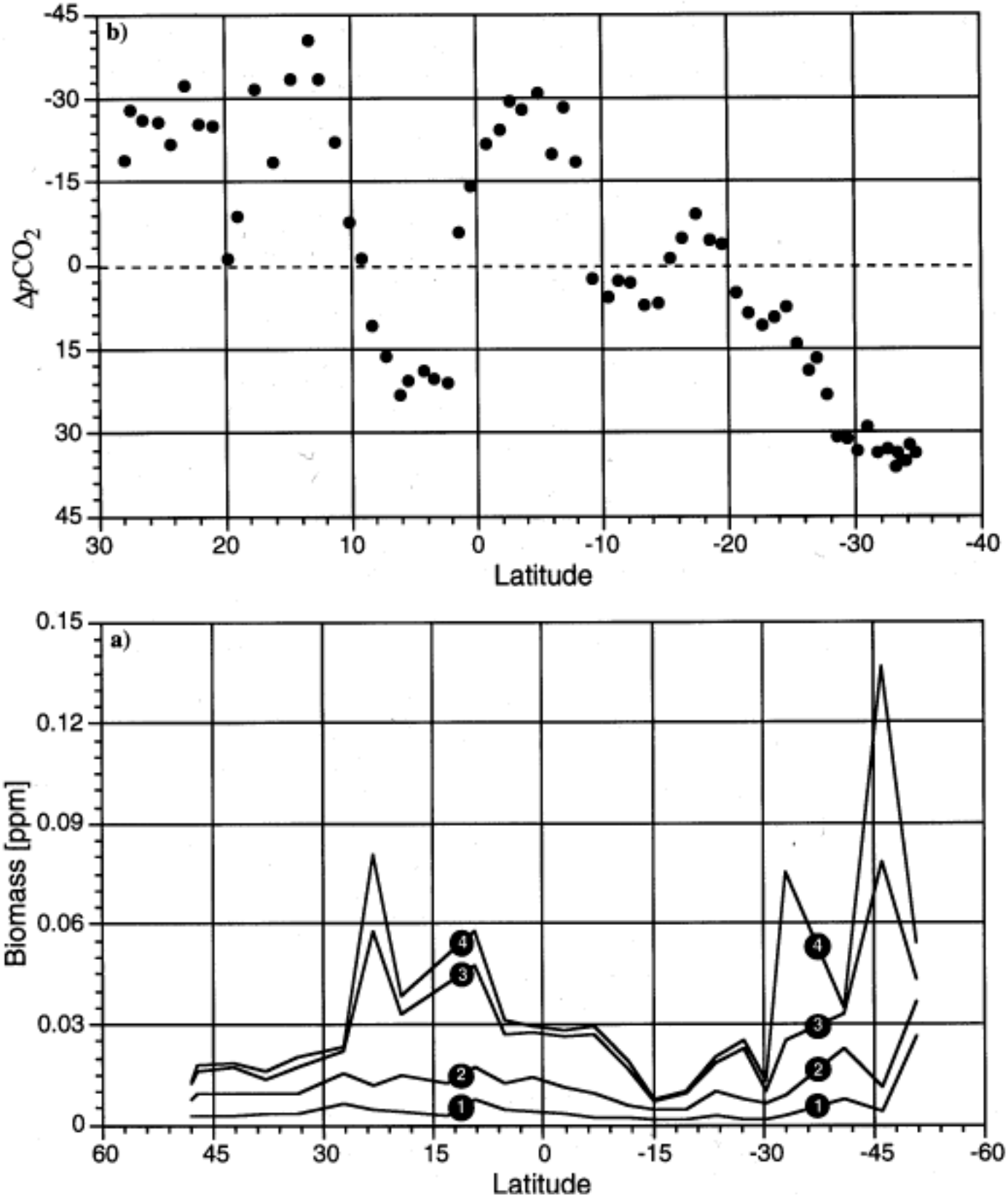

Fig. 38. Latitudinal compilations of **a)** ΔpCO_2, and **b)** biomass. For the latter, the size fractionation codes are as follows: 1 for 200–500 μm, 2 for 500–1,000 μm, 3 for 1,000–2,000 μm, and 4 for greater than 2,000 μm.

time. Some of the problems identified within this cruise report are almost entirely due to the short preparation time before the cruise. With fixed personnel resources and limited time, many seemingly mundane tasks required urgent or immediate attention, which reduced the opportunities for testing and commissioning new or borrowed equipment. This was particularly true for the pCO_2 system, which was substantially overhauled on board to correct a catalog of faults, as well as for some of the optics equipment, notably the PRR sensor which was supplied with incorrect wiring diagrams by the manufacturer. All of these problems in themselves, and with sufficient time, would not pose a major problem to an experienced team, but the cumulative effect of so many unforeseen problems had major implications for data acquisition at the start of AMT-1. Fortunately, this cruise report can claim valid and interesting data from all the equipment which proved troublesome in the early stages of the cruise, which is a clear testament to the scientists involved.

7.1 Lessons Learned

The short preparation time was also the reason for not working in any territorial waters during AMT-1, other than those of the UK. An application to the appropriate UK authorities requesting permission to sample in various territorial waters along the 20°W meridian (e.g., from Madeira to Senegal) and along the South American coast, was turned down on the grounds that the authorities involved required six months notice. Consequently, the program was modified to avoid these waters or to suspend station work or towing while in such waters. The area most effected by this was the upwelling region off West Africa, where a 390 nmi long area could not be worked. In an effort to derive the most useful science from these sampling restrictions, stations at the northern and southern edges of the upwelling region were scheduled and achieved (without interrupting the normal progress of the ship). Although both stations met *in situ* optical criteria for sun angles, potentially valuable data was not gathered in the intervening waters of the upwelling. Future AMT cruises will endeavor to secure permission to work in such waters given a sufficiently long cruise preparation time.

Most of the problems encountered with the optical sensors would have been obviated had there been sufficient time to test the equipment before sailing. As discussed earlier, preparation time for AMT-1 was extremely limited, and most of the time was spent ensuring the timely arrival of the equipment. The Satlantic sensors, for example, arrived a few days before the truck carrying the PML gear left for Grimsby. An important lesson is delays in funding require heroics just to schedule the availability of equipment and personnel and no time is left for testing the viability of the at-sea systems. The ensuing problems have to be resolved at sea, which necessarily reduces the likelihood of success and the amount of data collected.

7.2 Future Plans

Support for the AMT cruises has high priority for several reasons:

1. It provides an excellent mechanism to perform calibration activities related to intra-orbit variations of satellite sensors, since the same instruments can be used at high northern and southern latitudes. (This is especially important to establish whether there is any instrument bias involved in the significant differences between northern and southern hemisphere chlorophyll and productivity.)
2. It crosses six distinct biogeochemical oceanic provinces: the seasonally mixed North Atlantic, the North and South Atlantic central gyres, the North Equatorial Counter Current (NECC) and Amazon plume region, the equatorial upwelling regime, and the Antarctic frontal regions.
3. The cruise track encounters several distinct aerosol types, including those in the Northern Hemisphere, Saharan dust, and the more pristine South Atlantic, thereby offering a unique opportunity to address multiple atmospheric correction issues during one cruise.
4. The cruise also transects the Southern Anomaly which might impact the performance of polar orbiting satellites.
5. Coccolithophore enriched waters will be experienced at both ends of the transect.
6. The end points will be useful (but not definitive) for examining low sun angle effects on atmospheric corrections.

Support from the SIMBIOS Project will be for additional ship time to extend observations, standard equipment, shipping, and logistics. Participation by scientific personnel for data collection and analysis will be solicited for investigations to complement those planned by the current AMT group, including sun-photometry and profiles of apparent and inherent bio-optical properties on station. Extra days may be available to enable the transect to extend to 60°N (and perhaps with additional funds, to the north of Iceland).

Acknowledgments

The organization and implementation of a program such as AMT cannot be achieved without a dedicated team of people. In addition to the personnel sailing on AMT-1, there were those who have, and will continue to have, an important role in the success of the program. In particular, Jim Aiken was largely responsible for the initiation of the AMT program and maintained close contact with the ship and its personnel during the cruise, providing much appreciated advice, support, and encouragement. Malcolm Woodward provided his logistical expertise whenever it was needed and was an essential part of setting up the nutrient analyses.

Most importantly, Brian Hinde and NERC are acknowledged for their support in bringing the AMT program into reality.

Several colleagues at BAS are also deserving of commendation; without their support the AMT program would not have been possible. In particular, Barry Heywood, Frank Curry, John Hall, Graham Hughes, Julian Priddle, and Andrew Clarke are all thanked for their contributions. As on so many occasions, PML provided the underlying logistic and scientific support for many on board for which the director of PML is gratefully acknowledged. Support from NASA before and during the cruise was also excellent. Elaine Firestone, Dan Endres, and the rest of the SeaWiFS Project are all thanked for their efforts to ensure the success of AMT-1.

The success of any cruise depends upon a first-class ship and crew plus a wee bit of good luck. AMT-1 was fortunate to have an excess of the former and just enough of the latter to ensure the scientific goals were achieved. The RRS *James Clark Ross* is an exemplary research platform, not only because of the spacious and well equipped scientific facilities, but more importantly, because of her fine officers and crew. The scientific party is pleased to acknowledge the high level of professional competence continuously demonstrated by the ship's personnel (Table A1). In particular, Chris Elliott, John Harper, Stuart Wallace, Brian McJury, Ken Olley, and Robbie Watson were a continuing source of assistance and distinguished themselves repeatedly.

Appendices

Appendix A

RRS *James Clark Ross*

This appendix presents a summary of the scientific spaces, facilities, and equipment on board the RRS *James Clark Ross*.

AMT-1 Crew List

The 26 crew members of the the RRS *James Clark Ross* during AMT-1 are listed in Table A1.

Table A1. The crew list for RRS *James Clark Ross* during AMT-1.

Name		*Rank*
Elliott	Christopher	Master
Harper	John, R.	Chief Officer
Wallace	Stuart, I.	Second Officer
McJury	Brian, K.	Third Officer
Mee	Stephen, P.	Radio Officer
Cutting	David, J.	Chief Engineer
Kerswell	William, R.	Second Engineer
Caldwell	Robert, R.	Third Engineer
McAskill	Robert, J.	Third Engineer
Thomas	Norman, E.	Electrician
Olley	Kenneth, R.	Catering Officer
Watson	Robert	Bosun
Lang	Colin, D.	Bosun Mate
Dodd	Jonothan, M.	Seaman First Class
Bowen	Albert, M.	Seaman First Class
Moore	Stephen, P.	Seaman First Class
Watson	David, N.	Seaman First Class
Taylor	David, F.	Seaman First Class
Smith	Bruce	Motorman
Smith	Sydney, F.	Motorman
McManamy	Daniel Keir	Chef
Hunt	David, A.	Second Chef
Heeney	Robert, J.	Second Steward
Knowles	Jonathon, B.	Steward
Jones	Lee, J.	Steward
McAdam	Alister	Steward

Ship's Data

Port of Registry:	Stanley, Falkland Islands
Call Sign:	ZDLP
INMARSAT Voice:	00–871–144–4751
	00–874–144–4751
INMARSAT Fax:	00–871–144–4752
	00–874–144–4752
Grimsby Voice:	44–1–472–269–113
Grimsby Fax:	44–1–472–269–114
Endurance:	57 days at 12 kts
Propulsion:	Diesel electric, single fixed propeller, 8,500 SHP
Length Overall:	99.04 m
Breadth:	18.85 m
Full Load Draft:	6.40 m
Freeboard:	3.308 m
Officers:	11 (+1 on science cruises)
Ratings:	15 (+1 on science cruises)
Science Berths:	16 single (w/Pullman berth)
	4×4 berth
	Chief Scientist's Suite
Science Complement:	31 berths (maximum)

Working Deck Areas

All working deck areas are covered with a matrix of 1 T capacity bolt-down points at 1 m centers (0.5 m in some areas). Deck facilities include support for five laboratory containers (ISO 20 ft), four aft and one forward. The area coverage of the deck is as follows:

- After deck 20 m long (full deck width 370 m^2),
- Starboard deck 5 m wide to midship (150 m^2), and
- Forward deck, starboard side, main deck 130 m^2.

Cranage

There are three cranes forward and three cranes aft, presented by their safe working load (SWL) times (×) their boom extension:

a) Main forward cargo crane (20 T × 20 m),
b) Forward stores crane (2.5 T × 10 m),
c) Forward science crane (2 T × 4 m),
d) Aft cargo crane (10 T × 17 m or 3 T × 22 m),
e) Port science crane (2.5 T × 13 m), and
f) Starboard science crane (2.5 T × 10 m).

The forward science crane is fitted with winch and slip rings and both aft science cranes have winches.

Gantries

There are two articulated A-frames, one aft and one midships to starboard:

- SWL 20 T (7.5 T SWL articulated arm) 2×2 T handling winch aft, and
- SWL 30 T (static), 2×2 T handling winch (adjacent) midships.

Winch Systems

There are six winch systems on board: a main traction winch (30 T SWL) which serves both the aft and midships gantries, a CTD/hydrographic traction winch (10 T SWL), a biological drum winch (5 T SWL), a twin warp trawling system (2×35.8 T SWL), and two Gilson winches (5 T SWL). The drum specifications for these systems are as follows:

i) The main traction winch storage drums are a) super-aramid deep coring warp (8,000 m), b) standard coring warp (7,000 m), c) tapered trawl warp (15,000 m), and d) conducting cable (10,000 m);
ii) The CTD/hydrographic winch drum options are a) hydrographic wire (9,000 m), b) conducting cable (8,000 m), and c) a spare drum;
iii) The biological drum winch storage is 3,000 m; and
iv) The twin warp trawling system has a storage of 5,000 m (a net drum winch is available for mounting on the main deck).

The main traction winch and the CTD/hydrographic winches are fitted with inboard and outboard compensator systems.

Laboratories

All of the laboratories are on the Upper Deck, which is the main working deck for the ship. There are nine scientific laboratories of varying sizes:

1) Wet Laboratory (23.5 m^2),
2) Main Laboratory (44.2 m^2),
3) Rough Workshop (25.9 m^2),

4) Scientific Workshop (19.6 m^2),
5) Waterbottle Annex (18.1 m^2),
6) Chemistry Laboratory (18.1 m^2),
7) Preparation Laboratory (16.3 m^2),
8) Biochemistry Laboratory (10.6 m^2), and
9) Microbiology/Radioactive Laboratory (10.7 m^2).

Computer/Electronic/Control Spaces

There are six computer, electronic, or control spaces and all of them are located on the Forecastle Deck. Their names and sizes are as follows:

a) Underway Instrumentation and Control (UIC) Room (66.8 m^2) which incorporates the Winch Control Room,
b) Electronic Workshop (7.2 m^2),
c) Data Preparation Room (16.5 m^2),
d) Computer Room (19.2 m^2),
e) Paper and Magnetic Tape Ready-Use Store (4.6 m^2), and
f) Dark Room (7.4 m^2).

A local area network (LAN) with backup is installed for cruise instrumentation and equipment. The LAN is based on a thinnet and fiberoptic spine with access through thicknet transceivers. Ship instrumentation is continuously logged on the central computing systems. Facilities are available for data transmission via satellite to and from the ship.

Other Scientific Spaces

There are several other scientific spaces including, but not limited to, the following:

- Gravity Meter Room (5.2 m^2),
- Cool Specimen Room (13 m^2),
- Scientific Freezer (12.4 m^2),
- −60°C Scientific Freezer (1.5 m^2),
- Scientific Hold (118 m^2),
- Explosives Magazine (15 T),
- Hazardous Chemicals Lockers (main deck), and
- Storm Clothing Annex.

Navigation and Ship's Log

- Trimble 8-channel GPS receiver,
- Simrad EA 500 Navigational Sounder,
- Sub-bottom Profiler (3.5 KHz),
- Precision Echo Sounder (10 KHz),
- Furuno CSH50 Directional Sonar,
- RDI Type RD-VDM150 ADCP, and
- PC-based Ocean Logger.

Appendix B

XBT Log

The XBT Log is presented in Table B1. All of the XBTs deployed were T7s which have a nominal operating depth of 760 m.

Appendix C

CTD Bottle Log

The CTD bottle log is presented in Table C1. The SST is the temperature measured at the inlet of the uncontaminated sea water supply (approximately 7 m). Two CTD rosette bottles were tripped at each main depth and one bottle at each extra depth. Each CTD cast was to a depth of 200 m except station 268 which was to 100 m. Note that no sampling occurred on stations 274, 291–294, and 297.

Appendix D

Zooplankton Carbon Log

A summary of the Zooplankton Carbon Log is presented in Table D1.

Appendix E

Particulate Carbon Log

A summary of the Particulate Carbon Log is presented in Table E1.

Appendix F

Optical Profiling Log

The Optical Profiling Log is presented in Table F1.

Appendix G

Bridge Log

A summary of the Bridge Log is presented in Table G1.

Appendix H

Navigation Log

A summary of the Navigation Log is presented in Table H1. To keep the table uncluttered, the day and navigational labels only appear at the top of each column, the start of each new day, or when a hemispherical boundary is crossed (east to west and north to south).

Appendix I

UOR Tow Log

A summary of the UOR Tow Log is presented in Table I1. The total towing time and distance was 271.5 hours and 3,123 nmi (at 11.6 kts), respectively.

Appendix J

Pigment Extraction Log

The station and underway pigment extraction log is presented in Tables J1–J3. The former summarizes the station sampling program, and the latter two summarize the 2- and 4-hourly underway sampling program.

Appendix K

Primary Production and FRRF Log

A summary of the Primary Production and FRRF Log is presented in Table K1.

Appendix L

Underway Nutrient Sampling Log

A summary of the Nutrient Sampling Log is presented in Table L1.

Table B1. A summary of the XBT Log for AMT-1. The XBTs are numbered sequentially in the temporal order in which they were deployed. To keep the table uncluttered, hemispheric indicators are only given at the top of each column or when a hemispheric boundary was crossed. All times are in GMT.

No.	*Date*	*SDY*	*Time*	*Longitude*	*Latitude*	*No.*	*Date*	*SDY*	*Time*	*Longitude*	*Latitude*
1	26 September	269	0500	13° 08.0′ W	49° 13.8′ N	45	15 October	288	0001	38° 04.0′ W	25° 03.0′ S
2		269	1320	14 21.0	47 55.0	46		288	0733	39 12.2	26 9.7
3	27 September	270	0552	18 57.5	47 12.0	47		288	1543	40 8.3	27 7.3
4		270	0954	19 56.6	47 0.4	48		288	2358	41 7.0	28 8.0
5		270	2206	20 0.9	45 9.8	49	16 October	289	0737	42 19.4	28 18.1
6	28 September	271	0547	20 0.0	43 29.0	50		289	1538	43 22.9	30 15.5
7		271	1415	20 0.9	42 15.0	51		289	2359	44 33.0	31 19.0
8		271	2201	20 0.5	40 48.4	52	17 October	290	0736	45 41.8	32 24.6
9	29 September	272	0538	19 59.7	39 12.0	53		290	1543	46 31.0	33 11.1
10		272	1359	19 57.7	37 54.3	54		290	1658	46 37.1	33 16.0
11		272	2205	20 0.3	36 26.7	55	22 October	295	1114	55 33.7	39 38.7
12	30 September	273	1345	20 53.0	33 35.9	56		295	1259	55 36.9	40 1.5
13	2 October	275	1452	21 50.0	27 22.2	57		295	1450	55 30.7	40 25.0
14		275	2204	21 36.0	26 0.8	58		295	1632	55 20.7	40 46.9
15	3 October	276	0539	21 33.0	24 33.4	59		295	1901	55 17.1	41 5.9
16		276	1343	21 9.8	23 17.3	60		295	2053	55 22.0	41 31.4
17	4 October	277	0543	20 28.4	20 7.5	61		295	2301	55 28.0	42 3.0
18		277	1122	20 23.3	19 29.9	62	23 October	296	0056	55 33.0	42 30.0
19	5 October	278	1641	20 26.0	13 3.0	63		296	0256	55 39.0	42 57.0
20		278	2259	20 56.7	12 0.4	64		296	0506	55 46.1	43 27.3
21	6 October	279	0642	21 38.2	10 28.2	65		296	0630	55 51.2	43 47.3
22		279	1452	22 12.7	9 14.5	66		296	0653	55 52.4	43 52.8
23		279	2302	22 47.4	7 54.4	67		296	0917	55 58.1	44 28.7
24	7 October	280	1436	23 58.3	5 21.1	68		296	1027	56 0.6	44 45.3
25		280	2302	24 30.3	4 3.8	69		296	1204	56 6.0	45 6.0
26	8 October	281	0640	26 11.1	2 39.3	70		296	1331	56 10.8	45 27.6
27		281	1436	25 42.1	1 23.8	71		296	1438	56 13.1	45 42.6
28		281	1517	25 43.0	1 19.0	72		296	1517	56 14.6	45 51.3
29		281	2301	26° 18.9′ W	0° 00.3′ S	73		296	1632	56 17.1	46 0.5
30	9 October	282	1438	27 31.4	2 47.5	74		296	1728	56 18.2	46 8.3
31		282	2300	28 9.2	4 7.1	75		296	1814	56 20.5	46 18.7
32	10 October	283	0642	28 54.4	5 45.4	76		296	1911	56 23.9	46 32.0
33		283	1440	29 30.5	7 0.7	77		296	2012	56 27.6	46 46.4
34	11 October	284	0731	30 58.0	10 12.7	78		296	2105	56 31.0	46 58.7
35		284	1547	31 33.1	11 28.1	79		296	2238	56 36.7	47 20.2
36	12 October	285	0018	32 10.6	12 46.8	80	24 October	297	0052	56 43.8	47 50.8
37		285	0740	32 51.8	14 18.8	81		297	0504	56 56.0	48 49.7
38		285	1551	33 26.8	15 34.5	82		297	0710	57 2.0	49 17.8
39		285	2359	34 5.0	16 57.4	83		297	0904	57 8.5	49 43.6
40	13 October	286	0737	34 48.4	18 24.6	84		297	1205	57 18.6	50 23.8
41		286	1552	35 26.6	19 38.2	85		297	1237	57 20.4	50 31.1
42	14 October	287	0022	36 3.0	21 9.0	86		297	1305	57 22.1	50 37.6
43		287	0749	36 48.3	22 35.0	87		297	1334	57 23.4	50 43.7
44		287	1547	37 23.3	23 47.5						

Table C1. The CTD bottle log for AMT-1. The Z_i entries refer to the bottle numbers filled when taking water from the CTD rosette. No extra bottles were taken on station 284 (denoted by the NT code).

Station Number		268	269	270	271	272	273	275	276	277	278	279	280	281
SST (7 m) [°C]		16.6	17.4	18.0	19.4	21.7	23.4	24.4	25.1	25.4	28.8	28.1	28.0	27.1
Main Depths [m]	Z_1	7	7	7	7	7	7	7	7	7	7	7	7	7
	Z_2	20	20	20	30	30	50	50	40	20	30	20	40	30
	Z_3	30	30	30	50	60	70	80	60	30	50	40	60	60
	Z_4	50	40	40	60	80	90	100	80	40	70	60	80	80
	Z_5	70	50	50	70	90	110	120	100	50	100	80	100	100
Extra Depths [m]	Z_6	80	60	60	80	100	130	130	120	70	120	100	70	90
	Z_7	90	70	70	90	120	150	140	140	100	140	120	90	70
Station Number		282	283	284	285	286	287	288	289	290	295	296	297	
SST (7 m) [°C]		26.3	16.6	25.9	25.5	25.0	23.2	22.8	19.2	17.0	6.9	8.6	5.4	
Main Depths [m]	Z_1	7	7	7	7	7	7	7	7	7	7	7	7	
	Z_2	40	50	40	60	60	60	50	50	20	20	20	20	
	Z_3	70	80	70	120	120	80	80	80	40	40	30	30	
	Z_4	90	100	100	150	160	100	100	100	60	60	40	40	
	Z_5	120	140	140	180	180	120	120	120	80	80	60	50	
Extra Depths [m]	Z_6	80	90	NT	140	140	140	90	90	50	30	50	60	
	Z_7	100	110	NT	160	200	160	110	110	100	50	70	70	

Table D1. A summary of the Zooplankton Carbon Log for AMT-1. Depth is the maximum depth of the WP2 net cast and is in meters. The four digit numbers starting with "9" are the sample reference numbers and the $x \times y \,/\, z$ expression is decoded as follows: x is the number of replicates, y is the volume of the samples in milliliters, and z is the volume size fraction sampled in milliliters. On SDY 278, sample number 9367 (not listed) was collected to look at the (approximately) 200 μm size fraction.

Date	*SDY*	*Depth*	$>$ 2000 μm	1000–2000 μm	500–1000 μm	200–500 μm
25 Sept.	268	98	9207 3 × 50 / 1000	9208 3 × 50 / 1000	9209 3 × 50 / 1000	9210 3 × 50 / 1000
26 Sept.	269	200	9226 3 × 50 / 500	9227 3 × 50 / 1000	9228 3 × 50 / 1000	9229 3 × 50 / 1000
27 Sept.	270	200	9249 3 × 50 / 1000	9250 3 × 50 / 1000	9251 3 × 50 / 1000	9252 3 × 50 / 1000
28 Sept.	271	195	9258 3 × 50 / 1000	9259 3 × 50 / 1000	9260 3 × 50 / 1000	9261 3 × 50 / 1000
29 Sept.	272	205	9276 3 × 50 / 1000	9277 3 × 50 / 1000	9278 3 × 50 / 1000	9279 3 × 50 / 1000
30 Sept.	273	200	9290 3 × 50 / 1000	9291 3 × 50 / 1000	9292 3 × 50 / 1000	9293 3 × 50 / 1000
2 Oct.	275	200	9309 3 × 50 / 500	9310 3 × 50 / 500	9311 3 × 50 / 500	9312 3 × 50 / 500
3 Oct.	276	200	9323 3 × 50 / 500	9324 3 × 50 / 500	9325 3 × 50 / 500	9326 3 × 50 / 500
4 Oct.	277	200	9337 3 × 50 / 500	9338 3 × 50 / 500	9339 3 × 50 / 500	9340 3 × 50 / 500
5 Oct.	278	205	9363 3 × 50 / 500	9364 3 × 50 / 500	9365 3 × 50 / 500	9366 3 × 50 / 500
6 Oct.	279	200	9368 3 × 50 / 500	9369 3 × 50 / 500	9370 3 × 50 / 500	9371 3 × 50 / 500
7 Oct.	280	185	9382 3 × 50 / 500	9383 3 × 50 / 500	9384 3 × 50 / 500	9385 3 × 50 / 500
8 Oct.	281	200	9396 3 × 50 / 500	9397 3 × 50 / 500	9398 3 × 50 / 500	9399 3 × 50 / 500
9 Oct.	282	200	9410 3 × 50 / 500	9411 3 × 50 / 500	9412 3 × 50 / 500	9413 3 × 50 / 500
10 Oct.	283	200	9424 3 × 50 / 500	9425 3 × 50 / 500	9426 3 × 50 / 500	9427 3 × 50 / 500
11 Oct.	284	200	9438 3 × 50 / 500	9439 3 × 50 / 500	9440 3 × 50 / 500	9441 3 × 50 / 500
12 Oct.	285	200	9452 3 × 100 / 500	9453 3 × 100 / 500	9454 3 × 100 / 500	9455 3 × 100 / 500
13 Oct.	286	200	9466 3 × 100 / 500	9467 3 × 100 / 500	9468 3 × 100 / 500	9469 3 × 100 / 500
14 Oct.	287	190	9480 3 × 50 / 500	9481 3 × 50 / 500	9482 3 × 50 / 500	9483 3 × 50 / 500
15 Oct.	288	200	9494 3 × 50 / 500	9495 3 × 50 / 500	9496 3 × 50 / 500	9497 3 × 50 / 500
16 Oct.	289	185	9508 3 × 100 / 500	9509 3 × 100 / 500	9510 3 × 100 / 500	9511 3 × 100 / 500
17 Oct.	290	175	9522 3 × 50 / 500	9523 3 × 50 / 500	9524 3 × 50 / 500	9525 3 × 50 / 500
22 Oct.	295	200	9536 3 × 50 / 500	9537 3 × 50 / 500	9538 3 × 50 / 500	9539 3 × 50 / 1000
23 Oct.	296	200	9550 3 × 50 / 500	9551 3 × 50 / 500	9552 3 × 50 / 500	9553 3 × 50 / 500
24 Oct.	297	100	9564 3 × 50 / 500	9565 3 × 50 / 500	9566 3 × 50 / 500	9567 3 × 50 / 500

Table E1. A summary of the Particulate Carbon Log for AMT-1.

Date		*Sample*	*Particulate Size Fraction* [mm]						
Gregorian	SDY	*Depth* [m]	< 200	< 10	< 5	< 2	Total	Formalin	Lugol
25 September	268	7	9224	9223	9222	9221	9225	9211	9216
		20						9212	9217
		30						9213	9218
		50						9214	9219
		70						9215	9220
26 September	269	7	9234	9232	9231	9230	9235	9226	9229
		20						9227	9230
		40	9238	9237	9236	9235	9239	9228	9231
27 September	270	7	9248	9247	9246	9245		9240	9243
		30						9241	9244
		40	9243	9242	9241	9240	9244		
		50						9242	9245
28 September	271	7	9256	9255	9254	9253	9257	9258	9162
		30						9259	9263
		50	9269	9266	9267	9268	9270	9260	9264
		60						9261	9265
29 September	272	7	9272	9273	9274	9275	9271	9271	9275
		30						9272	9276
		60	9280	9281	9282	9283	9284	9273	9277
		90						9274	9278
30 September	273	7	9285	9286	9287	9288	9289	9290	9292
		110	9294	9295	9296	9297	9298	9291	9293
2 October	275	7	9304	9305	9306	9307	9308	9299	9303
		50						9300	9304
		100	9299	9300	9301	9302	9303	9301	9305
		130						9302	9306
3 October	276	7	9313	9314	9315	9316	9317	9307	9310
		40						9308	9311
		80	9318	9319	9320	9321	9322	9309	9312
4 October	277	7	9332	9334	9335	9336	9337	9349	9351
		30						9350	9352
		40	9327	9328	9329	9330	9331		
5 October	278	7	9358	9359	9360	9361	9362	9357	9363
		70	9353	9354	9355	9356	9357	9358	9364
6 October	279	7	9372	9373	9374	9375	9376	9365	9368
		40						9366	9369
		60	9377	9378	9379	9380	9381	9367	9370
7 October	280	7	9391	9392	9393	9394	9395	9382	9385
		40						9383	9386
		80	9386	9387	9388	9389	9390	9384	9387
8 October	281	7	9400	9401	9402	9403	9404	9327	9333
		30						9328	9334
		80	9405	9406	9407	9408	9409	9329	9335
9 October	282	7	9419	9420	9421	9422	9423	9396	9403
		40						9397	9404
		90	9414	9415	9416	9417	9418	9398	9405
10 October	283	7	9433	9434	9435	9436	9437	9427	9430
		50						9428	9431
		100	9428	9429	9430	9431	9432	9429	9432

Table E1. (cont.) A summary of the Particulate Carbon Log for AMT-1.

Date		*Sample*	*Particulate Size Fraction* [mm]						
Gregorian	SDY	*Depth* [m]	< 200	< 10	< 5	< 2	Total	Formalin	Lugol
11 October	284	7	9447	9448	9449	9450	9451	9443	9446
		70						9444	9447
		140	9442	9443	9444	9445	9446	9445	9448
12 October	285	7	9461	9462	9463	9464	9465	9452	9455
		60						9453	9456
		150	9456	9457	9458	9459	9460	9454	9457
13 October	286	7	9475	9476	9477	9478	9479	9466	9469
		60						9467	9470
		160	9470	9471	9472	9473	9474	9468	9471
14 October	287	7	9484	9485	9486	9487	9488	9472	9475
		60						9473	9476
		120	9489	9490	9491	9492	9493	9474	9477
15 October	288	7	9498	9499	9500	9501	9502	9480	9483
		50						9481	9484
		80	9503	9504	9505	9506	9507	9482	9485
16 October	289	7	9517	9518	9519	9520	9521	9494	9497
		50						9495	9498
		100	9512	9513	9514	9515	9516	9496	9499
17 October	290	7	9526	9527	9528	9529	9530	9500	9504
		20						9501	9505
		40	9531	9532	9533	9534	9535	9502	9506
		60						9503	9507
22 October	295	7	9540	9541	9542	9543	9544	9536	9539
		20	9545	9546	9547	9548	9549	9537	9540
		40						9538	9541
23 October	296	7	9554	9555	9556	9557	9558	9544	9547
		20						9545	9548
		40	9559	9560	9561	9562	9563	9546	9549
24 October	297	7	9568	9569	9570	9571	9572	9557	9560
		30	9573	9574	9575	9576	9577	9558	9561
		50						9559	9562

Table F1. The Optical Profiling Log for AMT-1. The *Type* codes are as follows: "P" indicates a regular profiling cast and "S" indicates a ship shadow cast. Depth is in meters.

SDY	*Type*	*SeaOPS*		*PRR-600*		*Depth*	*Cloud*	*SDY*	*Type*	*SeaOPS*		*PRR-600*		*Depth*	*Cloud*
268	P	↑†				62	1/8	281	P	↑	↓	↑	↓	153	5/8
269	P	↑				102	8/8	282	P	↑	↓	↑	↓	162	4/8
270	P	↑	↓	↑	↓	66	7/8	283	P	↑	↓	↑	↓	186	1/8
271	P	↑	↓‡	↑		109	3/8	284	P	↑	↓	↑	↓	207	3/8
272	P	↑	↓	↑	↓	156	2/8	285	P	↑	↓	↑	↓	230	7/8
273	P	↑	↓	↑	↓	190	3/8	286	P	↑	↓	↑	↓	213	3/8
275	P	↑	↓	↑	↓	176	3/8	287	P	↑	↓	↑	↓	206	6/8
	S	↑	↓	↑	↓	36	3/8	288	P	↑	↓	↑	↓	212	5/8
276	P	↑	↓	↑	↓	171	2/8	289	P	↑	↓	↑	↓	179	7/8
277	P	↑	↓	↑	↓	89	3/8	290	P	↑	↓	↑	↓	187	4/8
	S	↑	↓	↑	↓	36	3/8	295	P	↑	↓	↑	↓	65	8/8
278	P	↑	↓	↑	↓	142	5/8	296	P	↑	↓	↑	↓	109	3/8
279	P	↑	↓	↑	↓	156	4/8	297	P	↑	↓	↑	↓	55	7/8
280	P	↑	↓	↑	↓	142	6/8								

† Noisy cast. ‡ Partial cast.

Table G1. A summary of the Scientific Bridge Log for AMT-1. All times are in GMT.

Date	*SDY*	*Longitude*	*Latitude*	*Time*	*Activity*
23 September	266	8° 06.7′ W	50° 48.3′ N	1535	Left Portsmouth dock.
		1 55.5	50 37.2	2000	Anchored off Swanage Bay.
24 September	267	1° 57.1′ W	50° 35.0′ N	0803	Left anchorage.
		2 39.1	50 25.0	1500	Proceeding on passage; Heading 247°.
25 September	268	5° 34.6′ W	49° 33.3′ N	0030	Changed heading to 255°.
		8 21.8	49 2.7	0950	UOR deployed.
		9 8.9	48 55.8	1242	Stopped on station.
		9 9.1	48 56.2	1436	Resumed passage.
		11 1.8	48 33.7	2202	UOR recovered.
26 September	269	13° 10.9′ W	48° 13.3′ N	0600	UOR deployed.
		14 52.7	47 55.9	1231	UOR recovered.
		14 52.7	47 55.9	1236	Stopped on station.
		14 50.7	47 55.2	1436	Resumed passage.
		14 50.7	47 55.2	1444	UOR deployed.
		16 39.8	47 34.8	2158	UOR recovered.
27 September	270	18° 58.8′ W	47° 11.8′ N	0600	UOR deployed.
		19 56.6	47 00.4	1000	UOR recovered; Stopped on station.
		19 59.1	47 00.2	1130	Resumed passage; Heading 180°.
		19 59.2	46 58.3	1145	UOR deployed.
		20 00.9	45 9.8	2158	UOR recovered.
28 September	271	20° 00.2′ W	43° 29.0′ N	0600	UOR deployed.
		20 0.9	42 15.1	1232	UOR recovered.
		20 0.9	42 15.1	1238	Stopped on station.
		20 1.9	42 15.2	1408	Resumed passage.
		20 1.9	42 15.2	1415	UOR deployed.
		20 0.5	40 48.4	2200	UOR recovered.
29 September	272	19° 59.6′ W	39° 08.9′ N	0556	UOR deployed.
		19 59.7	37 54.3	1233	UOR recovered.
		19 59.7	37 54.3	1235	Stopped on station.
		19 59.4	37 54.7	1355	Resumed passage.
		19 59.4	37 54.7	1405	UOR deployed.
		20 0.3	36 26.7	2204	UOR recovered.
		20 0.3	36 25.8	2207	Changed heading to 198°.
		20 0.1	36 23.3	2220	Changed heading to 192°.
30 September	273	20° 10.3′ W	35° 48.6′ N	0558	Changed heading to 195°.
		20 31.6	34 47.6	0558	UOR deployed.
		20 53.0	33 35.9	1221	UOR recovered.
		20 53.0	33 35.9	1236	Stopped on station.
		20 53.0	33 35.9	1354	Resumed passage.
		20 53.0	33 35.9	1402	UOR deployed.
		20 51.8	33 13.9	1600	Changed heading to 100°.
1 October	274	17° 28.6′ W	32° 40.6′ N	0600	Arrived at Madeira.
		16 54.1	32 38.1	0844	Changed heading to 219°.
2 October	275	21° 50.0′ W	27° 22.8′ N	1400	Stopped on station.
		21 50.0	27 22.2	1500	Resumed passage; Heading 170°.
		21 50.0	27 22.2	1508	UOR deployed.
		21 36.1	26 9.4	2202	UOR recovered.
3 October	276	21° 22.9′ W	24° 31.1′ N	0551	UOR deployed.
		21 9.8	23 17.3	1235	UOR recovered.
		21 9.8	23 17.3	1238	Stopped on station.
		21 8.0	23 16.8	1349	Resumed passage.
		21 9.8	23 15.5	1410	UOR deployed.
		20 51.1	21 50.4	2200	UOR recovered.

Table G1. (cont.) A summary of the Scientific Bridge Log for AMT-1. All times are in GMT.

Date	*SDY*	*Longitude*	*Latitude*	*Time*	*Activity*
4 October	277	20° 30.4′ W	20° 13.9′ N	0554	UOR deployed.
		20 22.2	19 27.0	1020	UOR recovered.
		20 23.3	19 29.9	1042	Stopped on station.
		20 23.3	19 29.9	1208	Resumed passage; UOR deployed; Heading 181°.
		20 22.3	19 20.2	1321	UOR recovered.
5 October	278	20° 25.7′ W	13° 13.0′ N	1500	UOR deployed.
		20 26.0	13 3.3	1600	UOR recovered; Stopped on station.
		20 26.5	13 1.9	1700	Resumed passage; Heading 204°.
		20 26.5	13 1.9	1708	UOR deployed.
		20 56.7	12 0.4	2258	UOR recovered.
6 October	279	21° 39.2′ W	10° 26.3′ N	0654	UOR deployed.
		22 12.7	9 14.5	1356	UOR recovered.
		22 12.7	9 14.5	1401	Stopped on station.
		22 13.1	9 14.0	1456	Resumed passage; UOR deployed.
		22 47.4	7 54.4	2300	UOR recovered.
7 October	280	23° 29.9′ W	6° 28.4′ N	0654	UOR deployed.
		23 58.3	5 21.1	1356	UOR recovered.
		23 58.3	5 21.1	1400	Stopped on station.
		23 58.0	5 21.4	1448	Resumed passage.
		23 58.0	5 21.4	1458	UOR deployed.
		23 58.0	4 4.0	2258	UOR recovered.
8 October	281	25° 11.7′ W	2° 37.7′ N	0650	UOR deployed.
		25 42.1	1 23.8	1358	UOR recovered.
		25 42.1	1 23.8	1400	Stopped on station.
		25 42.1	1 32.5	1445	Resumed passage.
		25 42.1	1 32.5	1452	UOR deployed.
		26° 18.9′ W	0° 00.3′ S	2258	UOR recovered.
9 October	282	26° 57.3′ W	1° 36.4′ S	0648	UOR deployed.
		27 31.4	2 47.5	1355	UOR recovered.
		27 31.4	2 47.5	1400	Stopped on station.
		27 31.9	2 47.4	1500	Resumed passage.
		27 31.9	2 47.4	1505	UOR deployed.
		28 9.1	4 6.8	2258	UOR recovered.
10 October	283	28° 55.1′ W	5° 46.9′ S	0651	UOR deployed.
		29 30.5	7 0.7	1355	UOR recovered.
		29 30.5	7 0.7	1400	Stopped on station.
		29 30.9	7 0.9	1448	Resumed passage.
		29 31.6	7 2.1	1500	UOR deployed.
		29 57.5	7 57.6	2034	UOR recovered.
11 October	284	30° 59.8′ W	10° 16.7′ S	0753	UOR deployed.
		31 33.1	11 28.1	1455	UOR recovered.
		31 33.1	11 28.1	1458	Stopped on station.
		31 33.6	11 28.5	1600	Resumed passage; UOR deployed.
		32 10.0	12 46.0	2357	UOR recovered.
12 October	285	32° 52.6′ W	14° 20.5′ S	0750	UOR deployed.
		33 26.8	15 34.5	1453	UOR recovered.
		33 26.8	15 34.5	1503	Stopped on station.
		33 27.3	15 35.2	1600	Resumed passage.
		33 27.3	15 35.2	1602	UOR deployed.
		34 5.0	16 57.2	2358	UOR recovered.

Table G1. (cont.) A summary of the Scientific Bridge Log for AMT-1. All times are in GMT.

Date	*SDY*	*Longitude*	*Latitude*	*Time*	*Activity*
13 October	286	34° 49.1′ W	18° 26.2′ S	0748	UOR deployed.
		35 21.6	19 38.2	1456	UOR recovered.
		35 21.6	19 38.2	1459	Stopped on station.
		35 21.8	19 38.9	1555	Resumed passage.
		35 21.8	19 38.9	1557	UOR deployed.
		35 40.2	20 20.7	1933	UOR recovered.
14 October	287	36° 49.2′ W	22° 36.6′ S	0759	UOR deployed.
		37 23.2	23 47.2	1455	UOR recovered.
		37 23.2	23 47.2	1500	Stopped on station.
		37 23.3	23 47.4	1600	Resumed passage.
		37 23.3	23 47.4	1615	UOR deployed.
		37 50.5	24 47.2	2200	Changed heading to 222°.
		38 4.7	25 3.6	2356	UOR recovered.
15 October	288	39° 15.1′ W	26° 12.6′ S	0750	UOR deployed.
		40 8.5	27 2.3	1453	UOR recovered.
		40 8.5	27 2.3	1455	Stopped on station.
		40 8.3	27 7.0	1600	Resumed passage.
		40 8.3	27 7.0	1608	UOR deployed.
		41 9.0	28 9.7	2352	UOR recovered.
16 October	289	42° 20.5′ W	29° 19.3′ S	0745	UOR deployed.
		43 23.3	30 17.2	1453	UOR recovered.
		43 23.3	30 17.2	1458	Stopped on station.
		43 23.5	30 17.6	1600	Resumed passage.
		43 23.5	30 17.6	1616	UOR deployed.
		44 33.5	31 21.0	2356	UOR recovered.
17 October	290	45° 41.7′ W	32° 27.1′ S	0745	UOR deployed.
		46 25.8	33 11.1	1454	UOR recovered.
		46 25.8	33 11.1	1459	Stopped on station.
		46 24.5	33 10.8	1554	Resumed passage.
		47 0.1	33 23.7	2000	Changed heading to 256°.
19 October	292	53° 56.3′ W	34° 53.0′ S	0050	Changed heading to 254°.
22 October	295	55° 14.0′ W	40° 57.0′ S	1719	Stopped on station.
		55 15.4	40 57.3	1819	Resumed passage.
23 October	296	56° 17.1′ W	46° 00.2′ S	1600	Stopped on station.
		56 16.8	46 0.9	1654	Resumed passage.
24 October	297	57° 25.0′ W	50° 48.3′ S	1402	Stopped on station.
		57 25.3	50 48.6	1444	Resumed passage.
		58 29.3	51 54.3	2257	Anchored in Mare Harbour.

Table H1. A summary of the Navigation Log for AMT-1. All times are in GMT.

SDY Time	*Longitude*	*Latitude*	*SDY Time*	*Longitude*	*Latitude*	*SDY Time*	*Longitude*	*Latitude*
264 1500	0° 04.4′ W	53° 34.7′ N	266 2300	1° 55.6′ W	50° 37.2′ N	0700	13° 41.5′ W	48 8.6′ N
1600	0° 02.0′ E	53° 35.1′ N	267 0000	1° 55.6′ W	50° 37.2′ N	0800	13 57.1	48 5.8
1700	0 21.3	53 30.2	0100	1 55.6	50 37.2	0900	14 13.0	48 2.4
1800	0 42.2	53 24.5	0200	1 55.6	50 37.2	1000	14 29.1	47 59.7
1900	1 2.4	53 18.6	0300	1 55.5	50 37.3	1100	14 44.8	47 57.3
2000	1 17.7	53 8.3	0400	1 55.5	50 37.2	1200	14 52.4	47 55.6
2100	1 32.5	52 58.0	0500	1 55.5	50 37.3	1300	14 51.0	47 55.3
2200	1 47.8	52 48.6	0600	1 55.5	50 37.2	1400	14 54.9	47 54.4
2300	1 55.7	52 37.8	0700	1 55.5	50 37.1	1500	15 10.0	47 51.9
265 0000	1° 53.9′ E	52° 26.3′ N	0800	1 57.1	50 35.0	1600	15 24.9	47 49.6
0100	1 53.2	52 14.5	0900	1 54.1	50 34.9	1700	15 39.7	47 46.7
0200	1 51.0	52 2.3	1000	1 57.6	50 35.0	1800	15 54.9	47 43.5
0300	1 48.3	51 49.9	1100	1 57.2	50 34.5	1900	16 10.2	47 40.2
0400	1 45.7	51 36.5	1200	2 12.6	50 28.2	2000	16 25.8	47 37.2
0500	1 42.1	51 22.1	1300	2 34.4	50 26.2	2100	16 39.7	47 34.9
0600	1 32.3	51 8.8	1400	2 38.5	50 25.2	2200	16 54.7	47 32.6
0700	1 14.0	50 58.7	1500	2 58.9	50 18.8	2300	17 9.7	47 30.2
0800	0 55.3	50 48.3	1600	3 18.1	50 13.8	270 0000	17° 25.0′ W	47° 27.9′ N
0900	0 38.5	50 40.7	1700	3 36.0	50 9.4	0100	17 39.9	47 25.7
1000	0 18.2	50 35.9	1800	3 52.2	50 4.6	0200	17 55.0	47 22.7
1100	0° 04.3′ W	50° 32.3′ N	1900	4 9.5	49 59.9	0300	18 10.3	47 19.8
1200	0 27.8	50 35.6	2000	4 27.6	49 54.9	0400	18 25.9	47 17.2
1300	0 48.3	50 39.3	2100	4 46.4	49 49.7	0500	18 42.7	47 14.5
1400	1 2.0	50 43.6	2200	5 6.4	49 44.8	0600	18 58.9	47 11.7
1500	1 6.7	50 48.3	2300	5 24.4	49 36.4	0700	19 15.0	47 8.7
1600	1 6.7	50 48.3	268 0000	5° 44.1′ W	49° 31.6′ N	0800	19 31.2	47 5.3
1700	1 6.7	50 48.3	0100	6 2.8	49 27.0	0900	19 46.8	47 2.4
1800	1 6.7	50 48.3	0200	6 21.2	49 24.1	1000	19 59.6	47 0.3
1900	1 6.7	50 48.3	0300	6 39.2	49 21.8	1100	19 59.1	47 0.8
2000	1 6.7	50 48.3	0400	6 56.5	49 19.1	1200	19 59.2	46 58.5
2100	1 6.7	50 48.3	0500	7 13.7	49 15.7	1300	19 59.4	46 47.9
2200	1 6.7	50 48.3	0600	7 31.1	49 12.8	1400	19 59.8	46 37.0
2300	1 6.7	50 48.3	0700	7 49.0	49 9.1	1500	19 59.9	46 25.9
266 0000	1 6.7′ W	50° 48.3′ N	0800	8 6.5	49 5.7	1600	20 0.2	46 14.9
0100	1 6.7	50 48.3	0900	8 21.7	49 2.7	1700	20 0.7	46 4.0
0200	1 6.7	50 48.3	1000	8 39.6	48 59.8	1800	20 0.9	45 53.4
0300	1 6.7	50 48.3	1100	8 57.6	48 57.4	1900	20 0.7	45 42.4
0400	1 6.7	50 48.3	1200	9 9.2	48 55.7	2000	20 0.5	45 31.4
0500	1 6.7	50 48.3	1300	9 8.8	48 55.9	2100	20 0.9	45 20.2
0600	1 6.7	50 48.3	1400	9 14.0	48 55.6	2200	20 0.9	45 9.9
0700	1 6.7	50 48.3	1500	9 28.7	48 53.5	2300	20 0.4	44 57.6
0800	1 6.7	50 48.3	1600	9 43.3	48 50.7	271 0000	20 0.1′ W	44° 45.0′ N
0900	1 6.7	50 48.3	1700	9 58.0	48 47.2	0100	19 59.6	44 32.0
1000	1 6.7	50 48.3	1800	10 12.9	48 42.8	0200	19 59.6	44 19.2
1100	1 6.7	50 48.3	1900	10 29.2	48 39.4	0300	19 60.0	44 6.6
1200	1 6.7	50 48.3	2000	10 46.0	48 36.5	0400	20 0.2	43 53.7
1300	1 6.7	50 48.3	2100	11 1.5	48 33.8	0500	20 0.0	43 41.1
1400	1 6.7	50 48.3	2200	11 18.2	48 30.7	0600	20 0.2	43 29.1
1500	1 5.3	50 45.1	2300	11 35.1	48 27.4	0700	19 59.9	43 18.3
1600	1 6.0	50 36.4	269 0000	11° 51.3′ W	48° 24.9′ N	0800	19 59.3	43 7.1
1700	1 22.9	50 31.3	0100	12 7.1	48 22.6	0900	19 58.9	42 55.8
1800	1 40.7	50 33.6	0200	12 23.4	48 20.3	1000	19 59.7	42 44.2
1900	1 55.5	50 37.2	0300	12 39.2	48 18.0	1100	20 0.1	42 32.5
2000	1 55.5	50 37.2	0400	12 55.1	48 15.7	1200	20 0.6	42 21.3
2100	1 55.5	50 37.2	0500	13 10.6	48 13.3	1300	20 1.5	42 15.1
2200	1 55.5	50 37.2	0600	13 25.7	48 11.1	1400	20 1.9	42 15.3

Table H1. (cont.) A summary of the Navigation Log for AMT-1. All times are in GMT.

SDY Time	*Longitude*	*Latitude*	*SDY Time*	*Longitude*	*Latitude*	*SDY Time*	*Longitude*	*Latitude*
271 1500	20° 01.1′ W	42° 07.5′ N	273 2300	19° 10.1′ W	32° 56.6′ N	276 0700	21° 21.0′ W	24° 18.9′ N
1600	20 0.3	41 56.2	274 0000	18° 55.6′ W	32° 54.5′ N	0800	21 19.2	24 7.9
1700	19 59.7	41 44.6	0100	18 40.9	32 52.8	0900	21 17.2	23 56.9
1800	19 59.4	41 33.0	0200	18 26.3	32 50.6	1000	21 15.2	23 45.8
1900	20 0.1	41 21.6	0300	18 11.8	32 48.1	1100	21 13.1	23 34.7
2000	20 0.5	41 10.1	0400	17 57.2	32 45.8	1200	21 11.0	23 23.4
2100	20 0.9	40 58.8	0500	17 42.8	32 43.4	1300	21 9.7	23 17.1
2200	20 0.5	40 48.4	0600	17 28.5	32 40.8	1400	21 9.8	23 15.6
2300	19 59.9	40 36.1	0700	17 14.3	32 38.8	1500	21 7.7	23 5.5
272 0000	19° 59.8′ W	40° 23.4′ N	0800	16 59.7	32 37.0	1600	21 5.1	22 54.3
0100	20 0.0	40 10.8	0900	16 55.7	32 35.5	1700	21 2.7	22 43.1
0200	20 0.1	39 58.2	1000	17 5.9	32 24.7	1800	21 0.3	22 32.3
0300	20 0.0	39 45.6	1100	17 16.0	32 14.0	1900	20 58.0	22 21.6
0400	20 0.1	39 32.8	1200	17 26.1	32 3.0	2000	20 55.6	22 11.2
0500	19 59.8	39 20.1	1300	17 36.5	31 51.9	2100	20 53.1	22 0.5
0600	19 59.6	39 8.3	1400	17 47.2	31 40.9	2200	20 51.1	21 50.5
0700	19 59.3	38 57.0	1500	17 58.2	31 30.2	2300	20 48.4	21 38.9
0800	19 58.7	38 45.6	1600	18 8.8	31 19.3	277 0000	20° 45.7′ W	21° 26.8′ N
0900	19 58.7	38 34.3	1700	18 19.4	31 8.5	0100	20 43.4	21 14.2
1000	19 58.8	38 23.0	1800	18 30.1	30 57.8	0200	20 41.1	21 1.7
1100	19 59.1	38 11.6	1900	18 40.6	30 47.0	0300	20 38.5	20 49.1
1200	19 59.5	38 0.2	2000	18 50.5	30 36.2	0400	20 35.6	20 36.7
1300	19 59.5	37 54.5	2100	18 60.0	30 25.2	0500	20 32.8	20 24.3
1400	19 59.4	37 54.5	2200	19 10.0	30 14.2	0600	20 30.2	20 13.0
1500	19 59.8	37 43.8	2300	19 20.3	30 3.5	0700	20 28.2	20 2.2
1600	20 0.4	37 32.6	275 0000	19° 30.5′ W	29° 52.9′ N	0800	20 26.1	19 51.4
1700	20 0.4	37 21.5	0100	19 40.6	29 42.4	0900	20 24.3	19 40.7
1800	20 0.5	37 10.5	0200	19 50.9	29 31.7	1000	20 22.9	19 29.7
1900	20 0.8	36 59.4	0300	20 1.2	29 20.8	1100	20 23.5	19 29.9
2000	20 1.2	36 48.1	0400	20 11.4	29 9.9	1200	20 23.7	19 30.1
2100	20 1.1	36 37.0	0500	20 21.6	28 58.8	1300	20 22.3	19 20.3
2200	20 0.3	36 26.7	0600	20 31.6	28 47.9	1400	20 21.8	19 8.6
2300	20 3.6	36 14.9	0700	20 41.4	28 37.3	1500	20 21.7	18 54.4
273 0000	20° 06.9′ W	36° 02.1′ N	0800	20 51.7	28 26.7	1600	20 21.6	18 40.1
0100	20 10.1	35 49.4	0900	21 1.8	28 16.2	1700	20 21.5	18 26.1
0200	20 14.0	35 37.0	1000	21 12.1	28 5.8	1800	20 21.5	18 12.0
0300	20 18.1	35 24.6	1100	21 22.5	27 55.3	1900	20 21.6	17 58.1
0400	20 22.6	35 12.2	1200	21 32.5	27 44.7	2000	20 21.7	17 44.0
0500	20 27.0	34 59.6	1300	21 41.8	27 33.5	2100	20 21.6	17 29.7
0600	20 31.5	34 47.7	1400	21 50.2	27 22.8	2200	20 21.9	17 15.5
0700	20 35.7	34 36.5	1500	21 49.9	27 22.3	2300	20 22.1	17 1.3
0800	20 39.6	34 25.4	1600	21 48.3	27 13.2	278 0000	20° 22.0′ W	16° 47.0′ N
0900	20 42.7	34 14.4	1700	21 46.1	27 2.3	0100	20 22.1	16 32.6
1000	20 45.5	34 3.4	1800	21 44.0	26 51.7	0200	20 22.3	16 18.0
1100	20 48.4	33 52.1	1900	21 41.7	26 41.0	0300	20 22.6	16 3.5
1200	20 51.8	33 41.0	2000	21 39.7	26 30.2	0400	20 23.0	15 49.0
1300	20 52.8	33 36.0	2100	21 37.8	26 19.4	0500	20 23.4	15 34.7
1400	20 52.6	33 35.6	2200	21 36.1	26 9.4	0600	20 23.7	15 20.3
1500	20 52.0	33 24.9	2300	21 33.9	25 57.7	0700	20 23.9	15 6.2
1600	20 51.8	33 14.0	276 0000	21° 31.6′ W	25° 45.4′ N	0800	20 24.1	14 52.0
1700	20 38.5	33 11.3	0100	21 29.9	25 32.8	0900	20 24.5	14 37.9
1800	20 23.6	33 8.6	0200	21 28.1	25 20.0	1000	20 24.8	14 23.7
1900	20 8.7	33 6.2	0300	21 26.4	25 7.3	1100	20 24.8	14 9.6
2000	19 54.0	33 3.6	0400	21 25.1	24 54.6	1200	20 24.9	13 55.3
2100	19 39.3	33 1.2	0500	21 23.9	24 41.7	1300	20 25.2	13 41.2
2200	19 24.6	32 59.0	0600	21 22.8	24 30.0	1400	20 25.5	13 26.9

Table H1. (cont.) A summary of the Navigation Log for AMT-1. All times are in GMT.

SDY Time	*Longitude*	*Latitude*	*SDY Time*	*Longitude*	*Latitude*	*SDY Time*	*Longitude*	*Latitude*
278 1500	20° 25.7′ W	13° 13.1′ N	280 2300	24° 30.2′ W	4° 03.9′ N	283 0700	28° 55.7′ W	5° 48.3′ S
1600	20 26.0	13 3.2	281 0000	24° 35.4′ W	3° 53.0′ N	0800	29 0.6	5 59.4
1700	20 26.5	13 2.0	0100	24 40.7	3 41.9	0900	29 5.7	6 10.1
1800	20 31.4	12 51.9	0200	24 46.1	3 30.9	1000	29 10.8	6 20.9
1900	20 36.5	12 41.6	0300	24 51.5	3 20.0	1100	29 15.9	6 31.5
2000	20 41.7	12 31.1	0400	24 56.7	3 9.1	1200	29 20.7	6 40.9
2100	20 47.0	12 20.6	0500	25 2.0	2 58.2	1300	29 26.3	6 52.3
2200	20 52.4	12 10.1	0600	25 7.3	2 47.0	1400	29 30.5	7 0.7
2300	20 56.7	12 0.4	0700	25 12.3	2 36.4	1500	29 31.5	7 2.0
279 0000	21° 02.0′ W	11° 48.4′ N	0800	25 17.1	2 26.1	1600	29 36.6	7 12.0
0100	21 7.4	11 36.5	0900	25 22.1	2 15.7	1700	29 41.6	7 22.3
0200	21 12.8	11 24.5	1000	25 26.7	2 5.4	1800	29 46.3	7 32.6
0300	21 18.3	11 12.5	1100	25 31.3	1 54.8	1900	29 50.9	7 43.0
0400	21 23.5	11 0.2	1200	25 35.2	1 44.3	2000	29 55.5	7 52.8
0500	21 28.6	10 48.1	1300	25 38.6	1 33.6	2100	29 59.7	8 2.4
0600	21 34.2	10 36.4	1400	25 42.1	1 23.8	2200	30 5.1	8 14.7
0700	21 39.6	10 25.4	1500	25 42.6	1 22.1	2300	30 10.7	8 27.1
0800	21 44.7	10 15.1	1600	25 46.8	1 12.0	284 0000	30° 16.1′ W	8° 39.6′ S
0900	21 50.1	10 4.8	1700	25 51.1	1 1.7	0100	30 21.6	8 52.1
1000	21 55.3	9 54.6	1800	25 55.7	0 51.3	0200	30 27.1	9 4.3
1100	22 0.2	9 44.3	1900	26 0.3	0 40.9	0300	30 32.7	9 16.4
1200	22 4.7	9 34.0	2000	26 4.9	0 30.3	0400	30 38.4	9 28.7
1300	22 9.1	9 23.6	2100	26 9.5	0 19.9	0500	30 44.1	9 41.1
1400	22 12.6	9 14.5	2200	26 14.4	0 9.4	0600	30 49.7	9 53.6
1500	22 13.2	9 13.8	2300	26 18.8	0 0.2	0700	30 55.1	10 6.0
1600	22 17.4	9 4.1	282 0000	26° 24.1′ W	0° 12.1′ S	284 0800	31° 00.3′ W	10° 17.7′ S
1700	22 21.7	8 53.9	0100	26 29.2	0 24.6	0900	31 5.3	10 28.4
1800	22 25.7	8 44.1	0200	26 34.1	0 37.3	1000	31 10.3	10 38.8
1900	22 29.5	8 33.9	0300	26 38.9	0 49.7	1100	31 15.0	10 49.1
2000	22 33.9	8 23.7	0400	26 43.9	1 2.1	1200	31 19.7	10 59.3
2100	22 38.4	8 13.8	0500	26 48.8	1 14.6	1300	31 24.5	11 9.4
2200	22 43.0	8 3.6	0600	26 53.6	1 27.0	1400	31 29.1	11 19.6
2300	22 47.4	7 54.5	0700	26 58.2	1 38.2	1500	31 33.1	11 28.2
280 0000	22° 52.9′ W	7° 43.6′ N	0800	27 2.9	1 48.3	1600	31 33.5	11 28.4
0100	22 58.6	7 32.5	0900	27 7.8	1 58.5	1700	31 38.3	11 37.6
0200	23 4.0	7 21.4	1000	27 12.6	2 8.7	1800	31 43.1	11 47.6
0300	23 9.5	7 10.3	1100	27 17.3	2 18.7	1900	31 47.6	11 57.7
0400	23 14.8	6 59.3	1200	27 22.0	2 28.8	2000	31 51.5	12 8.0
0500	23 20.1	6 48.4	1300	27 27.0	2 38.8	2100	31 55.9	12 18.0
0600	23 25.4	6 37.6	1400	27 31.4	2 47.5	2200	32 0.8	12 27.6
0700	23 30.3	6 27.7	1500	27 32.0	2 47.3	2300	32 5.8	12 37.4
0800	23 34.5	6 18.3	1600	27 36.2	2 56.1	285 0000	32° 10.6′ W	12° 46.7′ S
0900	23 38.8	6 8.7	1700	27 40.9	3 5.7	0100	32 16.3	12 58.2
1000	23 43.0	5 59.1	1800	27 45.7	3 15.5	0200	32 21.7	13 10.0
1100	23 47.1	5 49.4	1900	27 50.1	3 24.3	0300	32 27.0	13 21.8
1200	23 51.1	5 39.5	2000	27 55.2	3 35.9	0400	32 32.1	13 33.9
1300	23 55.0	5 29.6	2100	27 60.0	3 46.4	0500	32 37.2	13 46.1
1400	23 58.2	5 21.1	2200	28 4.8	3 57.2	0600	32 42.7	13 58.3
1500	23 58.2	5 20.8	2300	28 9.2	4 7.0	0700	32 48.1	14 10.5
1600	24 1.5	5 12.1	283 0000	28° 14.9′ W	4° 19.6′ S	0800	32 53.4	14 22.1
1700	24 5.4	5 2.9	0100	28 20.8	4 32.3	0900	32 59.0	14 32.8
1800	24 9.2	4 53.4	0200	28 26.8	4 45.1	1000	33 4.3	14 43.4
1900	24 13.1	4 43.8	0300	28 32.8	4 58.0	1100	33 9.4	14 54.0
2000	24 17.1	4 33.8	0400	28 38.7	5 10.9	1200	33 14.1	15 4.7
2100	24 21.2	4 23.5	0500	28 44.6	5 23.7	1300	33 18.5	15 15.3
2200	24 25.9	4 13.4	0600	28 50.4	5 36.4	1400	33 23.0	15 25.8

Table H1. (cont.) A summary of the Navigation Log for AMT-1. All times are in GMT.

SDY Time	*Longitude*	*Latitude*	*SDY Time*	*Longitude*	*Latitude*	*SDY Time*	*Longitude*	*Latitude*
285 1500	33° 26.8′ W	15° 34.5′ S	287 2300	37° 57.5′ W	24° 55.9′ S	290 0700	45° 35.7′ W	32° 21.0′ S
1600	33 27.3	15 35.2	288 0000	38° 04.7′ W	25° 03.6′ S	0800	45 43.4	32 28.9
1700	33 32.0	15 44.8	0100	38 13.5	25 12.8	0900	45 51.0	32 37.3
1800	33 37.1	15 55.6	0200	38 22.2	25 21.7	1000	45 57.9	32 44.7
1900	33 42.2	16 6.5	0300	38 31.0	25 30.5	1100	46 4.4	32 51.1
2000	33 47.1	16 17.3	0400	38 40.1	25 39.3	1200	46 10.6	32 56.5
2100	33 51.6	16 27.8	0500	38 49.5	25 48.1	1300	46 16.0	33 1.7
2200	33 55.9	16 38.1	0600	38 58.9	25 56.9	1400	46 21.3	33 6.7
2300	34 0.5	16 48.1	0700	39 8.2	26 5.7	1500	46 25.7	33 11.1
286 0000	34° 05.0′ W	16° 57.3′ S	0800	39 16.0	26 13.6	1600	46 24.5	33 10.8
0100	34 10.7	17 8.6	0900	39 23.5	26 21.8	1700	46 30.7	33 16.0
0200	34 16.3	17 19.9	1000	39 30.8	26 30.2	1800	46 38.2	33 20.7
0300	34 21.8	17 31.6	1100	39 38.2	26 38.3	1900	46 49.0	33 22.1
0400	34 27.5	17 43.2	1200	39 46.1	26 45.8	2000	47 0.1	33 23.7
0500	34 33.2	17 54.8	1300	39 53.9	26 53.4	2100	47 11.4	33 25.7
0600	34 39.0	18 6.1	1400	40 1.9	27 0.9	2200	47 22.6	33 27.9
0700	34 44.8	18 17.3	1500	40 8.6	27 7.3	2300	47 34.5	33 31.0
0800	34 49.9	18 27.9	1600	40 8.3	27 7.0	291 0000	47° 48.1′ W	33° 34.2′ S
0900	34 54.9	18 38.0	1700	40 15.7	27 13.9	0100	48 2.4	33 37.0
1000	34 59.7	18 48.3	1800	40 23.3	27 21.9	0200	48 16.4	33 40.4
1100	35 4.2	18 58.8	1900	40 30.9	27 30.2	0300	48 30.6	33 44.4
1200	35 8.6	19 9.0	2000	40 38.4	27 38.5	0400	48 44.9	33 48.2
1300	35 13.2	19 19.1	2100	40 46.0	27 46.7	0500	48 59.2	33 51.9
1400	35 17.7	19 29.2	2200	40 54.0	27 54.9	0600	49 13.5	33 55.2
1500	35 21.6	19 38.2	2300	41 2.2	28 3.0	0700	49 27.5	33 58.1
1600	35 21.9	19 39.3	289 0000	41° 10.1′ W	28° 10.8′ S	0800	49 41.8	34 1.0
1700	35 26.2	19 49.3	0100	41 19.0	28 19.5	0900	49 56.4	34 3.8
1800	35 30.8	20 0.2	0200	41 27.9	28 28.3	1000	50 10.8	34 6.8
1900	35 35.6	20 11.2	0300	41 36.8	28 37.2	1100	50 25.4	34 9.5
2000	35 40.1	20 20.7	0400	41 46.1	28 46.0	1200	50 39.4	34 12.4
2100	35 45.3	20 31.0	0500	41 55.4	28 54.7	1300	50 53.1	34 15.0
2200	35 50.5	20 42.1	0600	42 4.8	29 3.5	1400	51 6.9	34 17.4
2300	35 55.4	20 53.8	0700	42 13.9	29 12.6	1500	51 21.0	34 20.3
287 0000	36° 01.0′ W	21° 05.1′ S	0800	42 22.1	29 21.0	1600	51 10.9	34 3.3
0100	36 7.1	21 16.3	0900	42 30.5	29 29.3	1700	51 51.5	34 26.1
0200	36 13.3	21 27.4	1000	42 39.2	29 37.5	1800	52 6.9	34 29.1
0300	36 19.5	21 38.6	1100	42 48.3	29 45.8	1900	52 22.3	34 32.5
0400	36 25.7	21 49.7	1200	42 57.4	29 54.0	2000	52 38.2	34 36.1
0500	36 32.0	22 1.4	1300	43 6.3	30 1.9	2100	52 53.8	34 39.7
0600	36 38.1	22 13.3	1400	43 15.3	30 9.9	2200	53 9.3	34 43.4
0700	36 43.8	22 25.3	1500	43 23.3	30 17.2	2300	53 24.9	34 47.0
0800	36 49.2	22 36.6	1600	43 23.5	30 17.6	292 0000	53° 40.6′ W	34° 50.1′ S
0900	36 54.1	22 47.3	1700	43 31.1	30 24.4	0100	53 56.3	34 53.0
1000	36 59.1	22 57.9	1800	43 40.1	30 32.5	0200	54 10.6	34 56.8
1100	37 4.3	23 8.2	1900	43 49.3	30 40.7	0300	54 24.4	35 0.5
1200	37 9.6	23 18.4	2000	43 58.6	30 49.2	0400	54 37.5	35 3.8
1300	37 14.1	23 28.6	2100	44 7.9	30 57.8	0500	54 51.1	35 4.4
1400	37 18.9	23 38.6	2200	44 17.0	31 6.0	0600	55 5.2	35 3.3
1500	37 23.2	23 47.2	2300	44 25.9	31 14.2	0700	55 19.9	35 2.3
1600	37 23.3	23 47.4	290 0000	44° 33.8′ W	31° 21.2′ S	0800	55 35.8	35 1.2
1700	37 27.0	23 55.6	0100	44 43.3	31 29.7	0900	55 51.6	35 0.4
1800	37 31.6	24 5.9	0200	44 52.3	31 38.4	1000	56 6.5	34 59.6
1900	37 36.0	24 16.0	0300	45 1.4	31 47.0	1100	56 13.5	34 54.7
2000	37 40.6	24 26.3	0400	45 10.4	31 55.6	294 1500	55° 33.7′ W	35° 11.6′ S
2100	37 45.6	24 36.6	0500	45 18.9	32 4.2	1600	55 23.2	35 20.4
2200	37 50.5	24 47.2	0600	45 27.3	32 12.5	1700	55 13.0	35 29.6

Table H1. (cont.) A summary of the Navigation Log for AMT-1. All times are in GMT.

SDY Time	*Longitude*	*Latitude*	*SDY Time*	*Longitude*	*Latitude*	*SDY Time*	*Longitude*	*Latitude*
294 1800	55° 12.3′ W	35° 43.0′ S	295 2000	55° 19.6′ W	41° 19.9′ S	296 2200	56° 34.4′ W	47° 11.5′ S
1900	55 12.8	35 56.5	2100	55 22.5	41 34.0	2300	56 38.0	47 25.3
2000	55 13.4	36 10.3	2200	55 25.5	41 48.4	297 0000	56° 41.0′ W	47° 39.3′ S
2100	55 13.7	36 24.3	2300	55 28.2	42 2.8	0100	56 44.4	47 53.4
2200	55 13.7	36 38.3	296 0000	55° 30.9′ W	42° 17.0′ S	0200	56 47.2	48 7.5
2300	55 13.6	36 52.1	0100	55 33.4	42 30.8	0300	56 49.8	48 21.4
295 0000	55° 13.8′ W	37° 05.9′ S	0200	55 36.0	42 44.4	0400	56 52.6	48 35.4
0100	55 14.3	37 19.4	0300	55 39.1	42 58.2	0500	56 55.8	48 49.2
0200	55 16.1	37 32.8	0400	55 42.3	43 12.2	0600	56 58.6	49 3.0
0300	55 18.4	37 46.4	0500	55 45.8	43 26.6	0700	57 1.9	49 16.5
0400	55 21.7	37 59.8	0600	55 49.5	43 40.8	0800	57 5.1	49 30.0
0500	55 23.5	38 13.5	0700	55 53.0	43 55.2	0900	57 8.4	49 43.4
0600	55 25.4	38 27.4	0800	55 55.8	44 10.0	1000	57 11.9	49 56.6
0700	55 27.3	38 41.3	0900	55 57.9	44 24.7	1100	57 15.1	50 9.9
0800	55 29.4	38 55.5	1000	55 59.8	44 39.2	1200	57 18.5	50 23.2
0900	55 31.3	39 9.5	1100	56 2.2	44 53.3	1300	57 21.9	50 36.6
1000	55 32.6	39 23.4	1200	56 6.1	45 7.1	1400	57 25.0	50 48.3
1100	55 33.5	39 36.4	1300	56 9.3	45 20.8	1500	57 25.9	50 51.4
1200	55 35.2	39 49.4	1400	56 12.1	45 34.2	1600	57 28.3	51 5.0
1300	55 37.0	40 1.9	1500	56 13.8	45 47.7	1700	57 31.0	51 18.8
1400	55 35.7	40 14.2	1600	56 17.1	46 0.2	1800	57 34.5	51 32.4
1500	55 29.5	40 27.0	1700	56 17.0	46 2.0	1900	57 41.6	51 44.0
1600	55 23.7	40 40.1	1800	56 19.7	46 15.8	2000	57 54.7	51 49.8
1700	55 17.8	40 53.5	1900	56 23.4	46 29.6	2100	58 6.7	51 54.2
1800	55 15.5	40 57.2	2000	56 26.9	46 43.6	2200	58 19.5	51 56.4
1900	55 17.1	41 5.9	2100	56 30.7	46 57.7	2300	58 29.3	51 54.3

Table I1. A summary of the UOR Tow Log for AMT-1. All times are in GMT. The minimum and maximum depths reached for each tow is given by $Z_{\min}$ and $Z_{\max}$, respectively.

	Before Station				*After Station*				
SDY	Hours	File	$Z_{\min}$	$Z_{\max}$	Hours	File	$Z_{\min}$	$Z_{\max}$	*Notes*
268	2.50	R995T01	10	70	7.50	R995T02	5	64	500 m wire before, 400 m after.
269	6.50	R995T03	4	65	7.25	R995T04	3	60	400 m wire.
270	4.00	R995T05	5	65	9.25	R995T06	4	62	400 m wire.
271	6.50	R995T07	4	64	7.75	R995T08	4	64	400 m wire.
272	6.50	R995T09	4	64	8.00	R995T10	4	64	400 m wire.
273	6.50	R995T11	4	64	2.00	R995T12	7	68	Heading for Madeira.
275	*Towing Suspended*				7.00	R995T13	10	78	500 m wire plus fairing.
276	6.50	R995T14	10	80	8.00	R995T15	15	75	500 m wire plus fairing.
277	4.50	R995T16	10	75	1.00	R995T17	15	80	500 m wire.
278	1.00	R995T18	10	80	6.00	R995T19	10	75	500 m wire.
279	7.00	R995T20	10	75	8.00	R995T21	12	78	
280	7.00	R995T22	15	78	6.00	R995T23	10	75	500 m wire.
281	7.00	R995T24	15	75	8.25	R995T25	20	85	
282	7.00	R995T26	15	75	8.00	R995T27	22	80	Did not reach shallow setting.
283	7.00	R995T28	22	78	5.50	R995T29	20	78	Changed servo.
284	7.00	R995T30	20	75	8.00	R995T31	19	76	Crank loose on bush.
285	7.00	R995T32	19	78	8.00	R995T33	20	75	Did not reach shallow setting.
286	7.00	R995T34	19	77	3.50	R995T35	18	75	
287	7.00	R995T36	17	78	8.00	R995T37	18	77	
288	7.00	R995T38	19	78	8.00	R995T39	15	75	
289	7.00	R995T40	16	76	8.00	R995T41	16	76	
290	7.00	R995T42	18	78	*Towing Completed*				Became poor at slow speed.

Table J1. Daily Pigment Extraction Log for AMT-1.

Station		268	269	270	271	272	273	275	276	277	278	279	280	281
Bottle	Z_1	POI	POI	POI	POI	POI	POI	POI	POI	POI	POI	POI	POI	POI
	Z_2	POI	POI	POI	POI	POIDA	POI	POI	POI	POI	POI	POI	POI	POI
	Z_3	POI	POI	POIDA	POIDA	POI	POIDA	POI	POIDA	POIDA	POIDA	POI	POI	POI
	Z_4	POI	POI	POI	POI	POI	POI	POIDA	POI	POI	POI	POI	POI	POI
	Z_5	POI	POI	POI	POI	POI	POI	POI	POI	POI	POI	POI	POI	POI
Station		282	283	284	285	286	287	288	289	290	295	296	297	
Bottle	Z_1	POI	POI	POI	POI	POI	POI	POI	POI	POI	POI	POI	POI	
	Z_2	POI	POI	POI	POI	POI	POI	POI	POI	POI	POI	POI	POI	
	Z_3	POI	POI	POI	POI	POI	POI	POI	POI	POI	POIDA	POI	POI	
	Z_4	POI	POI	POI	POI	POI	POI	POI	POI	POI	POI	POI	POI	
	Z_5	POI	POI	POI	POI	POI	POI	POI	POI	POI	POI	POI	POI	

P Pigment sample.

O Organic carbon sample.

I Inorganic carbon sample.

D Dissolved organic carbon sample.

A Particle absorption (filter papers) sample.

Table J2. The underway 2-hourly Pigment Extraction Log for AMT-1. Sample times are approximate and in GMT.

SDY	0100	0200	0300	0400	0500	0600	0700	0800	0900	1000	1100	1200
267												
268	6		7		8		9		10			
269	17		18		19		20		21		22	
270	29		30		31		32				33	
271		40		41		42		43		44		
272		50		51		52		53		54		
273		61		62		63		64		65		
274		71		72		73		74		75		
275		81				83		84		85		
276		91		92		93		94	95	96		
277				104		105		106		107	108	
278		115		116			117			118		119
279			126		127		128		129		130	
280	136		137	138			139		140			
281		148			149		150		151		152	
282	156		157		158		159		160		161	
283		167	168		169		170		171		172	
284			177			178		179		180		
285		186			187		188			189		190
286		196		197		198		199		200		201
287		206		207		208		209		210		211
288		216		217		218		219		220		
289		226		227		228		229	230			
290		236		237		238		240		241		
291		247		248			249		250		251	
292												
293												
294												
295		261	262		263		264		265		266	
296	272		273		274		275		276		277	
297	283		284		285		286		287		288	

Table J2. (cont.) The underway 2-hourly Pigment Extraction Log for AMT-1. Sample times are approximate and in GMT.

SDY	1300	1400	1500	1600	1700	1800	1900	2000	2100	2200	2300	2400
267					2		3		4		5	
268	11		12			14			15		16	
269	23		24		25		26		27		28	
270	34		35		36		37			38		
271	45		46		47				48			39
272	55		56		57		58			59		49
273	66		67		68		69				70	60
274	76				77				78			
275		86		87			88		89			80
276	97		99				100		101		102	90
277		109		110		111		112		113		103
278	120			121			121		123		124	114
279		131			132		133	134	135			125
280	141	142		143		144		145			147	
281		153			154					155		
282		162		163				164		165		
283		173		174			175				176	166
284	181		182			183				184	185	
285			191		192			193		194		
286			201		202			203		204		
287			212			213		214	215	216		
288	221		222		223			224			225	
289	231		232		233	234				235		
290	242		243		244			245			246	
291	252		253		254				255			
292												
293												
294							258		259		260	
295		267										
296	278			278		280		281			282	
297		289		290		291						

Table J3. The underway 4-hourly Pigment Extraction Log for AMT-1. Sample times are approximate and in GMT.

SDY	0100	0200	0300	0400	0500	0600	0700	0800	0900	1000	1100	1200
267												
268			P				PSDP					
269				P				PSDP				PSDP
270				P							PSDP	
271				P				PSDP				
272				P				PSDA				
273				P				PSDA				
274				P				P				
275				P				PS				
276				P				PSD				
277				P				PSD			PSDA	
278					P					PSDA		
279	P				P				PS			
280					P				PS			
281					P				PS			

Table J3. (cont.) The underway 4-hourly Pigment Extraction Log for AMT-1. Sample times are approximate and in GMT.

SDY	0100	0200	0300	0400	0500	0600	0700	0800	0900	1000	1100	1200
282					P				PS			
283				P						PS		
284				P						PS		
285		P			P					PS		
286		P			P					PS		
287						P				PS		
288						P				PS		
289		P				P				PS		
290		P				P					PS	
291			P									
292												
293												
294												
295		P			P						PS	
296					P				PS			
297	P				P			P				

Table J3. (cont.) The underway 4-hourly Pigment Extraction Log for AMT-1. Sample times are approximate and in GMT.

SDY	1300	1400	1500	1600	1700	1800	1900	2000	2100	2200	2300	2400
267					P				P			
268	PSDP			PSDP				P				
269				PSDP					P			
270			PSDP				PSDP			P		
271	PSDP				PSDP				P			
272	PSP				PSDA					P		
273	PSDA				P					P		
274	P				P				P			
275			PSD				P					P
276	PSD				PSD		P		P		P	
277				PSDA				P				
278	PSDA			PSDA				P				
279		P					P		P			
280	PS					P				P		
281		PS								PS		
282		PS						P				
283		PS					PS					P
284			PS							P		P
285			PS					P				
286			PS					P			P	
287			PS					P				
288			PS					P			P	P
289			PS			P						
290			PS				P				P	
291	PS			PS				PS				
292												
293												
294									P			
295			PSDA									
296	PS			PS					P			
297			PS			P						

Table K1. A summary of the Primary Production and FRRF Log for AMT-1.

Station		*Sample*	*Chlorophyll*		*Calcifi-*	*Photosynthesis*		*P-I*	
Date	*SDY*	*Depth*	*Total*	*Size*	*cation*	*Total*	*Size*	*Experiment*	*FRRF*
25 September	268	7	✓		✓	✓			✓
		20	✓		✓	✓			✓
		30	✓		✓	✓			✓
		50	✓		✓	✓		✓	✓
		70	✓		✓	✓			✓
26 September	269	7	✓		✓	✓			✓
		20	✓		✓	✓			✓
		30	✓			✓			✓
		40	✓		✓	✓		✓	✓
		50	✓			✓			✓
27 September	270	7	✓		✓	✓		✓	✓
		30	✓		✓	✓			✓
		40	✓		✓	✓			✓
		50	✓		✓	✓		✓	✓
		60	✓		✓	✓			✓
28 September	271	7	✓		✓	✓		✓	✓
		30	✓		✓	✓			✓
		50	✓		✓	✓			✓
		60	✓		✓	✓		✓	✓
		80	✓		✓	✓			✓
29 September	272	7	✓		✓	✓		✓	✓
		30	✓		✓	✓			✓
		60	✓		✓	✓			✓
		90	✓		✓	✓		✓	✓
		120	✓		✓	✓			✓
30 September	273	7	✓		✓	✓			✓
		50	✓		✓	✓			✓
		90	✓			✓			✓
		110	✓	✓	✓	✓	✓	✓	✓
		130	✓			✓			✓
2 October	275	7	✓		✓	✓			✓
		50	✓		✓	✓			✓
		80	✓			✓			✓
		100	✓	✓	✓	✓	✓	✓	✓
		130	✓			✓			✓
3 October	276	7	✓		✓	✓			✓
		40	✓			✓			✓
		60	✓		✓	✓			✓
		80	✓		✓	✓		✓	✓
		100	✓			✓			✓
4 October	277	7	✓		✓	✓			✓
		20	✓			✓			✓
		30	✓	✓	✓	✓	✓	✓	✓
		40	✓			✓			✓
		50	✓			✓			✓
5 October	278	7	✓	✓	✓	✓	✓		✓
		30	✓			✓			✓
		50	✓			✓			✓
		70	✓	✓	✓	✓	✓	✓	✓
		100	✓			✓			✓

Table K1. (cont.) A summary of the Primary Production and FRRF Log for AMT-1.

Station		*Sample*	*Chlorophyll*		*Calcifi-*	*Photosynthesis*		*P-I*	
Date	*SDY*	*Depth*	*Total*	*Size*	*cation*	*Total*	*Size*	*Experiment*	*FRRF*
6 October	279	7	✓	✓	✓	✓	✓		✓
		20	✓			✓			✓
		40	✓	✓	✓	✓	✓		✓
		60	✓	✓	✓	✓	✓	✓	✓
		80	✓			✓			✓
7 October	280	7	✓	✓	✓	✓	✓		✓
		40	✓			✓			✓
		60	✓			✓			✓
		80	✓	✓	✓	✓	✓	✓	✓
		100	✓			✓			✓
8 October	281	7	✓	✓	✓	✓	✓		✓
		30	✓			✓			✓
		60	✓			✓			✓
		80	✓	✓	✓	✓	✓	✓	✓
		100	✓			✓			✓
9 October	282	7	✓	✓	✓	✓	✓		✓
		40	✓			✓			✓
		70	✓			✓			✓
		90	✓	✓	✓	✓	✓	✓	✓
		120	✓			✓			✓
10 October	283	7	✓	✓	✓	✓	✓		✓
		50	✓			✓			✓
		80	✓			✓			✓
		100	✓	✓	✓	✓	✓	✓	✓
		140	✓			✓			✓
11 October	284	7	✓	✓	✓	✓	✓		
		70	✓			✓			✓
		100	✓			✓			✓
		140	✓	✓	✓	✓	✓	✓	✓
12 October	285	7	✓	✓	✓	✓	✓		✓
		60	✓			✓			✓
		120	✓			✓			✓
		150	✓	✓	✓	✓	✓	✓	✓
		180	✓			✓			✓
13 October	286	7	✓		✓	✓			✓
		60	✓			✓			✓
		120	✓			✓			✓
		160	✓	✓	✓	✓	✓	✓	✓
14 October	287	7	✓	✓		✓	✓		✓
		60	✓			✓			✓
		100	✓			✓			✓
		120	✓	✓		✓	✓	✓	✓
		140	✓			✓			✓
15 October	288	7	✓	✓		✓	✓		✓
		50	✓			✓			✓
		80	✓	✓		✓	✓	✓	✓
		100	✓			✓			✓
16 October	289	7	✓	✓	✓	✓	✓		✓
		50	✓			✓			✓
		80	✓			✓			✓
		100	✓	✓	✓	✓	✓	✓	✓
		120	✓			✓			✓

Table K1. (cont.) A summary of the Primary Production and FRRF Log for AMT-1.

Station		*Sample*	*Chlorophyll*		*Calcifi-*	*Photosynthesis*		*P-I*	
Date	*SDY*	*Depth*	*Total*	*Size*	*cation*	*Total*	*Size*	*Experiment*	*FRRF*
17 October	290	7	✓	✓	✓	✓	✓		✓
		20	✓			✓			✓
		40	✓	✓	✓	✓	✓	✓	✓
		60	✓			✓			✓
		80	✓			✓			✓
22 October	295	7	✓	✓	✓	✓	✓		✓
		20	✓			✓			✓
		30	✓			✓			✓
		40	✓	✓	✓	✓	✓	✓	✓
		60	✓			✓			✓
23 October	296	7	✓	✓	✓	✓	✓		✓
		20	✓			✓			✓
		30	✓			✓			✓
		40	✓	✓	✓	✓	✓	✓	✓
		60	✓			✓			✓
24 October	297	7	✓			✓			✓
		20	✓			✓			✓
		30	✓	✓		✓	✓	✓	✓
		40	✓			✓			✓
		60	✓			✓			✓

Table L1. A summary of the Nutrient Sampling Log for AMT-1. All times are in GMT.

SDY	1	2	3	4	5	6	7	8	9	10	11	12	13	14	15	16	17	18	19	20	21	22	23	24
267																	×				×			
268	×				×		×						×			×					×			
269	×							×				×				×						×		
270				×						×					×				×			×		
271				×				×					×				×				×			
272				×				×					×						×				×	
273			×					×					×				×					×		×
274				×				×					×				×				×			×
275				×				×						×					×					×
276				×				×					×				×				×			×
277				×				×			×					×						×		×
278				×				×					×		×						×			
279	×			×				×						×					×			×		
280					×				×					×				×				×		
281					×				×					×								×		
282				×							×			×						×				
283	×			×					×					×					×					×
284					×					×					×							×		
285	×				×					×					×									
286	×			×						×					×									
287						×				×					×					×				×
288						×				×					×					×			×	
289		×				×				×					×			×						
290		×				×				×					×				×				×	
291			×				×						×			×				×				
292	×																							
294																								
295		×			×				×		×						×							
296																								
297																								

Appendix M

AMT-1 Cruise Participants

The participants in AMT-1 are presented alphabetically.

Anthony Bale
Plymouth Marine Laboratory
Prospect Place
Plymouth PL1 3DH
United Kingdom
Voice: 44–1–752–633–425
Fax: 44–1–752–633–101
Net: a.bale@pml.ac.uk

Christopher Galienne
Institute of Marine Studies
University of Plymouth
Drake Circus
Plymouth PL4 8AA
United Kingdom
Voice: 44–1–752–232–457
Fax: 44–1–752–232–406
Net: cgallienne@plymouth.ac.uk

Stanford Hooker
NASA/GSFC/Code 970.2
Bldg. 28, Room W121
Greenbelt, MD 20771
USA
Voice: (301) 286–9503
Fax: (301) 286–1775
Net: stan@ardbeg.gsfc.nasa.gov

Samuel Laney
BNL/DAS/OASD
Bldg. 318
Upton, NY 11973
USA
Voice: (914) 358–4938
Fax: (914) 358–4938
Net: slaney@j51.com

Emilio Marañón
Dept. Biologia de Ogranismos y Sistemas
Universidad de Oviedo
E–33071 Oviedo, Spain
Voice: 34–8–510–4830
Fax: 34–8–510–4777
Net: emilio@vmesa.cpd.uniovi.es

Gerald Moore
Plymouth Marine Laboratory
Prospect Place
Plymouth PL1 3DH
United Kingdom
Voice: 44–1–752–633–416
Fax: 44–1–752–633–101
Net: g.moore@pml.ac.uk

Nigel Rees
Plymouth Marine Laboratory
Prospect Place
Plymouth PL1 3DH
United Kingdom
Voice: 44–1–752–633–416
Fax: 44–1–752–633–101
Net: n.rees@pml.ac.uk

David Robins
Plymouth Marine Laboratory
Prospect Place
Plymouth PL1 3DH
United Kingdom
Voice: 44–1–752–633–414
Fax: 44–1–752–633–101
Net: d.robins@pml.ac.uk

William Spooner
Southampton Oceanography Centre
Southampton SO9 5NH
United Kingdom
Voice: 44–1–703–593–253
Fax: 44–1–703–593–161
Net: wspooner@soc.ac.uk

Guy Westbrook
Institute of Marine Studies
University of Plymouth
Drake Circus
Plymouth PL4 8AA
United Kingdom
Voice: 44–1–752–232–459
Fax: 44–1–752–232–406
Net: awestbrook@plymouth.ac.uk

Glossary

A/D	Analog to Digital
ADCP	Acoustic Doppler Current Profiler
AMT	Atlantic Meridional Transect
AMT-1	The First AMT Cruise
BAS	British Antarctic Survey
BNL	Brookhaven National Laboratory
BSI	Biospherical Instruments, Incorporated
Case-1	Water whose reflectance is determined solely by absorption.
Case-2	Water whose reflectance is significantly influenced by scattering.
CHN	Carbon Hydrogen Nitrogen (analysis)
CHORS	Center for Hydro-Optics and Remote Sensing (San Diego State University)
C/N	Carbon-to-Nitrogen (ratio)
CTD	Conductivity, Temperature, and Depth
CWL	Center Wavelength
CZCS	Coastal Zone Color Scanner
DC	Direct Current
DCM	Deep Chlorophyll Maximum
DOC	Dissolved Organic Carbon
DOE	Department of Energy
EEZ	Exclusive Economic Zone
FEL	Not an acronym, but a lamp designator.
FRRF	Fast Repetition Rate Fluorometer
GF/F	Not an acronym; a specific type of glass fiber filter manufactured by Whatman.
GMT	Greenwich Mean Time
GPS	Global Positioning System
GSFC	Goddard Space Flight Center
GUI	Graphical User Interface
HPLC	High Performance Liquid Chromatography

IAPSO	International Association for the Physical Sciences of the Ocean
IBM	International Business Machines
IDL	Interactive Data Language
JCR	(RRS) *James Clark Ross*
JGOFS	Joint Global Ocean Flux Study
LAN	Local Area Network
LHCII	Light-Harvesting Complex II
MS-DOS	Microsoft-Disk Operating System
MVDS	Multichannel Visible Detector System
NASA	National Aeronautics and Space Administration
NECC	North Equatorial Counter Current
NERC	Natural Environmental Research Council
OCI	Ocean Color Irradiance
OCR	Ocean Color Radiance
OCTS	Ocean Color Temperature Sensor (Japan)
OPC	Optical Plankton Counter
ORKA	On-line Real-time Knowledge-based Analysis
PAR	Photosynthetically Available Radiation
PC	(IBM) Personal Computer
P-I	Production-Irradiance
PML	Plymouth Marine Laboratory
POC	Particulate Organic Carbon
PON	Particulate Organic Nitrogen
ppm	parts per million
PRIME	Plankton Reactivity in the Marine Environment
PRR	Profiling Reflectance Radiometer
PRT	Platinum Resistance Thermometer
PSII	Photosystem II
RAF	Royal Air Force
RDI	RD Instruments
RRS	Royal Research Ship
RTM	Reversing Thermometer
SBE	Sea-Bird Electronics
SDY	Sequential Day of the Year
SeaOPS	SeaWiFS Optical Profiling System
SeaWiFS	Sea-viewing Wide Field-of-view Sensor
SFP	Size-Fractionated Pigments
SHP	Shaft Horsepower
SIMBIOS	Sensor Intercomparison and Merger for Biological and Interdisciplinary Ocean Studies
SIRREX	SeaWiFS Intercalibration Round-Robin Experiment
SIS	Sensoren-Instrumente Systeme
S/N	Serial Number
SOC	Southampton Oceanography Center
SST	Sea Surface Temperature
Sun	Sun Microsystems
SWL	Safe Working Load
UIC	Underway Instrumentation and Control (Room)
UoP	University of Plymouth
UOR	Undulating Oceanographic Recorder
WMO	World Meteorological Organization
WP2	Not an acronym, but a standard net mesh size (200 μm).
XBT	Expendable Bathythermograph

Symbols

a	The absorption coefficient.
a_N	Normalized absorption coefficient.
$a_p(\lambda)$	Particulate absorption.
$\tilde{a}$	The measured value of a.
b	The scattering coefficient.
c	The beam attenuation coefficient $(a + b)$.
C	Chlorophyll concentration.
$\tilde{c}$	The measured value of c.
$E_d(0, \lambda)$	Surface irradiance.
$E_d(\lambda)$	Downwelling irradiance.
$E_s(\lambda)$	Incident solar irradiance.
F	Fluorescence.
F_0	Initial fluorescence.
F_m	Total sample maximal fluorescence (directly comparable to values measured by standard active fluorometers).
F_v	Variable fluorescence, $F_m - F_0$.
$K_d(\lambda)$	Diffuse attenuation coefficient.
$L_u(\lambda)$	Upwelling radiance.
$p\mathrm{CO}_2$	The partial pressure of CO_2.
$PB_{\max}$	Maximum biomass-specific photosynthetic rate.
R	Reflectance.
z	Depth.
$\beta(\theta)$	The scattering phase function.
$\Delta p\mathrm{CO}_2$	The difference in the partial pressure of CO_2 in the air and in the sea.
$\Delta\Phi_{\max}$	The ratio F_v/F_m which corresponds to the (normalized) maximum number of reaction centers in the chlorophyll population which are capable of photosynthesis.
θ	An angle.
λ	Wavelength of light.
σ	Standard deviation.
σ_t	The density of sea water determined from the *in situ* salinity and temperature, but at atmospheric pressure.

References

Aiken, J., 1981: A chlorophyll sensor for automatic, remote operation in the marine environment. *Mar. Ecol. Prog. Ser.,* **4,** 235–239.

——, 1985: The Undulating Oceanographic Recorder Mark 2. A multirole oceanographic sampler for mapping and modelling the biophysical marine environment. In: *Mapping Strategies in Chemical Oceanography.* A. Zirino, Ed., American Chemical Society, **209,** 315–332.

——, and I. Bellan, 1990: "Optical oceanography: an assessment of towed measurement." In: *Light and Life in the Sea.* P.J. Herring, A.K. Campbell, M. Whitfield, and L. Maddock, Eds., Cambridge University Press, 39–57.

Balch, W.M., P.M. Holligan, K.A. Kilpatrick, 1992: Calcification, photosynthesis and growth of the bloom-forming coccolithophore *Emiliania huxleyi. Contin. Shelf Res.,* **12,** 1,353–1,374.

Brewer, P.G., and J.P. Riley, 1965: The automatic determination of nitrate in sea water. *Deep-Sea Res.,* **12,** 765–772.

Culkin, F., and N.D. Smith, 1980: Determination of the concentration of KCl solution having the same electric conductivity at 15°C and infinite frequency as standard seawater of salinity 35 ppt (chlorinity 19.37394 ppt). *IEEE J. Ocean Eng.,* **5,** 22–25.

Falkowski, P.G., R. Greene, and R. Geider, 1992: Physiological limitations on phytoplankton productivity in the ocean. *Oceanography,* **5,** 84–91.

Hooker, S.B., and W.E. Esaias, 1993: An overview of the SeaWiFS Project. *Eos, Trans. AGU,* **74,** 241–246.

Joint Global Ocean Flux Study, 1991: JGOFS Core Measurements Protocols. *JGOFS Report No. 6,* Scientific Committee on Oceanic Research, 40 pp.

Joint, I.R., and A.J. Pomroy, 1983: Production of picoplankton and small nanoplankton in the Celtic Sea. *Mar. Biol.,* **77,** 19–27.

Kirkwood, D.S., 1989: Simultaneous determination of selected nutrients in seawater. *ICES CM1989/C:29,* 12 pp.

Kolber, Z., K.D. Wyman, and P.G. Falkowski, 1990: Natural variability in photosynthetic energy conversion efficiency: A field study in the Gulf of Maine. *Limnol. Oceanogr.,* **35,** 72–79.

——, and P. Falkowski, 1993: Use of active fluorescence to estimate phytoplankton photosynthesis *in situ. Limnol. Oceanogr.,* **38,** 1,646–1,665.

Lean, R.S., and B.K. Burnison, 1979: An evaluation of the errors in the ^{14}C method of primary production measurement. *Limnol. Oceanogr.,* **24,** 917–928.

McClain, C.R., W.E. Esaias, W. Barnes, B. Guenther, D. Endres, S.B. Hooker, G. Mitchell, and R. Barnes, 1992: Calibration and Validation Plan for SeaWiFS. *NASA Tech. Memo. 104566, Vol. 3,* S.B. Hooker and E.R. Firestone, Eds., NASA Goddard Space Flight Center, Greenbelt, Maryland, 41 pp.

Mueller, J.L., and R.W. Austin, 1995: Ocean Optics Protocols for SeaWiFS Validation, Revision 1. *NASA Tech. Memo. 104566, Vol. 25,* S.B. Hooker, E.R. Firestone, and J.G. Acker, Eds., NASA Goddard Space Flight Center, Greenbelt, Maryland, 66 pp.

The SeaWiFS Technical Report Series

Vol. 1

Hooker, S.B., W.E. Esaias, G.C. Feldman, W.W. Gregg, and C.R. McClain, 1992: An Overview of SeaWiFS and Ocean Color. *NASA Tech. Memo. 104566, Vol. 1,* S.B. Hooker and E.R. Firestone, Eds., NASA Goddard Space Flight Center, Greenbelt, Maryland, 24 pp., plus color plates.

Vol. 2

Gregg, W.W., 1992: Analysis of Orbit Selection for SeaWiFS: Ascending vs. Descending Node. *NASA Tech. Memo. 104566, Vol. 2,* S.B. Hooker and E.R. Firestone, Eds., NASA Goddard Space Flight Center, Greenbelt, Maryland, 16 pp.

Vol. 3

McClain, C.R., W.E. Esaias, W. Barnes, B. Guenther, D. Endres, S.B. Hooker, G. Mitchell, and R. Barnes, 1992: Calibration and Validation Plan for SeaWiFS. *NASA Tech. Memo. 104566, Vol. 3,* S.B. Hooker and E.R. Firestone, Eds., NASA Goddard Space Flight Center, Greenbelt, Maryland, 41 pp.

Vol. 4

McClain, C.R., E. Yeh, and G. Fu, 1992: An Analysis of GAC Sampling Algorithms: A Case Study. *NASA Tech. Memo. 104566, Vol. 4,* S.B. Hooker and E.R. Firestone, Eds., NASA Goddard Space Flight Center, Greenbelt, Maryland, 22 pp., plus color plates.

Vol. 5

Mueller, J.L., and R.W. Austin, 1992: Ocean Optics Protocols for SeaWiFS Validation. *NASA Tech. Memo. 104566, Vol. 5,* S.B. Hooker and E.R. Firestone, Eds., NASA Goddard Space Flight Center, Greenbelt, Maryland, 43 pp.

Vol. 6

Firestone, E.R., and S.B. Hooker, 1992: SeaWiFS Technical Report Series Summary Index: Volumes 1–5. *NASA Tech. Memo. 104566, Vol. 6,* S.B. Hooker and E.R. Firestone, Eds., NASA Goddard Space Flight Center, Greenbelt, Maryland, 9 pp.

Vol. 7

Darzi, M., 1992: Cloud Screening for Polar Orbiting Visible and IR Satellite Sensors. *NASA Tech. Memo. 104566, Vol. 7,* S.B. Hooker and E.R. Firestone, Eds., NASA Goddard Space Flight Center, Greenbelt, Maryland, 7 pp.

Vol. 8

Hooker, S.B., W.E. Esaias, and L.A. Rexrode, 1993: Proceedings of the First SeaWiFS Science Team Meeting. *NASA Tech. Memo. 104566, Vol. 8,* S.B. Hooker and E.R. Firestone, Eds., NASA Goddard Space Flight Center, Greenbelt, Maryland, 61 pp.

Vol. 9

Gregg, W.W., F.C. Chen, A.L. Mezaache, J.D. Chen, J.A. Whiting, 1993: The Simulated SeaWiFS Data Set, Version 1. *NASA Tech. Memo. 104566, Vol. 9,* S.B. Hooker, E.R. Firestone, and A.W. Indest, Eds., NASA Goddard Space Flight Center, Greenbelt, Maryland, 17 pp.

Vol. 10

Woodward, R.H., R.A. Barnes, C.R. McClain, W.E. Esaias, W.L. Barnes, and A.T. Mecherikunnel, 1993: Modeling of the SeaWiFS Solar and Lunar Observations. *NASA Tech. Memo. 104566, Vol. 10,* S.B. Hooker and E.R. Firestone, Eds., NASA Goddard Space Flight Center, Greenbelt, Maryland, 26 pp.

Vol. 11

Patt, F.S., C.M. Hoisington, W.W. Gregg, and P.L. Coronado, 1993: Analysis of Selected Orbit Propagation Models for the SeaWiFS Mission. *NASA Tech. Memo. 104566, Vol. 11,* S.B. Hooker, E.R. Firestone, and A.W. Indest, Eds., NASA Goddard Space Flight Center, Greenbelt, Maryland, 16 pp.

Vol. 12

Firestone, E.R., and S.B. Hooker, 1993: SeaWiFS Technical Report Series Summary Index: Volumes 1–11. *NASA Tech. Memo. 104566, Vol. 12,* S.B. Hooker and E.R. Firestone, Eds., NASA Goddard Space Flight Center, Greenbelt, Maryland, 28 pp.

Vol. 13

McClain, C.R., K.R. Arrigo, J. Comiso, R. Fraser, M. Darzi, J.K. Firestone, B. Schieber, E-n. Yeh, and C.W. Sullivan, 1994: Case Studies for SeaWiFS Calibration and Validation, Part 1. *NASA Tech. Memo. 104566, Vol. 13,* S.B. Hooker and E.R. Firestone, Eds., NASA Goddard Space Flight Center, Greenbelt, Maryland, 52 pp., plus color plates.

Vol. 14

Mueller, J.L., 1993: The First SeaWiFS Intercalibration Round-Robin Experiment, SIRREX-1, July 1992. *NASA Tech. Memo. 104566, Vol. 14,* S.B. Hooker and E.R. Firestone, Eds., NASA Goddard Space Flight Center, Greenbelt, Maryland, 60 pp.

Vol. 15

Gregg, W.W., F.S. Patt, and R.H. Woodward, 1994: The Simulated SeaWiFS Data Set, Version 2. *NASA Tech. Memo. 104566, Vol. 15,* S.B. Hooker and E.R. Firestone, Eds., NASA Goddard Space Flight Center, Greenbelt, Maryland, 42 pp., plus color plates.

Vol. 16

Mueller, J.L., B.C. Johnson, C.L. Cromer, J.W. Cooper, J.T. McLean, S.B. Hooker, and T.L. Westphal, 1994: The Second SeaWiFS Intercalibration Round-Robin Experiment, SIRREX-2, June 1993. *NASA Tech. Memo. 104566, Vol. 16,* S.B. Hooker and E.R. Firestone, Eds., NASA Goddard Space Flight Center, Greenbelt, Maryland, 121 pp.

Vol. 17

Abbott, M.R., O.B. Brown, H.R. Gordon, K.L. Carder, R.E. Evans, F.E. Muller-Karger, and W.E. Esaias, 1994: Ocean Color in the 21st Century: A Strategy for a 20-Year Time Series. *NASA Tech. Memo. 104566, Vol. 17,* S.B. Hooker and E.R. Firestone, Eds., NASA Goddard Space Flight Center, Greenbelt, Maryland, 20 pp.

Vol. 18

Firestone, E.R., and S.B. Hooker, 1995: SeaWiFS Technical Report Series Summary Index: Volumes 1–17. *NASA Tech. Memo. 104566, Vol. 18,* S.B. Hooker and E.R. Firestone, Eds., NASA Goddard Space Flight Center, Greenbelt, Maryland, 47 pp.

Vol. 19

McClain, C.R., R.S. Fraser, J.T. McLean, M. Darzi, J.K. Firestone, F.S. Patt, B.D. Schieber, R.H. Woodward, E-n. Yeh, S. Mattoo, S.F. Biggar, P.N. Slater, K.J. Thome, A.W. Holmes, R.A. Barnes, and K.J. Voss, 1994: Case Studies for SeaWiFS Calibration and Validation, Part 2. *NASA Tech. Memo. 104566, Vol. 19,* S.B. Hooker, E.R. Firestone, and J.G. Acker, Eds., NASA Goddard Space Flight Center, Greenbelt, Maryland, 73 pp.

Vol. 20

Hooker, S.B., C.R. McClain, J.K. Firestone, T.L. Westphal, E-n. Yeh, and Y. Ge, 1994: The SeaWiFS Bio-Optical Archive and Storage System (SeaBASS), Part 1. *NASA Tech. Memo. 104566, Vol. 20,* S.B. Hooker and E.R. Firestone, Eds., NASA Goddard Space Flight Center, Greenbelt, Maryland, 40 pp.

Vol. 21

Acker, J.G., 1994: The Heritage of SeaWiFS: A Retrospective on the CZCS NIMBUS Experiment Team (NET) Program. *NASA Tech. Memo. 104566, Vol. 21,* S.B. Hooker and E.R. Firestone, Eds., NASA Goddard Space Flight Center, Greenbelt, Maryland, 43 pp.

Vol. 22

Barnes, R.A., W.L. Barnes, W.E. Esaias, and C.R. McClain, 1994: Prelaunch Acceptance Report for the SeaWiFS Radiometer. *NASA Tech. Memo. 104566, Vol. 22,* S.B. Hooker, E.R. Firestone, and J.G. Acker, Eds., NASA Goddard Space Flight Center, Greenbelt, Maryland, 32 pp.

Vol. 23

Barnes, R.A., A.W. Holmes, W.L. Barnes, W.E. Esaias, C.R. McClain, and T. Svitek, 1994: SeaWiFS Prelaunch Radiometric Calibration and Spectral Characterization. *NASA Tech. Memo. 104566, Vol. 23,* S.B. Hooker, E.R. Firestone, and J.G. Acker, Eds., NASA Goddard Space Flight Center, Greenbelt, Maryland, 55 pp.

Vol. 24

Firestone, E.R., and S.B. Hooker, 1995: SeaWiFS Technical Report Series Summary Index: Volumes 1–23. *NASA Tech. Memo. 104566, Vol. 24,* S.B. Hooker and E.R. Firestone, Eds., NASA Goddard Space Flight Center, Greenbelt, Maryland, 36 pp.

Vol. 25

Mueller, J.L., and R.W. Austin, 1995: Ocean Optics Protocols for SeaWiFS Validation, Revision 1. *NASA Tech. Memo. 104566, Vol. 25,* S.B. Hooker and E.R. Firestone, Eds., NASA Goddard Space Flight Center, Greenbelt, Maryland, 66 pp.

Vol. 26

Siegel, D.A., M.C. O'Brien, J.C. Sorensen, D.A. Konnoff, E.A. Brody, J.L. Mueller, C.O. Davis, W.J. Rhea, and S.B. Hooker, 1995: Results of the SeaWiFS Data Analysis Round-Robin (DARR-94), July 1994. *NASA Tech. Memo. 104566, Vol. 26,* S.B. Hooker and E.R. Firestone, Eds., NASA Goddard Space Flight Center, Greenbelt, Maryland, 58 pp.

Vol. 27

Mueller, J.L., R.S. Fraser, S.F. Biggar, K.J. Thome, P.N. Slater, A.W. Holmes, R.A. Barnes, C.T. Weir, D.A. Siegel, D.W. Menzies, A.F. Michaels, and G. Podesta, 1995: Case Studies for SeaWiFS Calibration and Validation, Part 3. *NASA Tech. Memo. 104566, Vol. 27,* S.B. Hooker, E.R. Firestone, and J.G. Acker, Eds., NASA Goddard Space Flight Center, Greenbelt, Maryland, 46 pp.

Vol. 28

McClain, C.R., K.R. Arrigo, W.E. Esaias, M. Darzi, F.S. Patt, R.H. Evans, J.W. Brown, C.W. Brown, R.A. Barnes, and L. Kumar, 1995: SeaWiFS Algorithms, Part 1. *NASA Tech. Memo. 104566, Vol. 28,* S.B. Hooker, E.R. Firestone, and J.G. Acker, Eds., NASA Goddard Space Flight Center, Greenbelt, Maryland, 38 pp., plus color plates.

Vol. 29

Aiken, J., G.F. Moore, C.C. Trees, S.B. Hooker, and D.K. Clark, 1995: The SeaWiFS CZCS-Type Pigment Algorithm. *NASA Tech. Memo. 104566, Vol. 29,* S.B. Hooker and E.R. Firestone, Eds., NASA Goddard Space Flight Center, Greenbelt, Maryland, 34 pp.

Vol. 30

Firestone, E.R., and S.B. Hooker, 1996: SeaWiFS Technical Report Series Summary Index: Volumes 1–29. *NASA Tech. Memo. 104566, Vol. 30,* S.B. Hooker and E.R. Firestone, Eds., NASA Goddard Space Flight Center, Greenbelt, Maryland, 43 pp.

Vol. 31

Barnes, R.A., A.W. Holmes, and W.E. Esaias, 1995: Stray Light in the SeaWiFS Radiometer. *NASA Tech. Memo. 104566, Vol. 31,* S.B. Hooker, E.R. Firestone, and J.G. Acker, Eds., NASA Goddard Space Flight Center, Greenbelt, Maryland, 76 pp.

Vol. 32

Campbell, J.W., J.M. Blaisdell, and M. Darzi, 1995: Level-3 SeaWiFS Data Products: Spatial and Temporal Binning Algorithms. *NASA Tech. Memo. 104566, Vol. 32,* S.B. Hooker, E.R. Firestone, and J.G. Acker, Eds., NASA Goddard Space Flight Center, Greenbelt, Maryland, 73 pp., plus color plates.

Vol. 33

Moore, G.F., and S.B. Hooker, 1996: Proceedings of the First SeaWiFS Exploitation Initiative (SEI) Team Meeting. *NASA Tech. Memo. 104566, Vol. 33,* S.B. Hooker and E.R. Firestone, Eds., NASA Goddard Space Flight Center, Greenbelt, Maryland, 53 pp.

Vol. 34

Mueller, J.L., B.C. Johnson, C.L. Cromer, S.B. Hooker, J.T. McLean, and S.F. Biggar, 1996: The Third SeaWiFS Intercalibration Round-Robin Experiment (SIRREX-3), 19–30 September 1994. *NASA Tech. Memo. 104566, Vol. 34,* S.B. Hooker, E.R. Firestone, and J.G. Acker, Eds., NASA Goddard Space Flight Center, Greenbelt, Maryland, 78 pp.

Vol. 35

Robins, D.B., A.J. Bale, G.F. Moore, N.W. Rees, S.B. Hooker, C.P. Gallienne, A.G. Westbrook, E. Marañón, W.H. Spooner, and S.R. Laney, 1996: AMT-1 Cruise Report and Preliminary Results. *NASA Tech. Memo. 104566, Vol. 35,* S.B. Hooker and E.R. Firestone, Eds., NASA Goddard Space Flight Center, Greenbelt, Maryland, 87 pp.

REPORT DOCUMENTATION PAGE

Form Approved
OMB No. 0704-0188

1. AGENCY USE ONLY *(Leave blank)*	2. REPORT DATE	3. REPORT TYPE AND DATES COVERED
	April 1996	Technical Memorandum

4. TITLE AND SUBTITLE
SeaWiFS Technical Report Series
Volume 35–AMT-1 Cruise Report and Preliminary Results

5. FUNDING NUMBERS
Code 970.2

6. AUTHOR(S)
David B. Robins, Anthony J. Bale, Gerald F. Moore, Nigel W. Rees, Stanford B. Hooker, Christopher P. Gallienne, Anthony G. Westbrook, Emilio Marañón, William H. Spooner, and Samuel R. Laney
Series Editors: Stanford B. Hooker and Elaine R. Firestone

7. PERFORMING ORGANIZATION NAME(S) AND ADDRESS(ES)
Laboratory for Hydrospheric Processes
Goddard Space Flight Center
Greenbelt, Maryland 20771

8. PERFORMING ORGANIZATION REPORT NUMBER
96B00063

9. SPONSORING/MONITORING AGENCY NAME(S) AND ADDRESS(ES)
National Aeronautics and Space Administration
Washington, D.C. 20546–0001

10. SPONSORING/MONITORING AGENCY REPORT NUMBER
TM–104566, Vol. 35

11. SUPPLEMENTARY NOTES
Elaine R. Firestone: General Sciences Corporation, Laurel, Maryland; David B. Robins, Anthony J. Bale, Gerald F. Moore, and Nigel W. Rees: Plymouth Marine Laboratory, Plymouth, United Kingdom; Christopher P. Gallienne and Anthony G. Westbrook: University of Plymouth, Plymouth, United Kingdom; Emilio Marañón and William H. Spooner: IMS/University of Southampton, Southampton, United Kingdom; and Samuel R. Laney: Brookhaven National Laboratory, Upton, New York

12a. DISTRIBUTION/AVAILABILITY STATEMENT
Unclassified–Unlimited
Subject Category 48
Report is available from the Center for AeroSpace Information (CASI),
7121 Standard Drive, Hanover, MD 21076–1320; (301)621-0390

12b. DISTRIBUTION CODE

13. ABSTRACT *(Maximum 200 words)*

This report documents the scientific activities on board the Royal Research Ship (RRS) *James Clark Ross* during the first Atlantic Meridional Transect (AMT-1), 21 September to 24 October 1995. The ship sailed from Grimsby (England) for Montevideo (Uruguay) and then continued on to Stanley (Falkland Islands). The primary objective of the AMT program is to investigate basic biological processes in the open Atlantic Ocean over very broad spatial scales. For AMT-1, the meridional range covered was approximately 50°N to 50°S or nearly 8,000 nmi. The measurements to be taken during the AMT cruises are fundamental for the calibration, validation, and continuing understanding of remotely sensed observations of biological oceanography. They are also important for understanding plankton community structure over latitudinal scales and the role of the world ocean in global carbon cycles. During AMT-1 a variety of instruments were used to map the physical, chemical, and biological structure of the upper 200 m of the water column. Ocean color measurements were made using state-of-the-art sensors, whose calibration was traceable to the highest international standards. New advances in fluorometry were used to measure photosynthetic activity, which was then used to further interpret primary productivity. A unique set of samples and data were collected for the planktonic assemblages that vary throughout the range of the transect. These data will yield new interpretations on community composition and their role in carbon cycling. While the various provinces of the Atlantic Ocean were being crossed, the partial pressure of CO_2 was related to biological productivity. This comparison revealed the areas of drawdown of atmospheric CO_2 and how these areas relate to the surrounding biological productivity. These data, plus the measurements of light attenuation and phytoplankton optical properties, will be used as a primary input for basin-scale biological productivity models to help develop ecosystem dynamics models which will be important for improving the forecasting abilities of modelers. The AMT program is also attempting to meet the needs of international agencies in their implementation of Sensor Intercomparison and Merger for Biological and Interdisciplinary Ocean Studies (SIMBIOS), a program to develop a methodology and operational capability to combine data products from the various ocean color satellite missions.

14. SUBJECT TERMS
SeaWiFS, Oceanography, Atlantic Meridional Transect, AMT, Cruise Report, Instrumentation, Cruise Track, Cruise Synopsis

15. NUMBER OF PAGES
87

16. PRICE CODE

17. SECURITY CLASSIFICATION OF REPORT	18. SECURITY CLASSIFICATION OF THIS PAGE	19. SECURITY CLASSIFICATION OF ABSTRACT	20. LIMITATION OF ABSTRACT
Unclassified	Unclassified	Unclassified	Unlimited